

NUCLEAR DATA AND MEASUREMENTS SERIES

ANL/NDM-142

Neutron Scattering and Models: Molybdenum

by

A.B. Smith

November 1997

**ARGONNE NATIONAL LABORATORY,
ARGONNE, ILLINOIS 60439, U.S.A.**

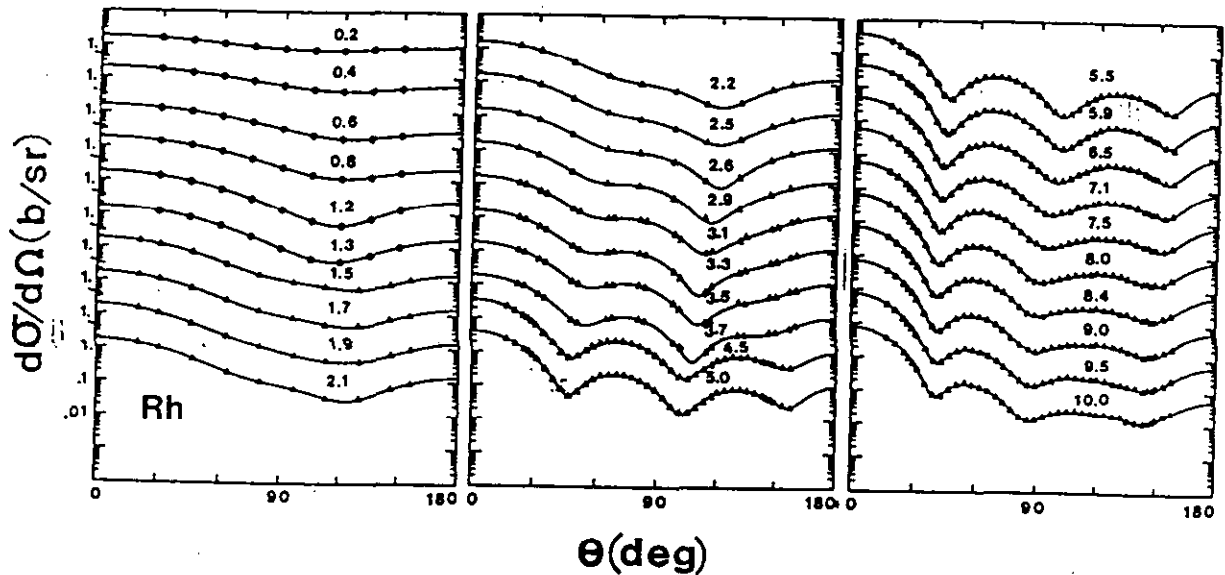
NUCLEAR DATA AND MEASUREMENTS SERIES

ANL/NDM-142

NEUTRON SCATTERING AND MODELS:- MOLYBDENUM

by
A. B. Smith

July, 1999



ARGONNE NATIONAL LABORATORY, ARGONNE, ILLINOIS

Operated by THE UNIVERSITY OF CHICAGO

for the U. S. DEPARTMENT OF ENERGY

under Contract W-31-109-Eng-38

Argonne National Laboratory

Argonne National Laboratory, with facilities in the states of Illinois and Idaho, is owned by the United States Government, and operated by the University of Chicago under provisions of a contract with the Department of Energy.

Disclaimer

This report was prepared as an account of work sponsored by an agency of the United States Government. Neither the United States Government nor any agency thereof, nor any of their employees, makes any warranty, express or implied, or assumes any legal liability or responsibility for the accuracy, completeness, or usefulness of any information, apparatus, product, or process disclosed, or represents that its use would not infringe privately owned rights. Reference herein to any specific commercial product, process, or service by trade name, trademark, manufacturer, or otherwise, does not necessarily constitute or imply its endorsement, recommendation, or favoring by the United States Government or any agency thereof. The views and opinions of authors expressed herein do not necessarily state or reflect those of the United States Government or any agency thereof.

Reproduced from the best available copy.

Available to DOE and DOE contractors from the Office of Scientific and Technical Information, P. O. Box 62, Oak Ridge, TN 37831; prices available from (423) 576-8401.

Available to the public from the National Technical Information Service, U. S. Department of Commerce, 5285 Port Royal Road, Springfield, VA 22161.

Nuclear Data and Measurement Series

The Nuclear Data and Measurement Series presents results of studies in the field of microscopic neutron data. The primary objective is the dissemination of information in the comprehensive form required for nuclear-technology applications. This Series is devoted to: a) measured microscopic nuclear parameters, b) experimental techniques and facilities employed in measurements, c) the analysis, correlation and interpretation of nuclear data, and d) the compilation and evaluation of nuclear data. Contributions to this Series are reviewed to assure technical competence and, unless otherwise stated, the contents can be formally referenced. This Series does not supplant formal journal publication, but it does provide the more extensive information required for technological applications (e.g., tabulated numerical data) in a timely manner.

PUBLICATIONS IN THE ANL/NDM SERIES

A listing of recent issues in this series is given below. Issues and/or titles prior to ANL/NDM-130 can be obtained from the National Technical Information Service, U. S. Department of Commerce, 5285 Port Royal Road, Springfield, VA 22161, or by contacting the author of this report at the following address:-

Technology Development Division
Argonne National Laboratory
9700 South Cass Avenue
Argonne, IL 60439
USA

- A. B. SMITH AND P. T. GUENTHER
Fast-Neutron Interaction with the Fission Product ^{109}Rh
ANL/NDM-130, September 1993
- A. B. SMITH AND P. T. GUENTHER
Fast-Neutron Scattering from Vibrational Palladium Nuclei
ANL/NDM-131, October 1993
- A. B. SMITH
Neutron Interaction with Doubly-Magic ^{40}Ca
ANL/NDM-132, December 1993
- A. B. SMITH
Neutron Scattering at $Z = 50$:- Tin
ANL/NDM-133, September 1994
- A. B. SMITH, S. CHIBA AND J. W. MEADOWS
An Evaluated Neutronic File for Elemental Zirconium
ANL/NDM-134, September 1994
- A. B. SMITH
Neutron Scattering from Uranium and Thorium
ANL/NDM-135, February 1995
- A. B. SMITH
Neutron Scattering and Models:- Iron
ANL/NDM-136, August 1995
- A. B. SMITH
Neutron Scattering and Models:- Silver
ANL/NDM-137, July 1996
- A. B. SMITH
Neutron Scattering and Models:- Chromium
ANL/NDM-138, June 1996
- W. P. POENITZ AND S. E. AUMEIER
The Simultaneous Evaluation of the Standards and Other Cross Sections of Importance for Technology
ANL/NDM-139, September 1997
- J. T. Daly and D. L. Smith
A Compilation of Information on the $^{31}\text{P}(p,\gamma)^{32}\text{S}$ Reaction and Properties of Excited Levels in ^{32}S
ANL/NDM-140, November 1997

- A. B. SMITH
Neutron Scattering and Models:- Titanium
ANL/NDM-141, July 1997
- A. B. SMITH
Neutron Scattering and Models:- Molybdenum
ANL/NDM-142, July 1999
- R. E. MILLER AND D. L. SMITH
*A Compilation of Information on the $^{31}\text{P}(p,\gamma)^{33}\text{Cl}$ Reaction
and Properties of Excited Levels in ^{33}Cl*
ANL/NDM-143, July 1997
- R. E. MILLER AND D. L. SMITH
*A Compilation of Information on the $^{31}\text{P}(p,\gamma)^{28}\text{Si}$ Reaction
and Properties of Excited Levels in ^{28}Si*
ANL/NDM-144, November 1977.
- R. D. LAWSON AND A. B. SMITH
*Abares-A Neutron Spherical Optical-Statistical Model Code:
A Users Manual*
ANL/NDM-145, June 1998.
- R. T. KLANN AND W. P. POENITZ
*Non-destructive Assay of EBR-II Blanket Elements Using
Resonance Transmission Analysis*
ANL/NDM-146, August 1998.

ANL/NDM-142

NEUTRON SCATTERING AND MODELS:- MOLYBDENUM*

by

A. B. Smith

Argonne National Laboratory
Argonne, Illinois
and
The University of Arizona
Tucson, Arizona

July, 1999

Keywords:

Measured $d\sigma/d\Omega_{el}$ and $d\sigma/d\Omega_{inel}$ for 4.5 \rightarrow 10 MeV neutrons incident on elemental molybdenum. Comprehensive model interpretations dealing with $^{92,96,98,100}\text{Mo}$ and elemental molybdenum, including:- spherical optical-statistical, first and second order vibrational coupled-channels, and dispersive models. Provision of a "general regional" model for applied and other purposes.

*This work supported by the United States Department of Energy under contract W-31-109-Eng-38, and by the Nuclear and Energy Engineering Program, College of Engineering and Mines, The University of Arizona, Tucson Arizona.

TABLE OF CONTENTS

Abstract -----	1
I. Preamble -----	1
II. Experimental Procedures -----	2
III. Experimental Results -----	3
IV. Model Development	
IV-1. Data Base -----	4
IV-2. Spherical Optical Model -----	5
IV-3. Volume Absorption -----	7
IV-4. Dispersive Optical Model -----	8
IV-5. First-order Vibrational Model -----	10
IV-6. First-order Vibrational Model with Dispersion ---	13
IV-7. First-order Vibrational Model with the 3 ⁻ Quadrupole Level -----	13
IV-8. First- and Second-Order Vibrational Model -----	14
V. Physical Discussion -----	15
VI. General Molybdenum Potential for Applied and Other Purposes -----	24
VII. Recommendations -----	26
VIII. Summary Comment -----	27
Acknowledgments -----	29
References -----	29
Tables (12) -----	35
Figures (27) -----	51

NEUTRON SCATTERING AND MODELS:- MOLYBDENUM

by

Alan B. Smith

ABSTRACT

A comprehensive interpretation of the fast-neutron interaction with elemental and isotopic molybdenum at energies of ≤ 30 MeV is given. New experimental elemental-scattering information over the incident energy range 4.5 \rightarrow 10 MeV is presented. Spherical, vibrational and dispersive models are deduced and discussed, including isospin, energy-dependent and mass effects. The vibrational models are consistent with the "Lane potential". The importance of dispersion effects is noted. Dichotomies that exist in the literature are removed. The models are vehicles for fundamental physical investigations and for the provision of data for applied purposes. A "regional" molybdenum model is proposed. Finally, recommendations for future work are made.

I. PREAMBLE

The naturally occurring isotopes of molybdenum span one of the larger isotopic ranges in the periodic table. The lightest, ^{92}Mo , is even in proton number and has a filled $1g_{9/2}$ neutron shell with even-parity excited states due to mixtures of $p_{1/2}^2 g_{9/2}^2$ and $g_{9/2}^4$ proton configurations [AT65]. It is essentially a spherical nucleus with a small β_2 of ≈ 0.087 . Vibrations will be primarily with the proton core [MBA75]. As the isotopic mass increases from ^{94}Mo through ^{98}Mo neutrons fill the $2d_{5/2}$ sub-shell, and for ^{100}Mo the two additional neutrons are in the $1g_{7/2}$ sub-shell [Law80]. Such a shell representation is an oversimplification as the character of the isotopes rapidly changes from that of the essentially spherical ^{92}Mo to nuclei making a transition from collective vibrators to the deformed rotors [BH75] which are typical of the unstable ^{104}Mo and ^{106}Mo isotopes. These increasingly complex structures have been interpreted as quadrupole deformations leading to potential

surfaces that describe the low-energy excited structures, even to the inversion of excited yrast 0^+ and 2^+ levels in ^{98}Mo [GG71]. Neutron and proton scattering from the molybdenum isotopes has been studied in the context of spherical optical-statistical and, to a lesser extent, direct-reaction models. As the isotopic mass and collectivity of the isotopes increases discrepancies appear ([Com78], [Rap+79], [SGW75]). A number of reported results do not agree with conventional isovector potential concepts ([Lan62], [Sat69]). In addition, sub-coulomb-barrier (p,n) results have suggested anomalously strong imaginary potentials at the low energies which can be examined using neutron-induced processes [JGK79]. These reported dichotomies suggest that something is wrong with the experimental data and/or the modeling in a rapidly changing collective environment. Relatively little attention has been given to the correlation of neutron and proton scattering. The present work considerably enhances the elemental neutron-scattering data for molybdenum in the 4 - 10 MeV transitional region where dispersive effects can be expected. From this new data, and the data found in the literature, were constructed comprehensive isotopic and elemental molybdenum neutron scattering and total cross section (σ_t) data bases not here-to-fore used in physical interpretations. Particular attention was given to collective, isospin and dispersive effects as they change from isotope to isotope. These considerations suggest that interpretations of neutron and proton data are reasonably consistent with each other and with generally accepted physical concepts. In particular, the isospin dichotomies of some previously work are removed. At the same time, the results lead to questions, for example, dealing with the influence of shell closures on the absorptive portion of the potential.

The isotopes of molybdenum are very prominent fission products and have large neutron inelastic-scattering cross sections, how large has been a matter of technical debate ([GK85], [GH92]). This has led to international study groups under the auspices of the NEA, to some new measurements [BWW97] and to extensive modeling [KWK98]. In addition, molybdenum is a material in ferrous alloys proposed for use in a wide range of neutronic applications, such as controlled fusion devices. This report endeavors to provide new experimental information and comprehensive model analyses that meet many of these applied needs.

II. EXPERIMENTAL PROCEDURES

The measurements were made using the fast-neutron time-of-flight method [CL55] and the Argonne multi-angle detection system. The particular apparatus and method have been widely described elsewhere [Smi+92] and will not be further discussed here. The measurement samples were 2 cm diameter 2 cm long cylinders of high-purity elemental molybdenum metal. The

neutron source was the $D(d,n)^3\text{He}$ reaction [Dro87] within a gas target assembly, providing incident-neutron energy spreads at the sample of ≈ 300 keV at 4.5 MeV, decreasing to ≈ 100 keV at 10.0 MeV. The neutron source was pulsed at a 2 MHz rate with a burst duration of ≈ 1 nsec. Source intensity was increased by the use of a harmonic klystron bunching system. The ten scattered-neutron flight paths were ≈ 5 m long, scattering angles were determined to within $\approx \pm 0.1^\circ$ and liquid-scintillation neutron detectors were placed at the ends of the flight paths. All cross sections were determined relative to the $H(n,n)$ standard [CSL83], and all the results were corrected for beam-attenuation, multiple-event, and angular-resolution effects using monte-carlo techniques [Smi91].

III. EXPERIMENTAL RESULTS

The measurements were made at approximately 0.5 MeV incident-energy intervals from 4.5 \rightarrow 10 MeV, and at forty or more scattering angles distributed between $\approx 17^\circ$ and 160° . The effective scattered-neutron resolution was $\approx < 500$ keV. This implies that several inelastically-scattered neutron groups were included with the elastic component. At some energies several sets of data were obtained at approximately the same scattering angles. In these cases the results were averaged at each scattering angle. The elastic-scattering results are summarized in Fig. III-A. The normalization uncertainty was estimated to be 2 \rightarrow 3 percent, and the statistical uncertainties varied from $\approx 1\%$ to larger values at the minima of the distributions. This set of elastic-scattering data is apparently the only elemental molybdenum neutron-scattering information available in the 4 \rightarrow 10 MeV energy range. Concurrent with the elastic-scattering measurements, elemental inelastic-scattering cross sections were determined corresponding to the excitation of levels at $\approx 0.7 \rightarrow 1.1$ MeV. The yrast 2^+ levels of most of the even isotopes must be prominent contributors to the excitation of this observed "level", with the addition of contributions from the odd isotopes [NDS]. Thus the measured values are "pseudo-integral" inelastic-scattering cross sections resulting from the excitation of a number of levels in the various isotopes making up the element. The observed inelastically-scattered neutron distributions appeared to have a significant direct-reaction component, evidenced by a forward peaking of the angular distributions. The inelastic cross sections are illustrated and discussed in Sections IV-5 and VI, below.

IV. MODEL DEVELOPMENT

IV-1. Data Base

The elastic-scattering data came from the files of The National Nuclear Data Center (Brookhaven National Laboratory) up to July 1998 (as cited in the references), some private Argonne files, and the present work. Some of the data sets contained a large number of elastic distributions on a fine energy mesh ([Lam+73], [SGW75]). In those cases, average distributions were constructed from the measured values at ≈ 200 keV intervals. Uncertainties were generally taken as specified by the original authors. There were obvious data differences beyond the respective uncertainties. The data samples are reasonably large and, hopefully, these differences averaged out in the fitting procedures. The isotopic elastic-scattering data bases extended from several-hundred keV to ≈ 26 MeV for $^{92,96,98,100}\text{Mo}$. The data for ^{94}Mo was far less comprehensive, and elastic-scattering data for the odd molybdenum isotopes ($\approx 25\%$ abundant) is essentially non-existent. The elemental elastic-scattering data is very detailed to 10 MeV. Above 10 MeV there are only two 14 MeV distributions, one of which is very old. This is a common neutron-scattering situation, the nearly complete lack of experimental information above 10 to 15 MeV. The experimental elastic-scattering data base is illustrated in Figs. IV-1-A to IV-1-E.

The isotopic and elemental σ_t data was also taken from the files of The National Nuclear Data Center (as cited in the references). Most of the data sets available at the Center were used. A few were abandoned as being discrepant and/or of a limited scope that would have very little effect on the overall picture. Only σ_t 's for ^{98}Mo and elemental Mo covered a large energy span. For the remainder of the isotopes σ_t were generally limited to energies of $\approx < 5$ MeV. Since the present interpretations are in the context of energy-averaged models, the σ_t data were averaged over 50 keV at incident energies below 0.5 MeV, over 100 keV between 0.5 and 5.0 MeV, and over 200 keV at higher incident energies. This smoothing averaged evident cross-section fluctuations, was consistent with the physical interpretations and reduced the number of data points in some of the sets to more manageable proportions. The σ_t data are illustrated in Fig. IV-1-F. Molybdenum inelastic-scattering information is very largely confined to energies of $\approx < 4$ MeV. The present results provide elemental inelastic-scattering values at higher energies. Some inelastic-scattering data was used in the interpretations as discussed in Sections IV-5 and VI.

IV-2. Spherical Optical Model (SOM)

The SOM parameters were primarily determined by fitting the differential elastic-scattering data, with subsequent comparisons with σ_t and inelastic-scattering data. The fitting procedures

minimized χ^2 defined by

$$\chi^2 = \sum_i \left[\frac{\sigma_{\text{exp}}(i) - \sigma_{\text{cal}}(i)}{\Delta\sigma_{\text{exp}}(i)} \right]^2, \quad (\text{IV-2-1})$$

where $\sigma_{\text{exp}}(i)$ denote measured elastic scattering, $\sigma_{\text{cal}}(i)$ the corresponding calculated values, and $\Delta\sigma_{\text{exp}}(i)$ the measurement uncertainties. All of the SOM calculations were carried out with the spherical optical-statistical-model code ABAREX [Mol82]. One version of this code deals with single isotopes (or averages thereof), and another comprehensively treats the element isotope by isotope. Compound-nucleus scattering processes were explicitly dealt with, following the formulations of Wolfenstein [Wol51] and Hauser-Feshbach [HF52], as modified for fluctuation and correlation effects by Moldauer [Mol80]. Fifteen discrete levels in ^{92}Mo to excitations of ≈ 3.0 MeV were considered, fifteen in ^{94}Mo to ≈ 2.8 MeV, thirteen in ^{95}Mo to ≈ 1.4 MeV, fifteen in ^{96}Mo to ≈ 2.5 MeV, fifteen in ^{97}Mo to ≈ 1.2 MeV, seventeen in ^{98}Mo to ≈ 2.3 MeV and fourteen in ^{100}Mo to ≈ 2.0 MeV. The corresponding excitation energies, spins and parities were taken from the respective Nuclear Data Sheets [NDS]. The excitation of higher-lying levels was represented using the statistical formalism and parameters of Gilbert and Cameron [GC65]. The excited levels were combined in the calculations to correspond to the resolutions of the respective experiments. Neutron radiative capture and other non-scattering neutron-induced reactions were assumed small and ignored.

The real potential was assumed to have the Saxon-Woods form, and the imaginary potential the derivative-Saxon-Woods form [Hod71]. The spin-orbit potential was taken to be real and of the Thomas form with the parameters fixed to those given by Walter and Guss [WG86]. The fitting procedure followed the five steps long used by the author [Smi+92]. First, six-parameter fits were carried out, varying real- and imaginary-potential strengths, radii and diffusenesses (all radii, r_i , are expressed in the reduced form where $R_i = r_i A^{1/3}$ and A is the target mass). From the six-parameter fits the real diffuseness, a_v , was fixed. Then the real radius, r_v , was determined from five-parameter fits, keeping a_v fixed. Four parameter fits then fixed the

imaginary radius, r_w , followed by three-parameter fits determining the imaginary diffuseness, a_w . Finally, two-parameter fits determined the real, J_v , and imaginary, J_w , potential strengths (herein potential strengths, J_i , are expressed as volume-integrals-per-nucleon). The results of fitting the ^{94}Mo scattering data were not used in determining parameter trends as that data base was very weak. The elemental data gives good information below 10 MeV but the results are unreliable at higher energies. All the isotopic-scattering measurements appear to have used the same measurement samples, and some of them seemed to contain significant oxygen. The use of common samples has the potential for systematic distortion of the isotopic measurements.

The SOM parameters deduced from fitting are summarized in Table IV-2-A. The a_v display no systematic trend with energy, the values are consistent within the uncertainties, and thus the weighted average was used in the subsequent fitting steps. There is some trend for the isotopic r_v to decrease with energy but the slope was only slightly outside the uncertainties, largely determined by the 20 and 26 MeV measurements from a single institution, and was not evident in the elemental results. Therefore, this slight energy dependence was ignored. The r_w show a tendency to decrease with energy. The effect becomes less acute as the target mass increases. The variation of r_w from isotope to isotope seems real, therefore the individual expressions of Table IV-2-A were used in the subsequent fitting steps. As noted previously at this laboratory [Smi+92], a_w tends to increase with energy in all cases, with larger values for the heavier targets as $E \rightarrow 0$. All of the SOM J_v values decrease with energy, while the SOM J_w increase with energy.

Illustrative comparisons of measured differential elastic scattering with the results of SOM calculations are shown in Figs. IV-1-A \rightarrow IV-1-E. The agreement is reasonably good. Fig. IV-1-F compares measured and SOM-calculated σ_t 's. The measured ^{92}Mo σ_t scatter by a few percent and only extend to ≈ 5.5 MeV. The calculated ^{92}Mo σ_t are slightly smaller than the measured quantities. The σ_t comparisons below ≈ 5.5 MeV are quite similar for the other isotopes. For ^{98}Mo the measured σ_t extend to much higher energies. These latter results are well described by the SOM calculations to 30 MeV or more. The agreement between the measured and calculated elemental elastic-scattering distributions is quite good over the entire measured energy

range. The SOM calculations qualitatively described the measured isotopic inelastic data over the region of large compound-nucleus contributions (e.g., up to ≈ 4 MeV). At higher energies direct reactions become significant, are inconsistent with the concept of the SOM, and thus are not described. Strength functions calculated with the SOM are compared with those deduced from measurements [MDH81] in Table IV-2-B. The agreement between measured and calculated S_0 values is reasonably good, and this is a difficult mass region of very small S_0 values. The comparison of S_1 values is less encouraging, particularly for the heavier and more collective targets. However, the measured S_1 values scatter by considerable amounts and thus the comparisons may not be too meaningful.

IV-3. Volume Absorption

As the energy increases the absorption term of the SOM shifts from a surface component to volume and surface contributions, and finally to a volume form. This transition is slowly energy dependent. The on-set of the volume component is uncertain, with a wide range of energies cited in the literature. For example, theoretical estimates suggest that volume absorption is the dominant component above ≈ 50 MeV [JLM77], while from experimental considerations it has been suggested that volume absorption is significant above ≈ 15 MeV [Rap+79]. In the present studies only the isotopic portions of elastic-scattering data are at high enough energies to be sensitive to volume absorption, and it is only relevant to the 20 and 26 MeV data from a single institution.

Two assessments of volume absorption were made. In the first of these, the volume-absorption strength of Rapaport et al. [Rap+79] was assumed and the entire SOM fitting procedure, described above, repeated. The resulting SOM parameters are summarized in Table IV-3-A. They are not significantly different from those of the SOM cited above. Thus, the inclusion of a volume absorption of the magnitude of ref. [Rap+79] did not appreciably alter the SOM parameterization. In the second assessment of volume absorption, three-parameter fits were carried out at 20 and 26 MeV, varying the real-potential, the volume-imaginary potential and the surface-imaginary potential, with the geometric parameters fixed to the above SOM values. The volume- and surface-imaginary potentials were assumed to have the same geometric parameters. The results of this fitting were "mixed". Generally, the resulting volume absorption was less than given in ref. [Rap+79], though the volume-absorption strengths scattered and, in one case, even went negative. Volume absorption may be a factor at higher energies, but the above considerations suggest that it is not a significant concern in the present studies. This conclusion tends to be supported by lower-energy proton-scattering studies [Cer+82]

IV-4. Dispersive Optical Model (DOM)

It is well known that there is a dispersion relationship linking real and imaginary optical potentials and reflecting causality ([Sat83], [Lip66], [Pas67], [Fes58]). This relationship can be expressed in the form

$$J(E)_v = J(E)_{HF} + \frac{P}{\pi} \int_{-\infty}^{+\infty} \frac{J_w(E')}{E - E'} dE', \quad (IV-4-1)$$

where J_{HF} is the local-equivalent Hartree-Fock potential, J_w is the strength of the imaginary potential, and "P" denotes the principle value of the integral. The integral can be broken into surface, ΔJ_s , and volume, ΔJ_{vo} , components

$$\Delta J_s(E) = \frac{P}{\pi} \int_{-\infty}^{+\infty} \frac{J_s(E')}{E - E'} dE' \quad (IV-4-2)$$

and

$$\Delta J_{vo}(E) = \frac{P}{\pi} \int_{-\infty}^{+\infty} \frac{J_{vo}(E')}{E - E'} dE'. \quad (IV-4-3)$$

Then $J_v(E) = J_{eff}(E) + \Delta J_s(E)$ and $J_{eff}(E) = J_{HF}(E) + \Delta J_{vo}(E)$, where $J_s(E)$ and $J_{vo}(E)$ are surface and volume imaginary-potential strengths, respectively. J_{HF} and ΔJ_{vo} are approximately linear functions of energy in the range of the present considerations. Combined they determine J_{eff} , the two components of which can not be experimentally distinguished. In the present work J_{HF} is approximately J_{eff} as ΔJ_{vo} is relatively small. Thus, the effect of Eq. IV-4-1 is essentially to add a surface component to the real Saxon-Woods potential consisting of some fraction of the J_s . The magnitude of the contribution can be evaluated following the methods of ref. [LGS87]. It was assumed that the imaginary potential was purely a surface term up to 26 MeV and then the imaginary potential linearly decreased with energy to zero at 60 MeV. Concurrently the volume imaginary contribution rises from zero at 26 MeV to 60 MeV where it reaches a strength equivalent to that of the surface component at 26 MeV, and remains constant at that value to higher energies. The J_s values from 0 → 26 MeV were taken from the SOM. The imaginary potential was assumed to zero at the Fermi Energy (E_F) and to have a quadratic energy dependence to zero energy. In addition, the entire imaginary potential was taken to symmetric about E_F [JLM77]. The dispersive contributions change from isotope to isotope due to

the changing E_F which increases from ≈ -10.3 MeV at ^{92}Mo to ≈ -6.8 MeV at ^{100}MeV . For the elemental interpretation a weighted average of the isotopic E_F 's was assumed. These approximations are qualitative but they should give an indication of the effect of the dispersion relationship. Somewhat different assumptions in the dispersion estimates did not particularly change the results. With the above assumptions, the fraction of the surface-imaginary potential added to the real potential was computed as a function of energy. A representative result obtained for ^{96}Mo is shown in Fig. IV-4-A. In this example, at zero energy approximately eight-tenths J_s is added to the real potential. That fraction falls with energy to zero at ≈ 30 MeV. The calculations also give the energy dependence of the above $\Delta J_s(E)$ integral contribution, as illustrated in Fig. IV-4-B.

With the above dispersion contribution, the entire SOM fitting was repeated. The resulting parameters are given in Table IV-4-A. In principle, the fitting should be iterated to converge on the dispersion effects. This was not done as the parameters did not greatly change from those of the SOM. The average a_v of the DOM is similar to that of the SOM (0.6445 and 0.6448 fm, respectively) and the r_v are systematically smaller than those of the SOM. The r_w and a_w resulting from both the DOM and SOM fitting scatter by considerable amounts. Given that scatter, the parameters of the two potentials are reasonably consistent. The DOM J_v are nearly constant with mass. The DOM parameters give approximately the same description of the experimental data as obtained with the SOM. For the elastic scattering this is illustrated by the ^{92}Mo results of Fig. IV-4-C. This figure is essentially identical to Fig. IV-1-A. Similar close agreement is obtained for elastic scattering from the other isotopes and the element. The total cross sections calculated with the SOM and DOM were essentially indistinguishable.

The above elemental calculations concurrently dealt with the seven isotopes of the natural element, assuming that isovector potentials were identically zero. The elemental DOM calculations were extended to include real- and imaginary-isovector potentials respectively defined by $V = V_0 - V_1 \cdot \eta$ and $W = W_0 - W_1 \cdot \eta$, where V_0 (W_0) are scalar potentials, V_1 (W_1) are vector potentials and $\eta = (N-Z)/A$ is the nuclear asymmetry. It was assumed that the isoscalar and isovector potentials had the same form and geometric parameters. This is a rather crude assumption as folding models and other considerations suggest that the vector potentials may be concentrated near the nuclear surface and there are suggestions that the vector potentials are energy dependent.

([GPT68], [Sat69]). However, the relative isovector contributions over the range of the molybdenum isotopes are quite small thus simple approximations are reasonable. In the present calculations it was assumed that $V_1 = 24$ MeV and $W_1 = 12$ MeV.

These magnitudes are a matter of some debate but the values used here are generally in the middle of those deduced from a number of neutron and proton studies ([Hod94], [BG69]), and are consistent with those deduced in the present work (see discussion below). Repeating the elemental DOM fitting with the isovector contributions leads to the elemental parameter values given in brackets in Table IV-4-A. The latter parameters are generally consistent within uncertainties with those obtained assuming the isovector strengths are identically zero. The largest parameter differences involve the imaginary potentials which are not very well defined. The conclusion drawn from the exercise is that the inclusion of the isovector potentials in the elemental fitting does not significantly effect the resulting parameters. This is not surprising as the isovector contributions are relatively minor.

IV-5. First-order Vibrational Model (CCM1)

There are a number of indications that the molybdenum isotopes are collective in nature, and increasingly so with mass. As an initial approximation these collective properties were represented with a first-order quadrupole vibrational model (this is a simplification as the quadrupole moment of, particularly, ^{100}Mo is $\neq 0$). This model couples the 0^+ ground state of the even isotopes to the yrast 2^+ state assuming a quadrupole vibrational parameter, β_2 . These yrast 2^+ states are at 1509 (^{92}Mo), 778 (^{96}Mo), 735 (^{98}Mo) and 536 (^{100}Mo) keV [NDS]. All of the CCM1 calculations used the coupled-channels method [Tam65], implemented with the calculational code ECIS96 [Ray96]. Compound-nucleus contributions were included in the calculations using the concepts, level structures and parameters employed in the above SOM calculations. $\beta_2^{\text{ave.}}$ parameters were constructed from an average of β_2^{em} electro-magnetic values [Ram+87] and of β_2^{pp} proton-scattering values (see citations to proton-scattering references). The β_2^{em} and the $\beta_2^{\text{ave.}}$ used in the calculations are summarized in Table IV-5-A. These $\beta_2^{\text{ave.}}$ are approximations as β_2^{em} , β_2^{pp} and β_2^{nn} may not be identical, and the various β_2^{pp} derived from experiments deviate by significant amounts. However, the $\beta_2^{\text{ave.}}$ approximation is a useful starting point in

the calculations.

With the above assumptions, the entire fitting procedure, outlined above, was repeated using the quadrupole model, resulting in the parameters of Table IV-5-A. The resulting a_v scattered about the average value of 0.6339 ± 0.0107 fm. The r_v obtained for the four isotopes were consistent with one another, and had an average value of 1.2160 ± 0.0044 fm. The ^{92}Mo CCM1 and SOM r_w values are very similar. This is not surprising as β_2 is small for ^{92}Mo . As β_2 increases for the heavier isotopes, the CCM1 low-energy r_w become increasing larger than that of the SOM. In both the SOM and CCM1 models the r_w decrease with increasing energy. There is considerable scatter of the a_w values resulting from the fitting. However, all the CCM1 isotopic a_w values increase with energy in qualitatively the same manner. The CCM1 J_v were deduced from fitting at energies above ≈ 1.5 MeV as lower-energy J_v tended to scatter. The J_v of Table IV-5-A follow a systematic mass dependence, and all decrease with energy. The uncertainties in the CCM1 J_w values are quite large, however the general trend of J_w is to increase with energy. The J_w magnitudes tend to be smaller than those resulting from the SOM.

The ^{92}Mo elastic scattering predicted by the CCM1 potential is compared with the data base in Fig. IV-5-A. This description is essentially identical to that obtained with the SOM. Similar comparisons for ^{96}Mo are shown in Fig. IV-5-B. In this instance the CCM1 model may be somewhat better at the highest energies of the data base, but the differences are marginal. For ^{98}Mo and ^{100}Mo the CCM1 gives elastic-scattering results similar to those obtained with the SOM (see Figs. IV-5-C and -D). σ_t calculated with CCM1 and SOM models are compared in Fig. IV-5-E. Above several MeV the two potentials give nearly identical results. For ^{92}Mo that is true throughout the energy range $0 \rightarrow 26$ MeV. This is encouraging as ^{92}Mo is essentially a spherical nucleus with a small β_2 . Therefore, the two models should give the same results, despite the fact that the fitting procedures used to derive the SOM and CCM1 potentials were entirely independent and used very different calculational codes. As the energy decreases below several MeV, the CCM1 σ_t 's fall increasingly below the SOM values as the mass increases. That trend is not particularly supported by measurements (see Fig. IV-1-F). This low-energy behavior marginally improves the description of strength

functions (compare Tables IV-5-B and IV-2-B). Strength functions and total cross sections are sensitive to the a_w at low energies where it is not well known.

The inelastic neutron excitation should be a good test of the CCM1 model, particularly that associated with the yrast 2^+ levels. These, and other inelastic cross sections, were calculated with the CCM1 model for the isotopes $^{92,96,98,100}\text{Mo}$ with the results compared with the measured values in Figs. IV-5-F, -G, -H and -I. The calculated ^{92}Mo angle-integrated results agree reasonably well with the measured values for the yrast 2^+ (1.509 MeV) level (and also give a reasonable description of the corresponding differential distributions). The $(n;n',\gamma)$ results are a bit lower above ≈ 2 MeV, possibly as a consequence of branching-ratio effects. The higher-energy results for the yrast 2^+ level are nicely accounted for with the direct reaction. The calculated inelastic excitations for the higher-lying ^{92}Mo levels are reasonably consistent with the experimental information. The exceptions are the 11 MeV value for the excitation of the 2.85 MeV level and the single measurement for the excitation of the composite of levels near 3 MeV. The former discrepancy is probably due to the omission of the direct excitation of the 3^- octupole level (not considered in the CCM1, see the CCM13 below), while the latter difference probably is due to the single measurement including only two of the three contributing levels considered in the calculations. Similar comparisons for the inelastic excitation of levels in ^{96}Mo are also reasonably encouraging. The measured excitations of the yrast 2^+ level (0.778 MeV) are somewhat lower than the calculated quantities near 4 MeV. This may suggest that the competition with the continuum inelastic scattering was not calculated quite correctly. The remainder of the ^{96}Mo comparisons are reasonably good, excepting several low-energy measurements for the excitation of the 1.626 MeV level which may be in error. The ^{98}Mo inelastic comparisons are, again, quite encouraging. There may be a modest concern for the continuum competition with the yrast 2^+ cross sections, and measured excitations near 2.2 MeV are much lower than calculated. In the latter case the cross sections are all small and it is likely that the measurements failed to include contributions from all four of the relevant levels. The inelastic comparisons for ^{100}Mo are also reasonable. Some of the ^{100}Mo comparisons at excitations of $\approx > 1.7$ MeV leave something to be desired but the correspondence between measured and calculated level structure is very uncertain. The calculated excitation of the 0.695 level is not as large as indicated by some of the experiments (for unknown reasons), however the cross sections in this instance are small.

The present inelastic-scattering comparisons are supported by the recent DWBA interpretations of Kawano et al. [KWK98]. Their calculated excitations of the yrast 2^+ states in ^{92}Mo , ^{98}Mo and ^{100}Mo are consistent with the present inelastic-scattering results though possibly slightly larger at the maxima of the energy distributions. The work of ref. [KWK98] does not consider the higher-energy excitations. Generally, the agreement between inelastic-scattering measurements and CC1 calculations for these four isotopes is quite good, and thus it is reasonable to use the CC1 as a vehicle for interpolating and extrapolating inelastic scattering cross sections of the even isotopes of molybdenum.

IV-6. First-order Vibrational Model with Dispersion (CC1D)

The interpretation of the CC1 (above) was repeated including the effects of the dispersion integral as outlined in Section IV-4. As for the SOM, the primary consequence is the addition of a surface term to the real Saxon-Woods potential. E_F 's, β_2 's and coupling schemes were the same as for the above CC1. With the additional dispersion effects the entire fitting procedure of the CC1 was repeated. The resulting CC1D parameters are given in Table IV-6-A. They gave essentially the same description of the differential and total cross sections of the four isotopes as obtained with the CC1, above, and illustrated in the figures of Section IV-5. There are some differences between the CC1 and CC1D parameters, qualitatively similar to those between the SOM and DOM. The potential strengths and mass dependencies are somewhat different from those of the CC1, as discussed in Section V. The S_0 strength functions of the CC1 and CC1D potentials are similar. The S_1 of the CC1D tend to be systematically larger than those obtained with CC1 potential.

IV-7. First-order Vibrational Model with the 3^- Octupole Level (CC13)

The first-order vibrational model (CC1) was extended to include the direct excitation of the 3^- octupole levels. The excitation energies of the octupole levels and their β_3 were taken from the Nuclear Data Sheets [NDS] and proton-scattering studies. They were: for ^{92}Mo an E_x of 2.840 MeV and $\beta_3 = 0.154$; for ^{96}Mo $E_x = 2.234$ MeV and $\beta_3 = 0.181$; for ^{98}Mo $E_x = 2.017$ MeV and $\beta_3 = 0.211$; and for ^{100}Mo $E_x = 1.900$ MeV and $\beta_3 = 0.211$. The β_2 parameters and other excitations were identical to those of the CC1. The choice of excitations and β_3 's is somewhat

subjective. With the addition of the above 3^- contributions, the entire fitting process described for the CCM1 in Section IV-5 was repeated. The resulting parameters are summarized in Table IV-7-A.

The CCM13 provides a description of the σ_t and elastic-scattering cross sections essentially identical to that obtained with the simpler CCM1 model. There may be some improvement in the comparisons of elastic scattering at the highest energies, but it is very marginal and, if present, probably is well within the variation of the parameters in the fitting procedures. The imaginary-potential strengths are smaller than those of the CCM1, as one would expect since the contribution of the 3^- state is now taken explicitly into account. There is only fragmentary experimental evidence for the neutron excitation of the 3^- levels at high enough energies for a reasonable assessment of the direct excitation. There is the 11 MeV value for ^{92}Mo shown as a contribution to the composite level of Fig. IV-5-F at $E_x \approx 2.8$ MeV [Bai+78]. In this particular case the experimental scattered-neutron angular distribution is limited to seven angles distributed between $\approx 40^\circ$ and 100° . However, these experimental results are in close agreement with the predictions of the CCM13.

IV-8. First and Second Order Vibrational Model (CCM12)

The first-order vibrational model (CCM1) was extended to the second order (CCM12) by including both one- and two-phonon vibrational levels. The selection of excited levels and their energies follows from the Nuclear Data Sheets [NDS] and proton-scattering studies. The assignments are not unambiguous, particularly for the heavier even isotopes, but they should provide a reasonable indication of the effect of including the two-phonon levels in the coupled-channels fitting processes. The assumed two-phonon level properties are outlined in Table IV-8-A. An example of the uncertainties is the first excited state in ^{98}Mo which is 0^+ . If this is member of the two-phonon triad the triad splitting must be very large. For that reason it was not taken to be a two-phonon level. The entire coupled-channel fitting procedure of the CCM1 was repeated using the above one- and two-phonon coupled level structure. The resulting model parameters are given in Table IV-8-B. The CCM12 gives a description of the elastic-scattering and total cross sections that is essentially equivalent to that obtained with the simple CCM1 model. There is not enough experimental information about the inelastic neutron-excitation of the two-phonon levels to provide a reasonable test of the model. The imaginary-potential values tend to be smaller than for the simple CCM1 as, again, more levels are explicitly addressed in the calculations.

V. PHYSICAL DISCUSSION

The a_v of all of the above potentials are essentially energy independent, and consistent with an average of $0.6358(\pm 0.0030)$ fm to within the respective uncertainties. There seems to be no trend of a_v with type of potential or target mass. All the r_v are essentially energy independent, and there is no significant deviation from the $R_v = r_v \cdot A^{1/3}$ mass dependence over the 92,96,98,100 Mo isotopic chain as has been suggested in the literature ([LBC69], [Cha+79]). For example, the r_v mass dependence of the CCM1, as determined by linear least-square fitting, is only marginally greater than the statistical uncertainties, and for the CCM1D significantly less than the statistical uncertainties. Any such comparisons are further mitigated by the well known Vr_v^n ambiguity. The r_v values of the non-dispersive potentials are consistent, within the respective uncertainties, with an average value of $1.2181(\pm 0.0036)$ fm, and those of the two dispersive models with an average of $1.1813(\pm 0.0027)$ fm. The r_v of the dispersive models are significantly smaller than those of the non-dispersive models, as expected from the addition of a surface real component to the potential in the dispersive interpretations. The dispersive effects are strongest at relatively low energies (e.g., below 20 MeV). In making comparisons between models deduced from low- and higher-energy data one should consider the dispersive result as the non-dispersive models have an energy-dependent distortion. The r_w decrease with energy, and the $E \rightarrow 0$ values are larger than those of the r_v . There is no clear difference between dispersive and non-dispersive r_w values. At ≈ 25 MeV all r_w values tend to converge to ≈ 1.0 fm. The suggestion from some (p,p) studies that $r_w > r_v$ [Rob+66] is not supported throughout the energy range of the present work. All a_w increase with energy but the scatter of the values precludes quantitative comparisons. No evidence for volume absorption could be identified to the maximum energies of the present interpretations (26 MeV), at higher energies it may be a factor [JLM77]. The J_v of all the non-dispersive vibrational models are similar. The vibrational and spherical dispersive models have similar J_v , smaller than those of the non-dispersive models by an amount approximately equivalent to the value of the dispersion integral, ΔJ_s . The real-potential isospin dependence of the dispersive vibrational model is smaller than that of the non-dispersive vibrational models and somewhat energy dependent. However, one should be cautious as the dispersive results are influenced by the variations in E_F . The J_w of all the vibrational potentials

(dispersive and non-dispersive) are approximately the same and generally smaller than the comparable quantity of the spherical potentials as direct channels are explicitly dealt with.

Lane and others ([Lan62], [GS58]) have pointed out that potential strengths are related to isospin through the expression

$$J_i = J_i^0(1 \pm \xi_i \cdot \eta), \quad (V-1)$$

where "+" refers to protons and "-" to neutrons, ξ_i and J_i^0 are constants and "i" can be "v" or "w" corresponding to real- or imaginary-potentials, respectively. For J_v of the present work, Eq. V-1 takes the values of Table V-A. Analogous values for the J_w are given in Table V-B. The J_v^0 of the four non-dispersive models have a rms deviation from the average of only 1.8% and the energy dependencies are similar, particularly for the three vibrational cases. All of the ξ_v are positive to well above the maximum energy of the present work, thus all of them are consistent with the Lane isospin dependence in the sense of Eq. V-1. The ξ_v of the non-dispersive models are in reasonable agreement, particularly those of the three vibrational models. Furthermore, the ξ_v of these three potentials are nearly energy independent with an average magnitude of ≈ 0.5067 , which is similar to the magnitude deduced from considerations of the nucleon-nucleon force [GPT68]. At 11 MeV Ferrer et al. [FCR77] deduced SOM's from the fitting of elastic neutron scattering from $^{92,96,98,100}\text{Mo}$ with results implying $\xi_v \approx 0.56$, very similar to the 0.51 of the present SOM (Table 5 of ref. [FCR77] was used). The corresponding J_v^0 magnitudes agree to within $\approx 8\%$. The ξ_v values of the present dispersive models are different from the non-dispersive cases, particularly having a slight positive energy dependence which may reflect the approximations involved in evaluating the dispersion integral. Both the spherical models (SOM and DOM) have negative values of ξ_w . Thus, in the sense of Eq. V-1, they are inconsistent with the Lane isospin dependence of the potential. This dichotomy has been noted before at this laboratory in lower-energy work [SGW75] and has been the subject of discussion in the literature ([Com78], [Rap+79], [FCR77]). Explanations have been sought in complex deuteron couplings [Com78]. In ref. [Rap+79] a "Lane consistent" potential was postulated which, when applied with DWBA methods and reasonable quadrupole deformations, gave a good description of the elastic scattering from the even isotopes of molybdenum. It was suggested that the "anomalous" isospin behavior of the molybdenum imaginary potentials is attributable to the omission of collective effects in the spherical models. The present work

determines the imaginary potentials from detailed fitting and clearly shows that the resulting potentials are "Lane consistent" if the collective vibrational excitations are reasonably taken into account. Some proton potentials support this conclusion [LHB71] with ξ_v values of ≈ 0.42 and ξ_w values of ≈ 1.48 . From the present work, it is concluded that the previous dichotomies were the result of inappropriate models. The effect is quite qualitative, and not dependent upon the details of the collective models as the CCM1, CCM1D, CCM13 and CCM12 all give approximately the same results.

All of the potentials of the present work extend to very low energies, a few-hundred keV or even an eV for strength functions. All the imaginary-potential strengths increase with energy as one would expect as additional channels open. This behavior well below the coulomb barrier gives no indication of the anomalously large absorptions suggested by some sub-coulomb-barrier (p,n) measurements [JGK79]. The same conclusion has been reached from recent (p,p) studies though, of course, they could not reach the low energies of the present work [Cer+82].

The J_v^0 values for the two dispersive models (DOM and CCM1D) are reasonably consistent but they should not be compared with with the corresponding quantities of the other, non-dispersive, models. The J_v of the DOM and CCM1D are the Hartree-Fock component, $J(E)_{HF}$, of Eq. IV-4-1 (plus a possible small contributions from the inherent energy dependence of the nucleon-nucleon force and the ΔJ_{v0} integral). For comparison with the other J_v values the value of the integral in Eq. IV-4-2 must be added. When this is done the CCM1D $J_v^0 \approx 454.0 - 2.9370 \cdot E$, and $\xi_v \approx 0.4901 + 0.0011 \cdot E$, values that are very similar to those of the CCM1. It should be noted that as the mass increases in the molybdenum isotopic sequence so does the asymmetry, while the magnitude of E_F decreases. The latter behavior has an impact on the dispersion relations which is not directly associated with the isospin dependence. To the author's knowledge, this effect has not been previously noted. The vibrational-model J_v^0 's of Table V-A have a magnitude and an energy dependence that is reasonably consistent with other models and with non-locality effects [PB62]. The corresponding ξ_v are essentially energy independent, and have magnitudes that agree with estimates based on the nucleon-nucleon force ([GMP70], [GPT68]). The imaginary potential results of Table V-B are not as well defined but, for the vibrational models, are quite reasonable. The J_w^0 magnitudes for the CCM12 and CCM13 are less than for the CCM1 as more channels have been explicitly dealt

with. All of the imaginary strengths increase with energy as one would expect from the opening of more channels. The vibrational ξ_w have reasonable magnitudes. They slightly increase with energy but this may only reflect the approximate representations of the models.

Inherent in the above isospin remarks are several assumptions. The isoscalar and isovector potentials were assumed to have the same Saxon-Woods form and geometries. The isovector potential is probably a surface potential [GPT68] as the proton and neutron density distributions are different, the later having the larger radius. It was assumed that the isovector effects are not sensitive to the exact form of the isovector potential [BG69]. It seems that no one has undertaken an extensive study using a surface isovector potential. Another qualification is the impact of shell closures. It has been pointed out by Lane et al. [Lan+59] that one should expect decreasing imaginary-potential strengths as closed shells are approached. Experimental evidence supports this postulate (refs. [VSM64], [SGW84] and the mass behavior of the S_0 strength function). In the present context of the even isotopes of molybdenum, this shell effect results in increasing imaginary strengths as the target mass increases from the closed neutron shell at ^{92}Mo to the heavier isotopes. Such a trend is opposite to that expected from the isovector term of the potential and may tend to reduce, or cancel, the isovector contribution. The two effects can not be experimentally separated by studying the even molybdenum isotopes (or similar isotopic sequences) thus resulting in an inherent uncertainty in the conclusions. In the present work we have generally ignored the shell effect on the imaginary potential (as have apparently all other studies of the isovector imaginary potential). That may be a questionable.

It is of interest to compare the CCM1 and CCM1D real potentials with results of the effective-mass approximation implied by the non-locality of the nucleon-nucleon interaction. In the present context, these comparisons are most promising for ^{92}Mo which is the least collective of the molybdenum isotopes and has a closed neutron shell, and thus the following comments are limited to that isotope. Early work by Brueckner et al. ([BLM54], [Bru+56]), Bethe [Bet56], Perey and Buck [PB62] and by Wyatt et al. [WWG60] have considered the velocity dependence (i.e., non-locality) of the nuclear potential. These concepts have been further developed by Brown et al. ([BGG63], [BDS79]) using a dynamic theory of vibrations. It is shown in refs. [BDS79], [MN81] and [Bau+82] that the non-locality leads to the expression

$$\frac{m^*}{m} = 0.64 + 0.36[1.0 + |E - E_F|/(2\hbar\omega_0)]^{-2}, \quad (\text{V-2})$$

where m is the nucleon mass, m^* the effective nucleon mass, E the energy, and $\hbar\omega_0 = 41/A^{1/3}$. Concurrently,

$$\frac{m^*}{m} = 1 - \frac{dV_L}{dE}, \quad (V-3)$$

where V_L is the local real potential. Well away from E_F Eq. V-2

leads to $\frac{m^*}{m}$ values of ≈ 0.68 , consistent with the nuclear matter

estimates. At E_F the $\frac{m^*}{m}$ ratio of Eq. V-2 clearly rises to unity.

This seems to be qualitatively consistent with the behavior of the shell-model potential in the low-MeV bound region where the

ratio $\frac{m^*}{m}$ tends to approach, or even exceed, unity at E_F ([BDS79, Coh65]). Turning to the present potentials, Eq. V-3 implies

$\frac{m^*}{m}$ = of 0.6884 from the CCM1 and 0.7448 from the CCM1D, well away from E_F . Either value is in reasonable agreement with the

predictions of Eq. V-2. Near E_F the $\frac{m^*}{m}$ ratio derived from the

CCM1D rises to well above unity and is similar to the values deduced from single-particle levels in ref. [Coh65]. The exact magnitude at E_F is sensitive to the high-energy extrapolation of

the imaginary potential used in the dispersion calculations [MN81]. The zero-value end point of the CCM1 J_v implied by the

linear energy dependence is ≈ 166 MeV, while that of the CCM1D J_v

is ≈ 200 MeV. The latter value is in good agreement with

equivalent global proton-potential interpretations [Bau+82], giving some support to the CCM1D. It is further noted that

commonly used "global" neutron potentials ([WG86], [Rap+79], [BG69]), not including dispersion effects, have zero values at

≈ 167 MeV, almost exactly the value of the present CCM1. None of them are consistent with the linear representation of the proton potentials over a wide energy range [Bau+82].

Potentials deduced from proton scattering can be compared with the above neutron potentials as the strength of neutron and proton potentials are interrelated through Eq. V-1. It would be nice to re-analyze the proton scattering data accumulated over the past few decades with contemporary models and techniques. Unfortunately, the requisite experimental data has largely vanished into the mists of time, and one must use the various proton potentials published at the time of the measurements. The corresponding interpretations are generally the result of SOM or DWBA analyses, with a few coupled-channels studies. The quality of both the proton data and its interpretation varies by

considerable amounts. By far the largest amount of proton information pertains to scattering from ^{92}Mo , with only sparse results for the other molybdenum isotopes. Furthermore, ^{92}Mo has a closed neutron shell and is a nearly spherical nucleus, thus it can be hoped that the interpretations should be less sensitive to uncertain collective effects. Therefore, the present comparisons are confined to ^{92}Mo .

The literature contains nineteen proton potentials based upon measurements, distributed from ≈ 7 to 61 MeV (see citations of the references). The corresponding J_v are illustrated in Fig. V-A. These are nuclear potential strengths, corrected for the coulomb contribution as appropriate using the conventional expression $V_c = 0.4Z/A^{1/3}$. The lowest-energy values are probably unreliable for the present purposes as they may be distorted by fluctuations, uncertain compound-nucleus and coulomb corrections, and by dispersive effects that increase at lower energies. Therefore, for the present comparisons, only the fourteen proton potentials at energies $\approx > 15$ MeV were used. The real strengths of these are reasonably described by the expression

$$J_v = 447.1 - 2.2418 \cdot E, \quad (\text{V-4})$$

as illustrated by the J_p curve in Fig. V-A. The same figure shows the J_v distributions of the above neutron CCM1 and CCM1D potentials. The J_v of the CCM1 has a sharper energy dependence than that of the proton potential. The energy dependence of Eq. V-4 is close to the global proton-potential values of ref. [Bau+82], while the J_v of the CCM1D has a slope similar to that of the proton potential, with an off-set of about 40 MeV-fm³. The sharper slope of the CCM1 J_v is a reflection of the dispersive effects which are strongly felt at the lower energies that influence the derivation of the neutron potentials. In contrast, the proton potentials were derived from measurements at higher energies where dispersion effects are relatively minor [Bau+82]. The coulomb barrier precludes proton studies at lower energies where dispersive effects are large. One should expect agreement between the CCM1D and proton J_v values, and not be surprised at discrepancies with the CCM1 J_v . If one compares the J_v of the CCM1D and proton potentials over the energy range of $\approx 15 \rightarrow 30$ MeV, the region of reasonable experimental overlap, one obtains the ξ_v of Eq. V-1 equal to 0.557, with essentially no energy dependence. This value is very similar to the $\xi_v = 0.45 \rightarrow 0.55$ indicated by the theory of nucleon-nucleon forces ([GPT68], [GMP70]), and consistent with the value deduced

from the asymmetry dependence of the coupled-channels neutron potentials (discussed above), and with proton behavior [Sat69]. Eq. V-4 and an $\xi_v = 0.557$ imply a $J_v^0 \approx 426.4 - 2.138 \cdot E$. Thus there is also good consistency between the J_v^0 of the proton-based results and those of the present CCM1D potential. Any small differences may well be due to the approximations used in the present determinations of dispersive effects. It should be emphasized that this good agreement is possible only when consideration is given to dispersive contributions. The importance of the dispersive effects in such comparisons is generally not recognized.

It would be nice to compare neutron and proton imaginary potentials in a manner analogous with the above. Unfortunately, the scatter in both neutron and proton imaginary-potential results precludes quantitative comparisons. The situation is further complicated by the uncertain and energy-dependent contribution of volume absorption.

Single-particle states in the molybdenum isotopes are not particularly well known. However, there are systematic trends as given, for example, in refs. [TM69] and [Coh65]. The molybdenum single-particle levels to binding energies of ≈ 10 MeV are $2d_{3/2}$, $1g_{7/2}$, $3s_{1/2}$ and $2d_{5/2}$. These should be related to the potentials deduced from the unbound neutron scattering. If one assumes that the geometries of the real-potentials in the bound region are fixed at the $E = 0$ values and that the bound potential is of the Saxon-Woods form, the binding energies of the above single particle states follow from the CCM1 and CCM1D potentials. Those calculated for the most spherical isotope, ^{92}Mo , with the CCM1D are qualitatively consistent with the systematics of binding-energies, with an average deviation from the systematic values of the above four single-particle levels of ≈ 0.5 MeV. In contrast, the corresponding CCM1 results are wide of the systematics, particularly for the lower binding energies. The dispersion contribution leads to the "Fermi-Surface Anomaly" which sharply reduces the real-potential strength in the first few MeV of the bound region in a manner required to describe the single-particle levels. The difference in the results obtained with the CCM1 and CCM1D are consistent with this behavior.

The asymmetry constant ξ_v of the spherical real potential can also be deduced from a sampling of neutron potentials. Following ref. [Chi+90], comparisons were made at an incident energy of 8 MeV, an energy that is sufficiently high to avoid low-energy structure effects, a region where the potentials are reasonably defined, where there is an abundance of independent potentials based upon experimental neutron information, and an energy that is not unduly perturbed by dispersive effects. The Argonne Group has reported 25 neutron potentials over the past

decade or so, extending from $A = 40 \rightarrow 238$ and asymmetry $\eta = 0 \rightarrow 0.277$, as given in this work and refs. ([Smi94], [SG93], [Smi97], [LGS89], [SS97], [Smi96], [SGL88], [Smi+92A], [LGS86], [Chi+92], [SGL86], [Smi97A], [Chi+90], [Smi95], [LGS87], and [SC96]) These indicate a decrease of r_v with the mass, A , that is expressed in the form

$$r_v = r_0 + r_1/A^{1/3}, \quad (V-5)$$

where r_0 and r_1 are constants. Least-square fitting to the data base gives $r_0 = 1.1673$ and $r_1 = 0.37083$. These values are very similar to those of refs. [Chi+90] and [Mol63], but lead to *somewhat smaller radii than given in some proton studies [Hod70]* and are larger than resulting from the present fitting. Comparisons of r_v are fraught with the Vr_v^2 ambiguity. The difference between Eq. V-5 and the simple $r_v A^{1/3}$ radial mass dependence is too small to be detected over the limited mass range of the molybdenum isotopes. The real-potential strengths are expressed by

$$J_v = K_0 [1 - \xi_v \eta] (r_0 + r_1/A^{1/3})^3, \quad (V-6)$$

where K_0 and ξ_v are constants. Again, least-square fitting the data, one obtains $K_0 = 232.96 \text{ MeV-fm}^3$ and $\xi_v = 0.447$. These values are reasonably consistent with those of ref. [Chi+90], and the ξ_v is similar to that derived above from comparisons of neutron and proton results for ^{92}Mo and with the values deduced from nucleon-nucleon interactions ([GPT68, GMP70]), and (p,n) studies [BFG69]. However, the value of ξ_v is approximately half that obtained from a simple analysis of potentials across a wide mass range ([FCR77], [HW72]). Using the latter method the resulting ξ_v also contains a size effect that approximately doubles the value of the constant. Eq. V-6 contains a size correction.

The β_2 values used in the above interpretations of the experimental neutron data are compromise averages of values deduced from electro-magnetic and proton-scattering studies. The resulting vibrational models give reasonable descriptions of the fragmentary experimental inelastic neutron scattering at higher energies where direct-vibrational reactions dominate. However, the neutron experimental information is far from definitive enough to provided quantitative guidance as to the behavior of

β_2 . Even proton β_2 's are fragmentary and conflicting. ^{92}Mo can be reasonably considered a proton-vibrational nucleus in the sense of the core-polarization model of Madsen, Brown and Anderson [MBA75]. Those authors predict in that case that the β_2^{nn} is somewhat smaller than β_2^{em} , and the β_2^{pp} much smaller. Applied to ^{92}Mo , their model gives the ratios $\beta^{\text{nn}}/\beta^{\text{em}} \approx 0.89$ and $\beta^{\text{pp}}/\beta^{\text{em}} \approx 0.73$. Experimental comparisons should be based upon the deformation length defined as $\delta_2 = \beta_2 \cdot r$, where the common assumption $r \approx r_v$ is used here. The β_2^{em} value given in ref. [Ram+87] is 0.1058, the radius used in its derivation is 1.2 fm, thus $\delta_2^{\text{em}} = 0.127$. The present models give $\delta_2^{\text{nn}} = 0.1018$, or the ratio $\delta^{\text{nn}}/\delta^{\text{em}} = 0.802$, which is $\approx 10\%$ smaller than indicated by Madsen et al. [MBA75]. This is reasonable agreement given the variations in the β^{pp} used in constructing the present averages, and certainly as close as one can determine from comparisons with the fragmentary ^{92}Mo neutron data for the excitation of the yrast 2^+ states. Generally, the δ_2 used in the present vibrational calculations are reasonably consistent with the δ_2 resulting from electro-magnetic and (p,p) and (α,α) scattering considerations ([BH75], [LHB71], [Mat+72] [Bar+72]). It is noted that the present δ_2^{nn} mass distribution displays the same anomaly at ^{98}Mo as the δ_2^{em} , δ_2^{pp} and $\delta_2^{\alpha\alpha}$ mass distributions, and that ^{98}Mo marks the closure of the $2d_{5/2}$ neutron sub-shell. It is also noted that any possible isovector dependence of δ_2 should be absent from considerations of (α,α) scattering yet $\delta_2^{\alpha\alpha}$ does not differ appreciably from δ_2^{em} or δ_2^{pp} suggesting that the isovector contribution to β_2 is small. Further considerations of such matters as isospin dependence of the β_2 are thwarted by the lack of detailed experimental information. For the heavier molybdenum isotopes the neutron shell is no longer closed and both proton and neutron cores contribute to the vibrations. In these cases the $\delta_2^{\text{em}} / \delta_2^{\text{pp}} / \delta_2^{\text{nn}}$ ratio estimates of ref. [MBA75] probably become no more than qualitative upper limits.

The present SOM can be compared with the frequently-used global neutron potentials, for example with that of ref [RKF79]. The latter is based upon spherical closed-shell nuclei and thus can best be compared with the present ^{92}Mo SOM results. The real

potential of ref. [RKF79] is very similar to the present ^{92}Mo SOM. The a_v agree to within $\approx 3.5\%$, and the r_v to within $\approx 2.5\%$. This is good agreement, particularly in view of the well known Vr_v^n ambiguity. Ref. [RKF79] suggests that there is a small mass dependence of r_v going from mass 40 to 208. Not surprisingly, this is not evident in the present work as all the molybdenum targets have approximately the same mass. The J_v are remarkably similar, differing only by $\approx 1.3\%$ at zero energy, and by $\approx 3\%$ at 25 MeV, both with a linear energy dependence. The present SOM isovector results reflect the rapidly increasing collective nature of the heavier molybdenum isotopes which is not consistent with the SOM. Generally, it is encouraging to note that the real global potential of ref. [RKF79] is consistent with the present ^{92}Mo SOM results. Some of the same data were used in both interpretations but the present data base was much larger, extended over a much wider energy range, and the interpretation used entirely different model calculations and fitting procedures. One would like to make similar comparisons between the present ^{92}Mo imaginary potential and that of the global model of ref. [RKF79]. Unfortunately, there are questions dealing with the imaginary potential of ref. [RKF79], the two branches of the reported potential are not continuous near 15 MeV.

VI. A GENERAL MOLYBDENUM POTENTIAL FOR APPLIED AND OTHER PURPOSES

The above models are descriptive of isotopic and elemental processes and illuminate various physical aspects of the neutron interaction with the isotopes of molybdenum. However, they may be awkward in applied use and in the extrapolation of the processes to experimentally unobserved isotopes. Therefore, a "regional" molybdenum neutron potential is proposed, based upon the above even-isotope potentials. It was assumed that the reactions could be approximated with a first-order vibrational model (e.g., the CC1). With this approximation the prominent direct processes are reasonably calculable while the model retains practical simplicity.

An inspection of molybdenum quadrupole deformation parameters leads to the approximation $\beta_2 = 1.275 \cdot \eta$ as derived from a least-square fit to β_2^{em} and β_2^{pp} values and the constraint that $\beta_2 = 0$ at $\eta = 0$. This isospin dependence is reasonably consistent with the above $\beta_2^{\text{ave.}}$ values. Then, averaging the above CC1 potential values and making small adjustments to improve the description of the neutron total cross sections, the "regional" molybdenum parameter set of Table VI-A was obtained. The real portion of this potential is "Lane consistent" and quite

well defined. The imaginary part is less certain, but it too is "Lane consistent" and the trends are qualitatively correct. The imaginary potential has magnitudes and energy behavior that depends upon the asymmetry, η . This is not surprising as the structure, and even the nature of the collective behavior, sharply depends on η and is primarily represented by the imaginary potential. This "regional" potential is strictly applicable to the energy range $E \approx 0 \rightarrow 30$ MeV, the range of the present considerations, and only to the molybdenum isotopes.

The above "regional" potential gives a good description of what is experimentally known of the neutron σ_t of the even molybdenum isotopes, as illustrated in Fig. VI-A. The σ_t 's of elemental molybdenum are far better known than those of the isotopes. It too is well described by the "regional" potential. In making the latter comparison the σ_t of each of the naturally occurring isotopes was calculated and then combined, weighting with the natural abundance. The "regional" potential provides descriptions of the neutron elastic scattering for the prominent even isotopes which approach that obtained with the CCM1 parameters, as illustrated in Figs. VI-B \rightarrow E. The "regional" potential description of the elemental elastic scattering is not quite as good, as illustrated in Fig. VI-F. As the energy increases above ≈ 5 MeV the calculated elemental elastic distributions tend to fall below the experimental values in the minima. This is not surprising as $\approx 25\%$ of the element consists of the odd isotopes. These, and ^{100}Mo , have low-lying excited states contributing to inelastic scattering which were not resolved from the elastic component in the experimental measurements as the energy increased. This unresolved inelastic contribution tends to fill in the minima of the observed "elastic" scattering angular distributions. The magnitude of the experimental perturbation is difficult to estimate. Further, it is difficult to calculate the elastic scattering from the two odd isotopes due to structure uncertainties. In the present work the simple approximation of an "equivalent" even isotope was used. This results in ^{95}Mo and ^{97}Mo models that are similar to that of ^{96}Mo with the appropriate mass change. With this concept the yrast 2^+ strength of ^{96}Mo is distributed over $1/2^+ \rightarrow 9/2^+$ levels [NDS] of the odd isotope. Such low-lying levels are present in both ^{95}Mo and ^{97}Mo , but there are also additional low-lying levels. Thus the modeling of the odd isotopes is not very quantitative, and this may contribute to some deterioration of the results of the elemental elastic-scattering calculations.

The "regional" potential can be used to calculate the even-isotope inelastic-scattering cross sections with results very similar to those shown in Section IV-5. It can also be used to calculate elemental inelastic-scattering cross sections.

However, making detailed comparisons with the comparable experimental values is difficult. In the seven naturally occurring molybdenum isotopes there are more than one hundred levels that potentially contribute to inelastic scattering up to excitations of ≈ 2 MeV. A number of the spins and parities are not well known and it is very difficult to make a correlation between experimental results and the contributing excited structure given the variations in energy scales and resolutions of the particular experimental sets. However, some reasonable comparisons are possible at excitations of $\approx 0.7 \rightarrow 1.0$ MeV, primarily corresponding to excitation of the yrast 2^+ levels in the even isotopes. These are also the excitations that explicitly contributed to the elemental inelastic-scattering results of the present measurements. Using the "regional" potential, the isotopic components were calculated and combined to obtain the elemental excitation cross sections. The calculated values were then compared with the available experimental information with the results shown in Fig. VI-G. The calculations did fairly well. In particular, the description of the higher-energy inelastic scattering of the present work is good. This is a limited test. However, combined with the successful description of elemental neutron σ_t and elastic-scattering cross sections, it tends to support the use of the "regional" potential to provide unmeasured elemental inelastic-scattering information. S_0 and S_1 strength functions calculated with the "regional" molybdenum potential are very similar to those obtained with the CCM1, and in qualitative agreement with the results of resonance measurements.

VII. RECOMMENDATIONS

The present interpretations are limited by the available experimental information. To substantively improve the calculational capability and physical understanding some careful measurements are required.

i) Quality neutron σ_t cross sections of the prominent naturally-occurring isotopes of molybdenum should be available up to at least 30 MeV. There is no technological obstacle to such measurements.

ii) There are limited molybdenum elastic-scattering results available for some of the isotopes at 11, 20 and 26 MeV; all from a single institution. What is needed is a detailed set of high-quality, isotopic elastic-scattering results from $\approx 5 - 30$ MeV, and even above. Such measurements are difficult but technically feasible.

iii) Excepting a very few values (essentially confined to ^{92}Mo), there are no isotopic neutron inelastic-scattering results above

≈ 4 MeV. There should be a detailed set of measured inelastic-scattering cross sections for each of the prominent even isotopes from threshold to $>\approx 10$ MeV. Only with such information can a better definition of β_2^{nn} be obtained. Again, such measurements are difficult but technically feasible.

iv) Over the years there have been a number of isotopic (p,p) and (p,n) studies. Unfortunately, the explicit experimental results have largely been lost. Therefore, it is difficult to correlate neutron and proton processes. Some good-quality differential (p,p), (p,p'), (p,n) and (α,α) measurements extending from the coulomb barrier to at least 30 MeV are recommended.

The following fifth recommendation is more general:-

v) Mechanisms should be established for the archival storage of nucleon scattering data. At present it is only so for neutron data. With the current situation, charged-particle experimental results reported in a qualitative manner in journals fade with time and are soon lost for future quantitative study. This unfortunate situation extends to a wide range of nuclear reactions and the relevant particles.

Unless significant portions of the above recommendations are addressed, there is little hope that the understanding of the neutron interaction with molybdenum can be significantly improved. Furthermore, it is noted that some of the above recommendations imply the availability of suitable isotopic molybdenum measurement samples. Current isotope availability is uncertain.

VIII. SUMMARY COMMENT

The present measurements provided a detailed knowledge of neutron scattering from elemental molybdenum over the energy range of $4 \rightarrow 10$ MeV where no information was previously available. A comprehensive elemental and isotopic molybdenum data base was assembled from the present work, from previous work at this laboratory, and from the literature, up to incident energies of ≈ 30 MeV. This data base was interpreted in detail using spherical-optical-statistical and coupled-channels models with and without dispersion effects. The resulting spherical models were consistent with global and regional models previously reported in the literature, and displayed the previously noted inconsistency of the imaginary potential with "Lane" isospin concepts. The coupled-channels models, including the quadrupole vibrational coupling of the ground and yrast 2^+ states, removed this inconsistency in a straight-forward manner and had isovector terms that are in agreement with those deduced from nucleon-nucleon forces. However, there remain questions regarding the form of the isovector potential (volume, surface,

etc.) and as to perturbations due to shell closures. The coupled-channels calculations used β_2^{nn} values somewhat less than β_2^{em} but larger than β_2^{pp} , in qualitative agreement with the core-polarization model. That model is less applicable to the heavier even molybdenum isotopes. While the coupled-channels models reasonably describe elastic-scattering, inelastic-scattering and σ_t of elemental and even-isotopic molybdenum, the inelastic neutron scattering data is not sufficient in either quantity or quality at higher energies, where direct reactions are dominate to critically asses the magnitudes of the β_i^{nn} . One model included second-order quadrupole effects coupling yrast one-phonon 2^+ and two-phonon $0^+-2^+-4^+$ levels to the ground state. Alternatively, yrast 2^+ quadrupole and 3^- octupole levels were coupled to the ground state. Both of the latter alternatives gave good descriptions of the measured data with predictable effects. However, the experimental data is not sufficient to quantitatively test either of the latter two options. Dispersive models were considered in both spherical and coupled-channels contexts. The results are particularly important at the lower energies of the neutron measurements. It is shown that comparisons with proton potentials should be made with the dispersive models as the proton potentials are generally at higher energies where dispersive components are small, while the majority of the neutron data has significant dispersive contributions. With this approach, comparisons of proton and neutron potentials lead to isovector components consistent with those obtained from other aspects of this study and the literature. The dispersion effect is probably one source of the long standing dichotomy between potentials deduced from low- and high-energy neutron data and between neutron and proton data. Generally the energy dependence of the dispersive spherical and coupled-channels real potentials is consistent with estimates of the local-equivalent Hartree-Fock potential and leads to reduced masses consistent with those derived from the dynamic theory of vibrations and from considerations of the systematics of bound single particle-states. Results of this study were combined to obtain a simple "regional" vibrational model that should be useful for calculating the neutron interaction with molybdenum and its isotopes for both basic and applied purposes. Experimental and administrative recommendations are suggested that are necessary for improving the understanding of the neutron interaction with molybdenum and its isotopes. One of these recommendations is of a far more general nature.

ACKNOWLEDGMENTS

The author is very much indebted to The National Nuclear Data Center (Brookhaven National Laboratory) for the provision of extensive experimental data files, and to Dr. J. Raynal for extensive guidance in the use of the code ECIS96.

REFERENCES

References with the subscript "e" were used in formulating the elastic-scattering data base, with "t" the σ_t data base, and with "p" the proton-scattering data base.

- [AT65] Auerbach N. and Talmi I., Nucl. Phys. 64 (1965) 458.
[Bai+78] Bainum D., Finlay R., Rapaport J., Hadizadeh M. and Carlson J., Nucl. Phys. A311 (1978) 492.
[Bar+72] Barrette J. et al., Phys. Rev. C1 (1972) 1339.
[Bau+82] Bauer M., Hernandez-Saldana E., Hodgson P. E. and Quintanilla J., J. Phys. G8 (1982) 525.
[BDS79] Brown G., Dehesa J. and Speth J., Nucl. Phys. A330 (1979) 290.
[Bet56] Bethe H., Phys. Rev. 103 (1956) 1353.
[BFG69] Batty C., Friedman E. and Greenlees G., Nucl. Phys. A127 (1969) 368.
[BG69] Becchetti F. Jr. and Greenlees G., Phys. Rev. 182 (1969) 1190.
[BGG63] Brown G., Gunn J. and Gould P., Nucl. Phys. 46 (1963) 598.
[BH75]_p Burger S. and Heymann G., Nucl. Phys. A243 (1975) 461.
[BLM54] Brueckner K., Levinson C. and Mahmoud H., Phys. Rev. 95 (1954) 217.
[BPS58]_t Bratenahl A., Peterson J. and Stoering J., Phys. Rev. 110 (1958) 927.
[Bru56] Brueckner K., Phys. Rev. 103 (1956) 1121.
[BWW97] Birn I., Wattecamps E. and Weigmann H., Proc. Conf. on Nucl. Data, Trieste (1997).
[Cal+60]_t McCallum G. et al., Nucl. Phys. 16 (1960) 313.
[Cao+99]_e Cao Jianhua et al., IAEA Report, INDC(CRP)-011/GT (1998).
[CC72]_e Cox S. and Cox E., Argonne National Laboratory Report, ANL-7935 (1972).
[Cer+82]_p Cereda E., Pignanelli M., Micheletti S., von Geramb H., Harakeh M., De Leo R., D'Erasmus G. and Pantakeo A., Phys. Rev. C26 (1982) 1941.
[CGB52]_t Coon J., Graves E. and Barschall H., Phys. Rev. 88 (1952) 562.
[Cha+79] Chapman R., Hyland M., Durrell J., Mo J., MacPhail M., Sharma H. and Merrill N., Nucl. Phys. A316 (1979) 40.

- [Chi+90] Chiba S., Guenther P., Lawson R. and Smith A., Phys. Rev. C42 (1990) 2487.
- [Chi+92] Chiba S., Guenther P., Smith A., Sugimoto M. and Lawson R., Phys. Rev. C45 (1992) 1260.
- [CL55] Cranberg L. and Levin J., Proc. Conf. on Peaceful Uses of Atomic Energy, Geneva 1958 (United Nations Press, New York, 1955).
- [Coh65] Cohen B., Am. J. Phys. 33 (1965) 1011.
- [Com78] Comfort J., Phys. Rev. Lett. 42 (1978) 30.
- [CP70]_{et} Coles R. and Porter D., Aldermaston Report, AWRE-0-89/70 (1970).
- [CSL83] Nuclear Standards File, IAEA Tech. Report 227, eds. Conde H., Smith A. and Lorenz A. (1983)
- [Dec+61]_t Decnninck et al., Phys. Rev. 22 (1961) 652.
- [Div68]_t Divadeenam T., Thesis, DA/B 28 (1968) 3834.
- [Dro87] Drog M., IAEA Report, IAEA-TECDOC-410 (1987).
- [FCR77]_e Ferrer J., Carlson J. and Rapaport J., Nucl. Phys. A275 (1977) 325.
- [Fes58] Feshbach H., Ann. Rev. Nucl. Sci. 8 (1958) 49.
- [FG71]_t Foster D. and Glasgow D., Phys. Rev. C3 (1971) 576.
- [FN63]_t Filippov V. and Nikolaev M., Atom. Energy 15 (1963) 493.
- [GC65] Gilbert A. and Cameron A., Can. J. Phys. 43 (1965) 1446.
- [GG71] Gneuss G. and Greiner W., Nucl. Phys. A171 (1971) 449.
- [GH92] Gruppelaar H. and Hogenbirk A. Proc. Specialist's Mtg. of Fission Product Nuclear Data, Tokai (NEA Press, Paris, 1992).
- [GK85] Gruppelaar H. and van der Kamp H. A. J., Proc. Specialist's Mtg. on Uses of the Optical Model for Calculation of Neut. Cross Sections below 20 MeV, Paris (NEA Press, Paris 1986).
- [Gla+69]_p Glashausser C. et al., Phys. Rev. 184 (1968) 1217.
- [GMP70] Greenlees W., Makifske W. and Pyle G., Phys. Rev. C1 (1970) 1145.
- [Goo52]_t Goodman L., Phys. Rev. 88 (1958) 686.
- [GPT68] Greenlees W., Pyle G. and Tang Y., Phys. Rev. 171 (1968) 1115.
- [GS58] Green A. and Sood P., Phys. Rev. 111 (1958) 1147.
- [HF52] Hauser W. and Feshbach H., Phys. Rev. 87 (1952) 362.
- [HL50]_t Hildebrand R. and Leith C., Phys. Rev. 80 (1950) 842.
- [Hod70]_t Hodgson P. E., Nucl. Phys. A150 (1970) 1.
- [Hod71] Hodgson P. E., Nuclear reactions and nuclear structure (Clarendon, Oxford, 1971).
- [Hod94] Hodgson P. E., The nucleon optical model (World Scientific, Singapore, 1994).
- [HW72] Holmqvist T. and Wiedling T., Nucl. Phys. A188 (1972) 24.

- [Jai+65]_t Jain A. et al., Phys. Rev. 137 (1965) 83.
- [JGK79] Johnson C., Galonsky A. and Kernell R., Phys. Rev. C20 (1979) 2052.
- [JLM77] Jeukenne J., Lejeune A. and Mahaux C., Phys. Rev. C16 (1977) 80.
- [Ken62]_t Kent D., Phys. Rev. 125 (1962) 331.
- [KR80]_p Kulkarni V. and Rapaport J., Can. J. Phys. 58 (1980) 146.
- [KWK98] Kawano T., Watanabe Y. and Kawai M., J. Nucl. Sci. Tech. (Japan), 35 (1998) 519.
- [Lam+73]_{et} Lambropoulos P., Smith A., Guenther P. and Whalen J., Nucl. Phys. A201 (1973) 1.
- [Lan+59] Lane A., Lynn J., Melkonian E. and Rae E., Phys. Rev. Lett. 2 (1959) 424.
- [Lan62] Lane A., Nucl. Phys. 25 (1962) 676; also Phys. Rev. Lett. 8 (1962) 171.
- [Lan+66]_t Langsford A. et al., Harwell Report, AERE-PR/NP 9 (1966) 36.
- [Law80] Lawson, R. D., The theory of the nuclear shell model (Clarendon, Oxford, 1980).
- [LBC69] Lutz H., Bartolini W. and Curtis T., Phys. Rev. 178 (1969) 1911.
- [LGS86] Lawson R., Guenther P. and Smith A., Phys. Rev. C34 (1986) 1599.
- [LGS87] Lawson R., Guenther P. and Smith A., Phys. Rev. C36 (1987) 1298.
- [LGS89] Lawson R., Guenther P. and Smith A., Nucl. Phys. A493 (1989) 267.
- [LHB71]_p Lutz H., Heikinen D. and Bartolini W., Phys. Rev. C4 (1971) 934.
- [LHH80]_t Larson D., Harvey J. and Hill N., Proc. Brookhaven Conf. on Data Evaluation (1980) 277.
- [Lip66] Lipperheide R., Nucl. Phys. 89 (1966) 97.
- [Mat+72] Matsuda K., Awaya Y., Nakanishi N. and Takeda S., J. Phys. Soc. Jap. 33 (1972) 298.
- [MBA75] Madsen V., Brown V. and Anderson J., Phys. Rev. C12 (1975) 1205.
- [McD+77]_e McDaniel F., Brandenburger J., Glasgow G. and Leighton H., Phys. Rev. C10 (1974) 1087.
- [McD+77]_e McDaniel F., Brandenburger J., Glasgow G., McEllistrem M. and Weil J., Univ. of Kenn. Report, A-KTY-77, 34 (1977).
- [MDH81] Mughabghab S., Divadeenam M. and Holden N. Neutron cross sections (Academic, New York, 1981).
- [MFC81]_p Moyer R., Finlay R. and Crawlet G., Nucl. Phys. A352 (1981) 221.
- [Mil52]_t Miller D., Phys. Rev. 88 (1952) 83.
- [MN81] Mahaux C. and Ngo H., Phys. Lett. 100B (1981) 285.

- [Mol63] Moldauer P., Nucl. Phys. 47 (1963) 65.
- [Mol80] Moldauer P., Nucl. Phys. A344 (1980) 185.
- [Mol82] Moldauer P., Spherical Optical-Statistical Model Code ABAREX, private communication (1982); extensively modified by R. Lawson and A. Smith and documented in the Argonne National Laboratory Report ANL/NDM-145 (1998); modifications for elemental use by S. Chiba.
- [NDS] Baglin C., Nucl. Data Sheets 66 (1992) 347; Muller H., Nucl. Data Sheets 44 (1985) 277; Burrows T., Nucl. Data Sheets 68 (1993) 635; Peker L., Nucl. Data Sheets 68 (1993) 165; Artna-Cohen A., Nucl. Data Sheets 70 (1993) 85; Singh B., Nucl. Data Sheets 67 (1992) 693; Singh B. and Szucs J., Nucl. Data Sheets 60 (1990) 1.
- [ND54]_t Nereson N. and Darden S., Phys. Rev. 94 (1954) 1678.
- [New+56]_t Newson H. et al., Phys. Rev. 102 (1956) 1580.
- [Pas67] Passatore G., Nucl. Phys. A95 (1967) 694.
- [Pas+80]_t Pasechnik M. et al., Proc. Kiev Conf. 1 (1980) 304.
- [PB62] Perey F. and Buck B., Nucl. Phys. 32 (1962) 353.
- [PBS60]_t Peterson J., Bratenahl A. and Stoering J., Phys. Rev. 120 (1960) 521.
- [Pop+85]_t Popov A. et al., Proc. of Conf. on Nucl. Data for Basic and Applied Purposes, eds. P. Young et al., 1 (1985) 313.
- [PP76]_p Perey C. and Perey F., At. Data and Nucl. Data Tables 17 (1976) 1.
- [PW80]_t Poenitz W. and Whalen J., Argonne National Laboratory Report, ANL/NDM-80 (1983).
- [Ram+87] Raman S., Malarkey C., Millet W., Nestor C. Jr. and Stelson P., At. Data and Nucl. Data Tables 36 (1987) 1.
- [Rap+79]_e Rapaport J., Cheena T., Bainum D., Finlay R. and Carlson J., Nucl. Phys. A313 (1979) 1.
- [Ray96] Raynal J., The coupled-channels code ECIS96, private communication (1996); see also CEA Report, CEA-N-2772 (1994).
- [RKF79] Rapaport J., Kulkarni V. and Finlay R., Nucl. Phys. A330 (1979) 15.
- [Rob+66] Robinson R. et al., Phys. Rev. 146 (1966) 816.
- [Sat69] Satchler G., Isospin in nuclear physics, ed. Wilkinson D. (North-Holland, Amsterdam, 1969).
- [Sat83] Satchler G., Direct nuclear reactions (Clarendon. Oxford, 1983).
- [SC96] Smith A. and Chiba S., Ann. Nucl. En. 23 (1996) 459.
- [Sch+75]_p Schulte K. et al., Nucl. Phys. A241 (1975) 272.
- [SE71]_p Sinha B. and Edwards V., Phys. Lett. 35B (1971) 391.
- [Set65]_t Seth K., Phys. Lett. 16 (1965) 306.
- [SG84]_e Smith A. and Guenther P., Nucl. Phys. A415 (1984) 1.
- [SG93] Smith A. and Guenther P., J. Phys. G19 (1993) 655.

- [SGL86] Smith A., Guenther P. and Lawson R., Nucl. Phys. A455 (1986) 344.
- [SGL88] Smith A., Guenther P. and Lawson R., Nucl. Phys. A483 (1988) 50.
- [SGW75]_{et} Smith A., Guenther P. and Whalen J., Nucl. Phys. A244 (1975) 213.
- [SGW84] Smith A., Guenther P. and Whalen J., Nucl. Phys. A415 (1984) 1.
- [SH67]_e Smith A. and Hayes R., Nucl. Phys. A93 (1967) 609.
- [Sin+72]_p Sinha B. et al., Nucl. Phys. A183 (1972) 401.
- [Smi91] Smith A., Argonne National Laboratory memorandum, (1991), unpublished.
- [Smi+92] Smith A. and Guenther P., Argonne National Laboratory Report ANL/NDM-127 (1992); Chiba S., Guenther P., Smith A., Sugimoto M. and Lawson R., Phys. Rev. C45 (1992) 1260; Budtz-Jorgensen C., Guenther P., Smith A. and Whalen J., Z. Phys. A306 (1982) 265; Smith A., Guenther P., Larsen R., Nelson C., Walker P. and Whalen J., Nucl. Instr. and Methods 50 (1977) 277; and references cited therein.
- [Smi+92A] Smith A., Guenther P., Whalen J. and Chiba S., J. Phys. G18 (1992) 629.
- [Smi94] Smith A., Nucl. Phys. A576 (1994) 165.
- [Smi95] Smith A., Nucl. Phys. A589 (1995) 201.
- [Smi96] Smith A., Nucl. Phys. A605 (1996) 269.
- [Smi97] Smith A., J. Phys. G24 (1997) 637.
- [Smi97A] Smith A., Nucl. Phys. A620 (1997) 249.
- [SPB77]_p deSwinarski R., Pham Dinh-Lien and Bagieu G., Can. J. Phys. 55 (1977) 43.
- [SS97] Smith A. and Schmidt D., J. Phys. G23 (1997) 197.
- [Str+61]_e Strizhak V. et al., ZET 41 (1961) 313.
- [Stu51]_t Stubbins W., Phys. Rev. 84 (1951) 902.
- [Swi+76]_p deSwinarski R. et al., Phys. Lett. 61B (1976) 37.
- [Tam65] Tamura T., Rev. Mod. Phys. 37 (1965) 679.
- [TE73]_p Tait W. and Edwards V., Nucl. Phys. A203 (1973) 193.
- [TM69] Takeuchi K. and Moldauer P., Phys. Lett. 28B (1969) 384.
- [Tut+77]_t Tutubal A. et al., Proc. Kiev Conf. 2 (1977) 65.
- [TY76]_e Tanaka W. and Yamanouti Y., Proc. Lowell Conf. on Neut. Physics (1976) 1328.
- [VMP60]_t Vincent L., Morgan I. and Prudhomme, Texas Nucl. Report, WADD-TR-60-215 (1960).
- [VSM64] Vonach W., Smith A. and Moldauer P., Phys. Lett. 11 (1964) 331.
- [WG86] Walter R. and Guss P., Proc. Conf. on Nucl. Data for Basic and Applied Sci., eds. Young P. et al., vol. 2, p. 277 (Gordon and Breach, New York, 1986),
- [WJ58]_t Weil J. and Jones K., Phys. Rev. 110 (1958) 466.

- [Wol51] Wolfenstein L., Phys. Rev. 82 (1951) 690.
[WWG60] Wyatt P., Wills J. and Green A., Phys. Rev. 119 (1960)
1031.

Table IV-2-A. SOM Parameters. Energies, E, in MeV.

Real-potential Diffuseness in fms.

Mo-elemental	0.6464±0.0126
⁹² Mo	0.6386±0.0174
⁹⁴ Mo	(0.6260±0.0176)*
⁹⁶ Mo	0.6347±0.0154
⁹⁸ Mo	0.6504±0.0145
¹⁰⁰ Mo	0.6526±0.0171
	Weighted Average = 0.6448±0.0067

Real-potential Radius in fms.

Mo-elemental	1.2247±0.0146
⁹² Mo	1.2286±0.0083
⁹⁴ Mo	(1.2387±0.0206)*
⁹⁶ Mo	1.2135±0.0082
⁹⁸ Mo	1.1943±0.0064
¹⁰⁰ Mo	1.2244±0.0155
	Weighted Average = 1.2111±0.0039

Imaginary-potential Radius in fms.

Mo-elemental	1.4193(±0.0324)-0.0161(±0.0054)·E
⁹² Mo	1.3068(±0.0152)-0.0099(±0.0017)·E
⁹⁴ Mo	(1.2735(±0.0637))*
⁹⁶ Mo	1.2555(±0.0187)-0.0062(±0.0021)·E
⁹⁸ Mo	1.2388(±0.0245)-0.0066(±0.0026)·E
¹⁰⁰ Mo	1.2243(±0.0259)-0.0046(±0.0027)·E

Imaginary-potential Diffuseness in fms.

Mo-elemental	0.4484(±0.0404)+0.0316(±0.0072)·E
⁹² Mo	0.2900(±0.0307)+0.0246(±0.0039)·E
⁹⁴ Mo	(0.5599(±0.0297))*
⁹⁶ Mo	0.4910(±0.0379)+0.0127(±0.0039)·E
⁹⁸ Mo	0.4676(±0.0292)+0.0160(±0.0028)·E
¹⁰⁰ Mo	0.5183(±0.0189)+0.0098(±0.0018)·E

Table IV-2-A. Continued--

Real-potential Strength, J_v , in $\text{MeV}\cdot\text{fm}^3$.

Mo-elemental	$419.8(\pm 1.915) - 1.9483(\pm 0.2799) \cdot E$
^{92}Mo	$437.4(\pm 1.240) - 2.3610(\pm 0.2799) \cdot E$
^{94}Mo	$(439.1(\pm 4.759) - 5.5500(\pm 0.9333) \cdot E)^*$
^{96}Mo	$429.2(\pm 1.330) - 2.6005(\pm 0.1475) \cdot E$
^{98}Mo	$428.2(\pm 1.128) - 2.5368(\pm 0.2096) \cdot E$
^{100}Mo	$425.6(\pm 1.132) - 2.8207(\pm 0.1160) \cdot E$

Imaginary-potential Strength, J_w , in $\text{MeV}\cdot\text{fm}^3$.

Mo-elemental	$46.95(\pm 2.419) + 0.947(\pm 0.341) \cdot E$
^{92}Mo	$46.54(\pm 3.766) + 2.377(\pm 0.396) \cdot E$
^{94}Mo	$(50.71(\pm 5.807) + 2.996(\pm 1.457) \cdot E)^*$
^{96}Mo	$54.87(\pm 4.328) + 1.977(\pm 0.461) \cdot E$
^{98}Mo	$55.70(\pm 3.559) + 1.997(\pm 0.353) \cdot E$
^{100}Mo	$70.07(\pm 1.694) + 1.201(\pm 0.152) \cdot E$

Spin-orbit Potential [WG85]

$$V_{\text{so}} = 5.767 - 0.015 \cdot E + 2 \cdot [(N-Z/A]$$

$$r_{\text{so}} = 1.103$$

$$a_{\text{so}} = 0.560$$

* ^{94}Mo values for any of the parameters are given for completeness. They were not used for determining systematic trends due to deficiencies in the experimental data base.

Table IV-2-B. Comparisons of measured [MDH81] and calculated (SOM) strength functions in units of 10^{-4} .

Isotope	S_0 -exp.	S_0 -cal.	S_1 -exp.	S_1 -cal.
^{92}Mo	0.5 ± 0.2	.4684	4.7 ± 1.5	5.842
$^{94}\text{Mo}^*$	0.53 ± 0.20	.5719	4.6 ± 2.0	7.775
^{96}Mo	0.43 ± 0.14	.6411	8.7 ± 2.8	6.793
^{98}Mo	0.54 ± 0.12	.6710	3.6 ± 0.6	7.455
^{100}Mo	0.73 ± 0.17	.8452	4.4 ± 0.9	6.751

* As noted in Table IV-2-A.

Table IV-3-A. SOM Parameters using the volume-absorption potential of ref. [Rap+79]. The energy, E, is in MeV.

Wt. Ave. $a_v = 0.6346 (\pm 0.0057)$ fm

Wt. Ave. $r_v = 1.2107 (\pm 0.0014)$ fm

Isotopic r_w values in fms

$${}^{92}\text{Mo}, = 1.3320 (\pm 0.0301) - 0.0093 (\pm 0.0043) \cdot E$$

$${}^{96}\text{Mo}, = 1.2596 (\pm 0.0167) - 0.0079 (\pm 0.0019) \cdot E$$

$${}^{98}\text{Mo}, = 1.2140 (\pm 0.0275) - 0.0054 (\pm 0.0029) \cdot E$$

$${}^{100}\text{Mo}, = 1.2424 (\pm 0.0344) - 0.0053 (\pm 0.0034) \cdot E$$

Isotopic a_w values in fms

$${}^{92}\text{Mo}, = 0.3043 (\pm 0.0260) + 0.0218 (\pm 0.0027) \cdot E$$

$${}^{96}\text{Mo}, = 0.5250 (\pm 0.0217) + 0.0125 (\pm 0.0023) \cdot E$$

$${}^{98}\text{Mo}, = 0.4705 (\pm 0.0329) + 0.0156 (\pm 0.0031) \cdot E$$

$${}^{100}\text{Mo}, = 0.5257 (\pm 0.0225) + 0.0102 (\pm 0.0024) \cdot E$$

Isotopic J_v values in Mev-fm³

$${}^{92}\text{Mo}, = 439.5 (\pm 0.9) - 2.6141 (\pm 0.1015) \cdot E$$

$${}^{96}\text{Mo}, = 426.5 (\pm 2.2) - 2.5615 (\pm 0.0974) \cdot E$$

$${}^{98}\text{Mo}, = 431.6 (\pm 1.0) - 2.8209 (\pm 0.0964) \cdot E$$

$${}^{100}\text{Mo}, = 423.7 (\pm 1.2) - 2.6895 (\pm 0.1210) \cdot E$$

Isotopic J_w values in MeV-fm³

$${}^{92}\text{Mo}, = 47.1 (\pm 5.1) + 2.6096 (\pm 0.5238) \cdot E$$

$${}^{96}\text{Mo}, = 56.9 (\pm 4.1) + 1.7120 (\pm 0.0974) \cdot E$$

$${}^{98}\text{Mo}, = 58.1 (\pm 3.9) + 1.7324 (\pm 0.3538) \cdot E$$

$${}^{100}\text{Mo}, = 68.6 (\pm 3.2) + 1.3621 (\pm 0.3184) \cdot E$$

Spin-orbit Potential is identical to that of Table IV-2-A.

Table IV-4-A. DOM Parameters. Energies, E, and Fermi Energies are in MeV.

Fermi Energies

^{92}Mo ,	-10.370
^{94}Mo ,	-8.424
^{95}Mo ,	-8.261
^{96}Mo ,	-7.988
^{97}Mo ,	-7.732
^{98}Mo ,	-7.284
^{100}Mo ,	-6.845

Weighted average = -8.121

Real-potential Diffuseness in fms.

Mo elemental,	0.6522(\pm 0.0125)
	[0.6879(\pm 0.0153)]*
^{92}Mo ,	0.6429(\pm 0.0129)
^{96}Mo ,	0.6433(\pm 0.0178)
^{98}Mo ,	0.6394(\pm 0.0076)
^{100}Mo ,	0.6445(\pm 0.0283)

Average = 0.6445(\pm 0.0021)

Real-potential Radius in fms.

Mo elemental,	1.1816(\pm 0.0118)
	[1.1955(\pm 0.0132)]*
^{92}Mo ,	1.1727(\pm 0.0077)
^{96}Mo ,	1.1768(\pm 0.0092)
^{98}Mo ,	1.1744(\pm 0.0076)
^{100}Mo ,	1.1873(\pm 0.0062)

Average = 1.1786(\pm 0.0026)

Table IV-4-A. Continued--

Imaginary-potential Radius in fms.

Mo elemental,	1.3894(±0.0293) - 0.01235(±0.00499) · E
	[1.3741(±0.0303) - 0.00630(±0.00481) · E] *
⁹² Mo,	1.2695(±0.0169) - 0.00859(±0.00109) · E
⁹⁶ Mo,	1.1894(±0.0171) - 0.00084(±0.00253) · E
⁹⁸ Mo,	1.2009(±0.0225) - 0.00552(±0.00249) · E
¹⁰⁰ Mo,	1.2409(±0.0432) - 0.00659(±0.00383) · E

Imaginary-potential Diffuseness in fms.

Mo elemental,	0.4658(±0.0275) + 0.0293(±0.0046) · E
	[0.4360(±0.0159) + 0.0225(±0.0026) · E] *
⁹² Mo,	0.3387(±0.0253) + 0.0248(±0.0021) · E
⁹⁶ Mo,	0.5299(±0.0271) + 0.0122(±0.0029) · E
⁹⁸ Mo,	0.5061(±0.0386) + 0.0192(±0.0038) · E
¹⁰⁰ Mo,	0.5141(±0.0292) + 0.0138(±0.0038) · E

Real-potential Strength, J_v , in MeV-fm³.

Mo elemental,	397.2(±1.65) - 1.8443(±0.3077) · E
	[404.7(±1.64) - 2.0268(±0.2424) · E] *
⁹² Mo,	401.7(±1.70) - 2.0856(±0.1949) · E
⁹⁶ Mo,	395.9(±1.80) - 2.0418(±0.2064) · E
⁹⁸ Mo,	398.6(±1.13) - 2.2693(±0.1269) · E
¹⁰⁰ Mo,	398.6(±2.23) - 2.0937(±0.2926) · E

Table IV-4-A. Continued--

Imaginary-potential strength, J_w , in $\text{MeV}\cdot\text{fm}^3$.

Mo elemental,	$48.4(\pm 3.4) + 0.7227(\pm 0.4353)\cdot E$
	$[59.9(\pm 3.8) + 0.0019(\pm 0.5312)\cdot E]^*$
^{92}Mo ,	$51.1(\pm 3.6) + 1.9816(\pm 0.3535)\cdot E$
^{96}Mo ,	$51.2(\pm 3.9) + 2.2691(\pm 0.4163)\cdot E$
^{98}Mo ,	$58.7(\pm 3.5) + 1.5886(\pm 0.2969)\cdot E$
^{100}Mo ,	$68.9(\pm 2.4) + 1.1510(\pm 0.2348)\cdot E$

Spin-orbit Potential identical to that of Table IV-2-A [WG85].

* The values in square brackets result from the inclusion of isovector real and imaginary strengths in the elemental calculations, as discussed in the text. These values were not used in calculating averages.

Table IV-5-A. CCM1 Model Parameters. Energies, E, in MeV.

Isotope	β_2^{em} [Ram+87]	β_2^{ave} (used in CCM1 cal.)
92	0.1058	0.0836
96	0.1720	0.1673
98	0.1684	0.1756
100	0.2309	0.2173

Real-potential Diffuseness in fms.

Weighted Ave. 0.6339±0.0107

Real-potential Radius in fms.

Weighted Ave. 1.2160±0.0044

Imaginary-potential Radius in fms.

^{92}Mo	1.3027(±0.0184) - 0.0106(±0.0019) · E
^{96}Mo	1.4173(±0.0318) - 0.0172(±0.0032) · E
^{98}Mo	1.4506(±0.0365) - 0.0186(±0.0037) · E
^{100}Mo	1.4695(±0.0254) - 0.0187(±0.0027) · E

Imaginary-potential Diffuseness in fms.

^{92}Mo	0.3122(±0.0333) + 0.0252(±0.0030) · E
^{96}Mo	0.3906(±0.0475) + 0.0252(±0.0046) · E
^{98}Mo	0.2783(±0.0439) + 0.0313(±0.0044) · E
^{100}Mo	0.3327(±0.0658) + 0.0261(±0.0058) · E

Real-potential Strength, J_v , in MeV-fm³.

^{92}Mo	443.3(±1.503) - 2.6555(±0.1641) · E
^{96}Mo	430.8(±0.875) - 2.5437(±0.0948) · E
^{98}Mo	430.4(±0.842) - 2.5589(±0.0916) · E
^{100}Mo	423.6(±1.309) - 2.5094(±0.1462) · E

Table IV-5-A. Continued--

Imaginary-potential Strength, J_w , in $\text{MeV}\cdot\text{fm}^3$.

^{92}Mo	$49.0(\pm 5.8) + 2.1523(\pm 0.5101) \cdot E$
^{96}Mo	$43.6(\pm 3.8) + 2.0028(\pm 0.3482) \cdot E$
^{98}Mo	$43.3(\pm 1.2) + 2.0529(\pm 0.3531) \cdot E$
^{100}Mo	$45.2(\pm 1.1) + 1.7274(\pm 0.3530) \cdot E$

Spin-orbit Potential is identical to that of Table IV-2-A [WG85].

Table IV-5-B. Strength functions calculated with the CCMI in units of 10^{-4} .

Isotope	S_0 -cal.	S_1 -cal.
^{92}Mo	0.529	6.656
^{96}Mo	0.465	6.265
^{98}Mo	0.358	5.365
^{100}Mo	0.521	4.274

Table IV-6-A. CCM1D Model Parameters. Energies, E, are in MeV.
Spin-orbit potential as per Table-IV-A.

Real-potential Diffuseness in fms.

Weighted Ave. 0.6281±0.0085

Real-potential Radius in fms.

Weighted Ave. 1.1840±0.0054

Imaginary-potential Radius in fms.

⁹² Mo	1.2641(±0.0131)-0.0104(±0.0015)·E
⁹⁶ Mo	1.3158(±0.0158)-0.0126(±0.0014)·E
⁹⁸ Mo	1.3194(±0.0384)-0.0124(±0.0035)·E
¹⁰⁰ Mo	1.4052(±0.0271)-0.0159(±0.0025)·E

Imaginary-potential Diffuseness in fms.

⁹² Mo	0.3243(±0.0414)+0.0286(±0.0035)·E
⁹⁶ Mo	0.3985(±0.0271)+0.0271(±0.0029)·E
⁹⁸ Mo	0.3457(±0.0531)+0.0303(±0.0047)·E
¹⁰⁰ Mo	0.3715(±0.0578)+0.0265(±0.0061)·E

Real-potential Strength, J_v , in MeV-fm³.

⁹² Mo	406.3(±1.1)-2.0161(±0.1058)·E
⁹⁶ Mo	400.8(±1.6)-2.1501(±0.1679)·E
⁹⁸ Mo	403.9(±1.0)-2.2784(±0.1052)·E
¹⁰⁰ Mo	395.1(±1.0)-2.1221(±0.1098)·E

Imaginary-potential Strength, J_w , in MeV-fm³.

⁹² Mo	45.9(±4.1)+2.0543(±0.3672)·E
⁹⁶ Mo	43.9(±3.7)+1.9042(±0.3352)·E
⁹⁸ Mo	38.3(±4.0)+2.1722(±0.3427)·E
¹⁰⁰ Mo	42.9(±3.9)+1.7946(±0.3579)·E

Table IV-7-A. Parameters for the first-order vibrational model
 with contributions from the 3^- level (CCM13). Energies, E,
 are in MeV. Spin-orbit potential of Table IV-2-A.

Real-potential Diffuseness in fms.

Weighted Ave. 0.6351(\pm 0.0064)

Real-potential Radius in fms.

Weighted Ave. 1.2179(\pm 0.0102)

Imaginary-potential Radius in fms.

^{92}Mo	1.3222(\pm 0.0290) - 0.0108(\pm 0.0025) · E
^{96}Mo	1.3250(\pm 0.0203) - 0.0116(\pm 0.0018) · E
^{98}Mo	1.3605(\pm 0.0425) - 0.0136(\pm 0.0035) · E
^{100}Mo	1.4132(\pm 0.0375) - 0.0150(\pm 0.0033) · E

Imaginary-potential Diffuseness in fms.

^{92}Mo	0.3363(\pm 0.0317) + 0.0223(\pm 0.0027) · E
^{96}Mo	0.4940(\pm 0.0335) + 0.0182(\pm 0.0030) · E
^{98}Mo	0.4674(\pm 0.0526) + 0.0217(\pm 0.0217) · E
^{100}Mo	0.3864(\pm 0.0577) + 0.0223(\pm 0.0051) · E

Real-potential strength, J_v , in MeV-fms³.

^{92}Mo	444.1(\pm 1.2) - 2.6024(\pm 0.1290) · E
^{96}Mo	432.9(\pm 1.1) - 2.5053(\pm 0.1113) · E
^{98}Mo	429.2(\pm 1.0) - 2.4026(\pm 0.1089) · E
^{100}Mo	424.9(\pm 1.0) - 2.4771(\pm 0.1124) · E

Imaginary-potential strength, J_w , in MeV-fm³.

^{92}Mo	40.2(\pm 3.7) + 2.2701(\pm 0.3264) · E
^{96}Mo	35.3(\pm 3.5) + 2.1816(\pm 0.3201) · E
^{98}Mo	31.6(\pm 4.0) + 2.2707(\pm 0.3407) · E
^{100}Mo	38.7(\pm 3.4) + 1.7535(\pm 0.3133) · E

Table IV-8-A. Excitations and deformations assumed for the CCM12 model.

Isotope	Level excitations in MeV	β_2
^{92}Mo	1.509 (2^+)	0.0836
	2.283 (4^+)	
	2.520 (0^+)	
	3.091 (2^+)	
^{96}Mo	0.778 (2^+)	0.1673
	1.147 (0^+)	
	1.498 (2^+)	
	1.870 (4^+)	
^{98}Mo	0.787 (2^+)	0.1756
	1.432 (2^+)	
	1.510 (4^+)	
	1.963 (0^+)	
^{100}Mo	0.536 (2^+)	0.2173
	1.136 (4^+)	
	1.464 (2^+)	
	1.504 (0^+)	

Table IV-8-B. CCM12 parameters derived by fitting with the one- and two-phonon model. Energies, E, are given in MeV.

Real-potential Diffuseness in fms.

Weighted Ave. 0.6282(\pm 0.0115)

Real-potential Radius in fms.

Weighted Ave. 1.2280(\pm 0.0063)

Imaginary-potential Radius in fms.

^{92}Mo	1.2710(\pm 0.0154) - 0.0084(\pm 0.0016) · E
^{96}Mo	1.2766(\pm 0.0277) - 0.0092(\pm 0.0026) · E
^{98}Mo	1.3296(\pm 0.0545) - 0.0126(\pm 0.0042) · E
^{100}Mo	1.3724(\pm 0.0425) - 0.0136(\pm 0.0036) · E

Imaginary-potential Diffuseness in fms.

^{92}Mo	0.3622(\pm 0.0388) + 0.0198(\pm 0.0033) · E
^{96}Mo	0.4775(\pm 0.0344) + 0.0151(\pm 0.0030) · E
^{98}Mo	0.4388(\pm 0.0561) + 0.0212(\pm 0.0050) · E
^{100}Mo	0.3937(\pm 0.0374) + 0.0199(\pm 0.0033) · E

Real-potential Strength, J_v , in MeV-fm³.

^{92}Mo	449.1(\pm 0.9) - 2.8030(\pm 0.0884) · E
^{96}Mo	439.3(\pm 1.1) - 2.7611(\pm 0.1206) · E
^{98}Mo	439.6(\pm 1.0) - 2.8173(\pm 0.1114) · E
^{100}Mo	434.4(\pm 1.1) - 2.8658(\pm 0.1154) · E

Imaginary-potential Strength, J_w , in MeV-fm³.

^{92}Mo	41.5(\pm 5.3) + 2.4751(\pm 0.4544) · E
^{96}Mo	43.1(\pm 4.0) + 2.0758(\pm 0.3666) · E
^{98}Mo	41.2(\pm 4.9) + 2.1451(\pm 0.3994) · E
^{100}Mo	46.6(\pm 3.9) + 1.7398(\pm 0.2949) · E

Spin-orbit Potential is identical to that of Table IV-2-A [WG85].

Table V-A. Real-potential Strengths of Eq. V-1. Strengths, J_V , are expressed as volume-integrals-per-nucleon in units of $\text{MeV}\cdot\text{fm}^3$, and energies, E , are given in MeV.

Potential	J_V^O	ξ_V
SOM	450.7-1.8800·E	+0.3517+0.0148·E
DOM	403.9-1.9886·E	+0.0989+0.0035·E
CCM1	465.0-2.8029·E	+0.5500-0.0007·E
CCM1D	417.4-1.8514·E	+0.2932+0.0075·E
CCM13	446.6-2.7784·E	+0.5631-0.0015·E
CCM12	465.1-2.7155·E	+0.4070-0.0047·E

Table V-B. Imaginary-potential Strengths of Eq. V-1. The notation is analogous to that of Table V-A.

Potential	J_W^O	ξ_W
SOM	20.25+3.67·E	-9.76+0.508·E
DOM	25.60+2.77·E	-7.35+0.343·E
CCM1	53.20+2.60·E	+1.20+0.015·E
CCM1D	51.30+2.24·E	+1.27-0.008·E
CCM13	39.87+2.33·E	+0.80+0.001·E
CCM12	36.60+3.26·E	+0.66+0.024·E

Table VI-A. Parameters of the "regional" molybdenum vibrational model. Energies, E , are in MeV, dimensions in fms, and strengths, J_i , in volume-integrals-per-nucleon ($\text{MeV}\cdot\text{fm}^3$).

Real Potential

Diffuseness $a_v = 0.6339$

Radius $r_v = 1.2160$

Strength $J_v = J_v^0 (1 - \xi_v \eta)$

where $J_v^0 = 465.0 - 2.8029 \cdot E$

and $\xi_v = 0.5503$

Imaginary Potential

Diffuseness $a_w = (-0.2107 + 6.317 \cdot \eta) + (0.04271 - 0.2429 \cdot \eta) \cdot E$

Radius $r_w = (+1.114 + 2.3063 \cdot \eta) - (0.00155 + 0.1147 \cdot \eta) \cdot E$

Strength $J_w = J_w^0 (1 - \xi_w \eta)$

where $J_w^0 = 53.2 + 2.60 \cdot E$

and $\xi_w = 1.198 + 0.015 \cdot E$

Spin-Orbit Potential

Diffuseness $a_{so} = 0.560$

Radius $r_{so} = 1.103$

Potential $v_{so} = 5.767 - 0.015 \cdot E + 2 \cdot \eta$ (MeV)

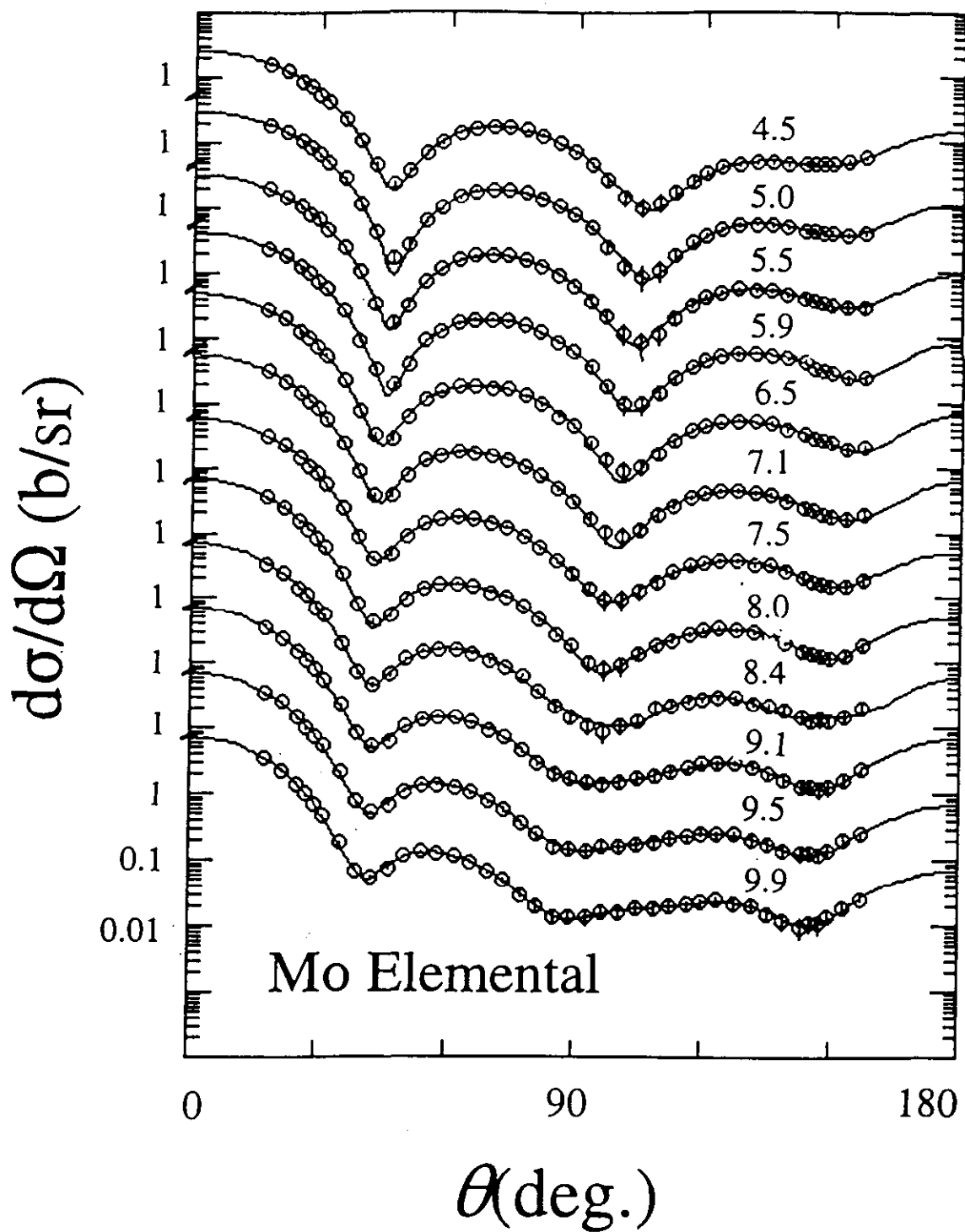


Fig. III-A. The present elemental molybdenum elastic-scattering results. The measured values are indicated by symbols, while curves illustrate the results of least-square fitting the experimental results with legendre-polynomial expansions. Approximate incident-neutron energies are numerically indicated. The figure (as are all figures in this paper) is presented in the laboratory coordinate system.

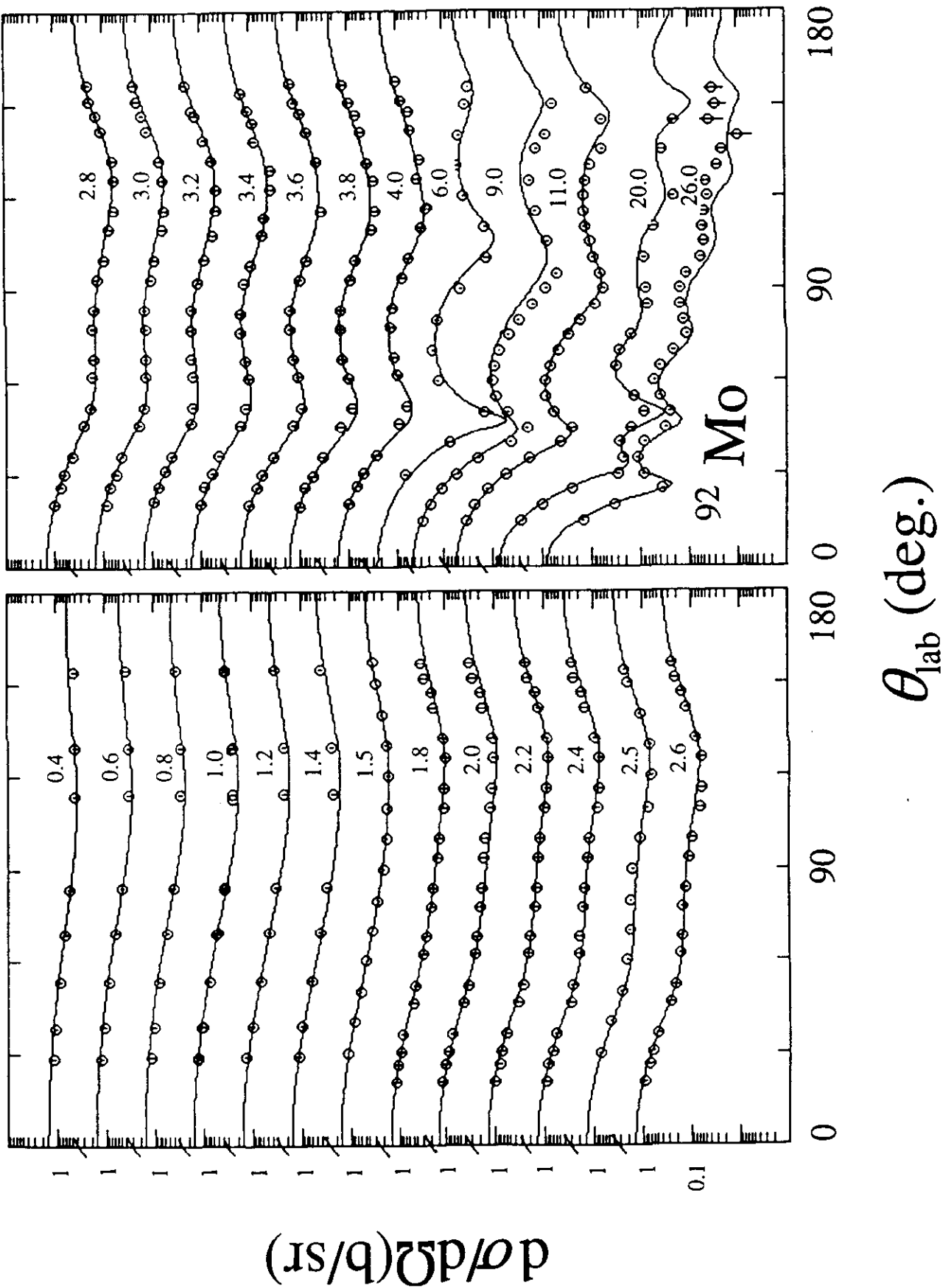


Fig. IV-1-A. Comparison of measured and calculated differential elastic-scattering cross sections of ^{92}Mo . Symbols indicate the experimental values and curves the results of SOM calculations using the potential described in the text. Incident neutron energies are numerically noted in MeV.

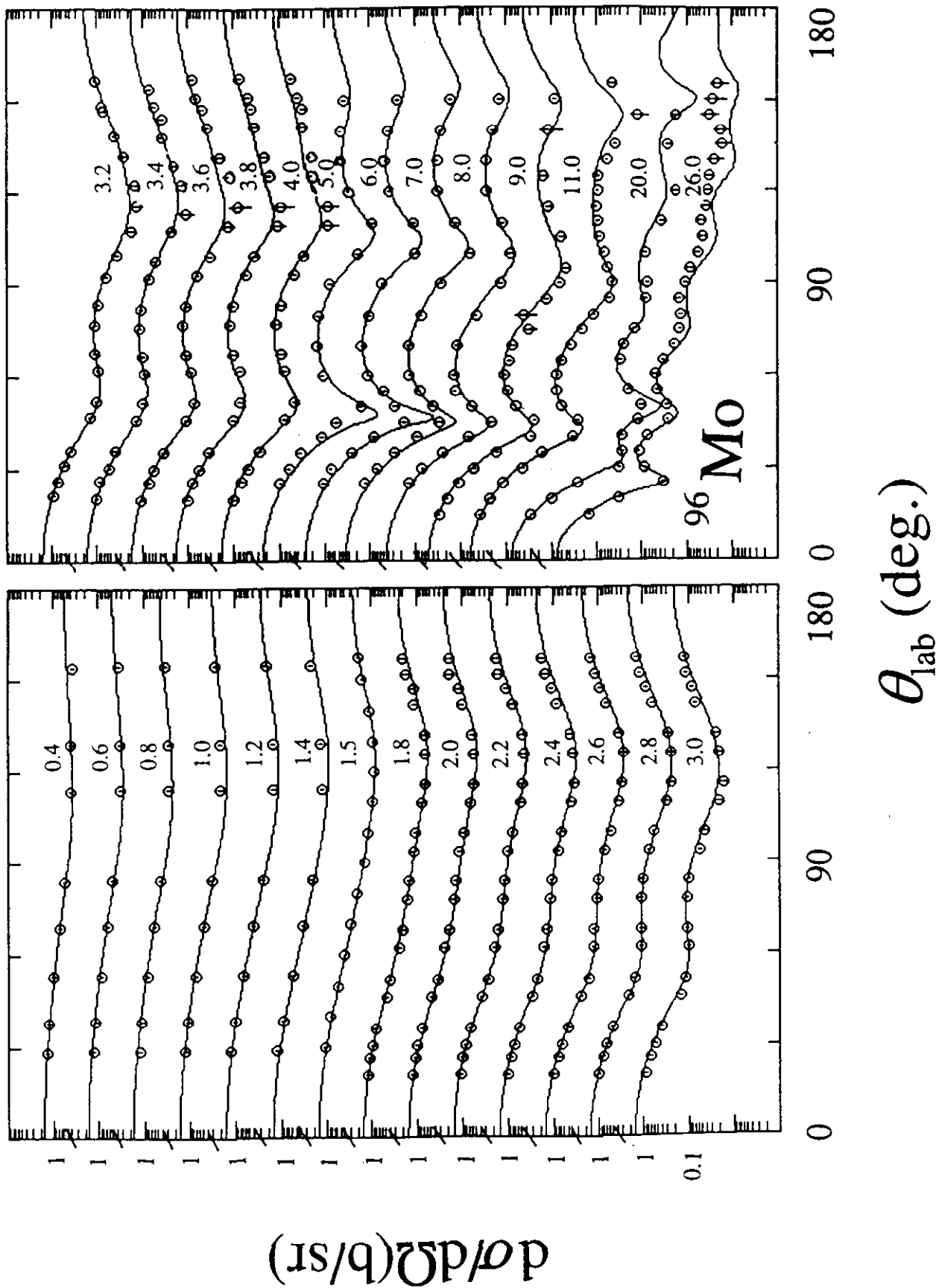
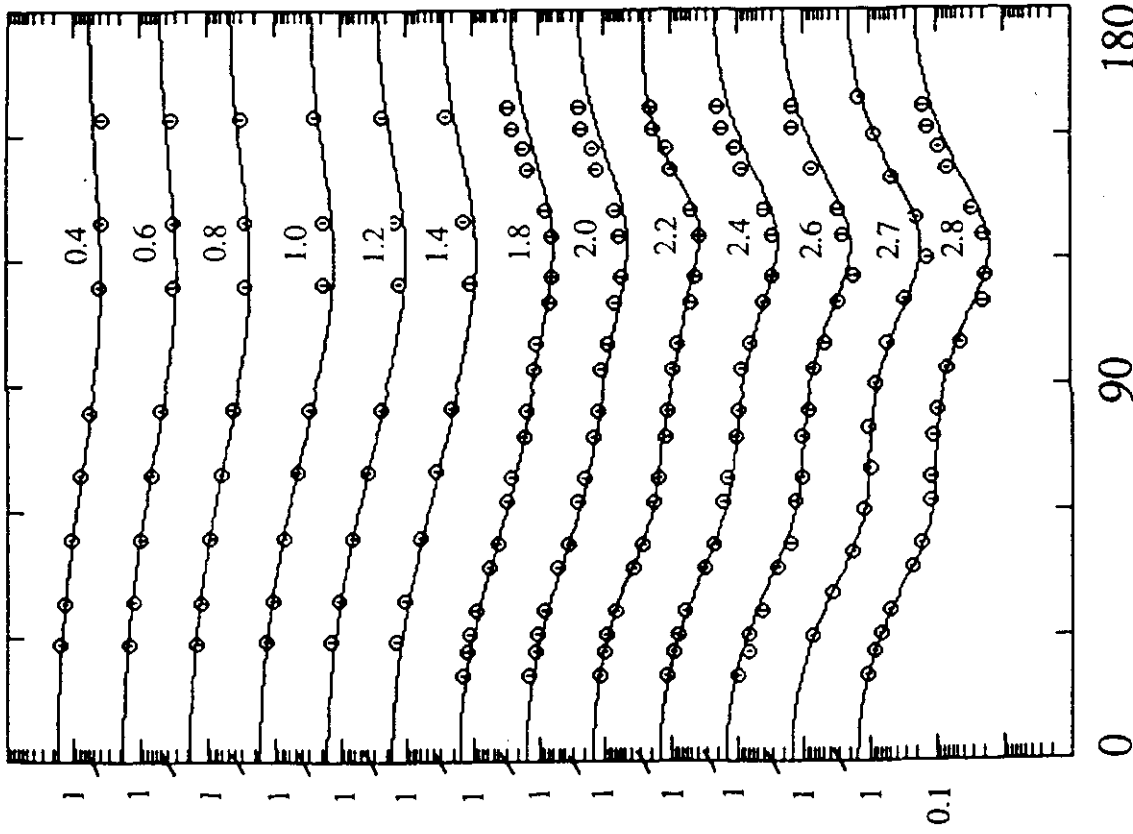
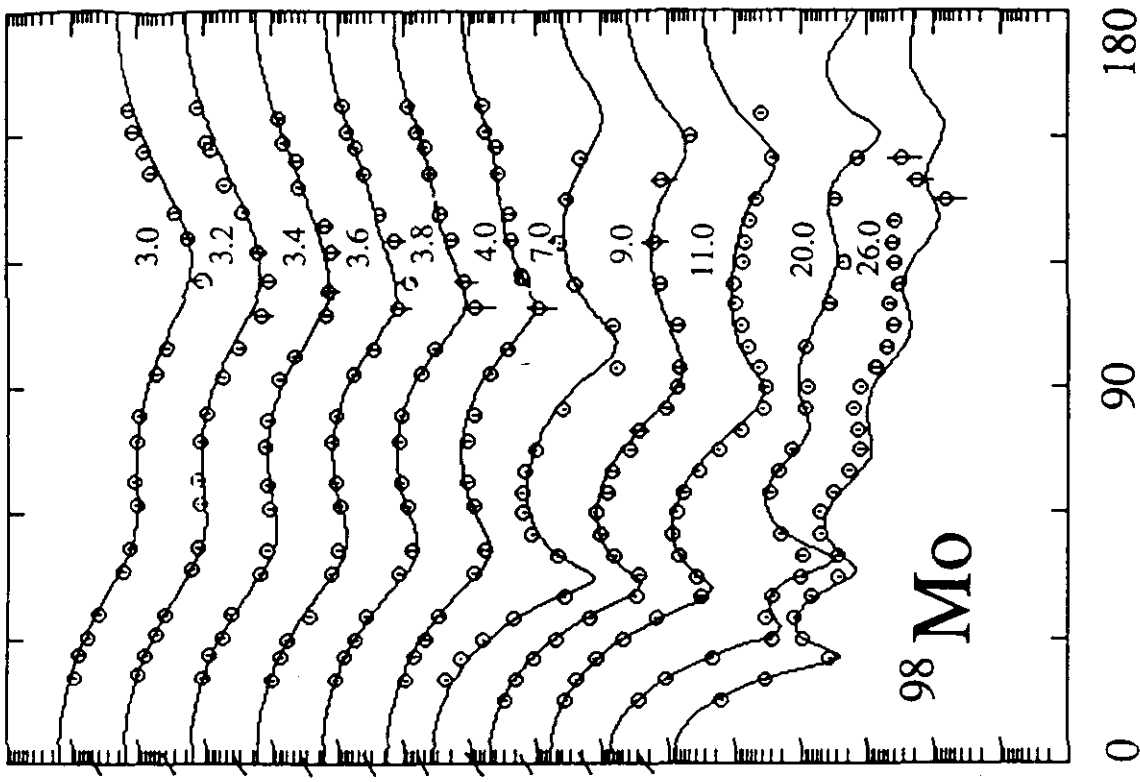
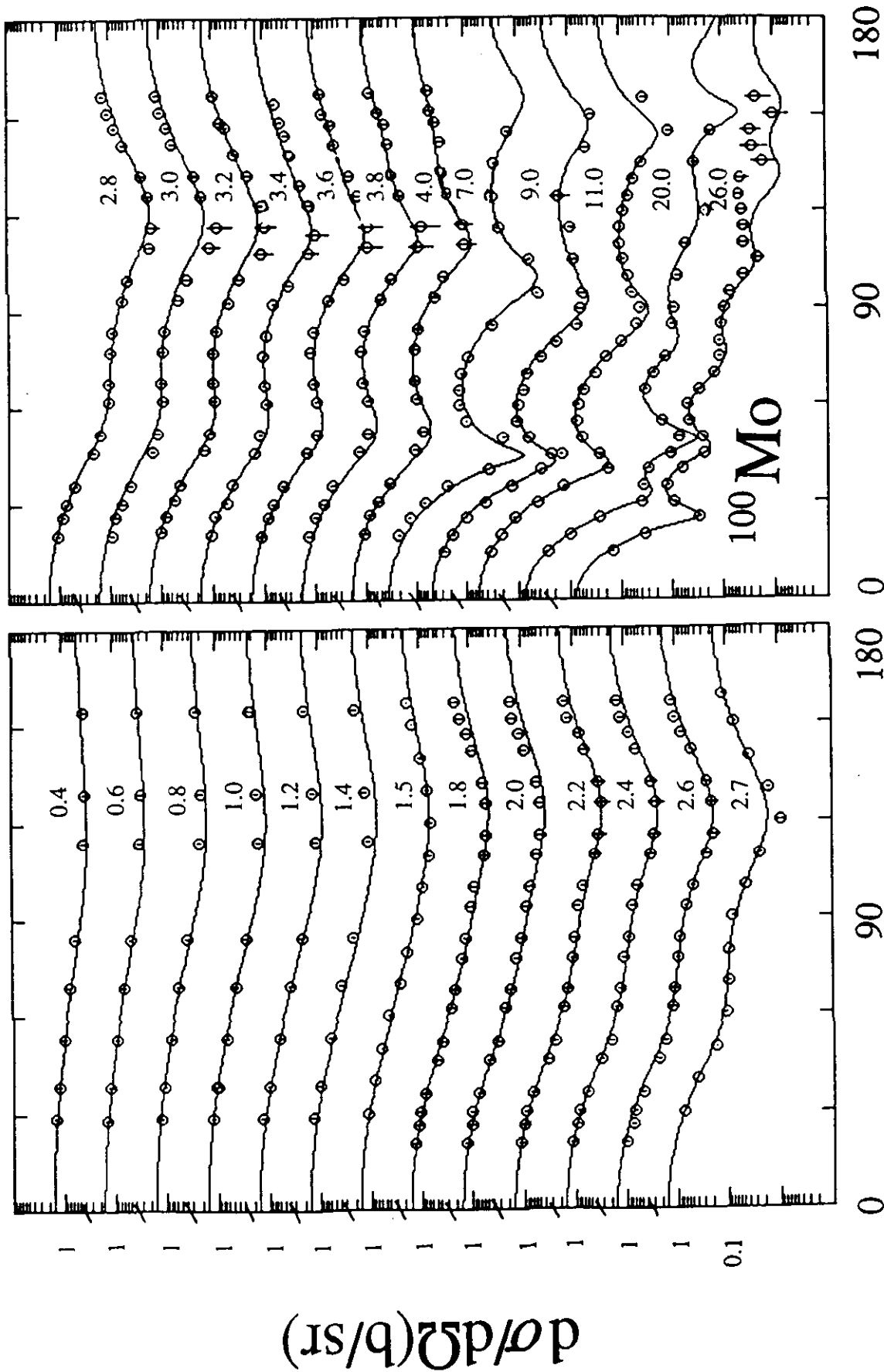


Fig. IV-1-B. Comparison of measured and calculated differential elastic-scattering cross sections of ^{96}Mo . The notation is identical to that of Fig. IV-1-A.



θ_{lab} (deg.)

Fig. IV-1-C. Comparison of measured and calculated differential elastic-scattering cross sections of ^{98}Mo . The notation is identical to that of Fig. IV-1-A.



θ_{lab} (deg.)

Fig. IV-1-D. Comparison of measured and calculated differential elastic-scattering cross sections of ^{100}Mo . The notation is identical to that of Fig. IV-1-A.

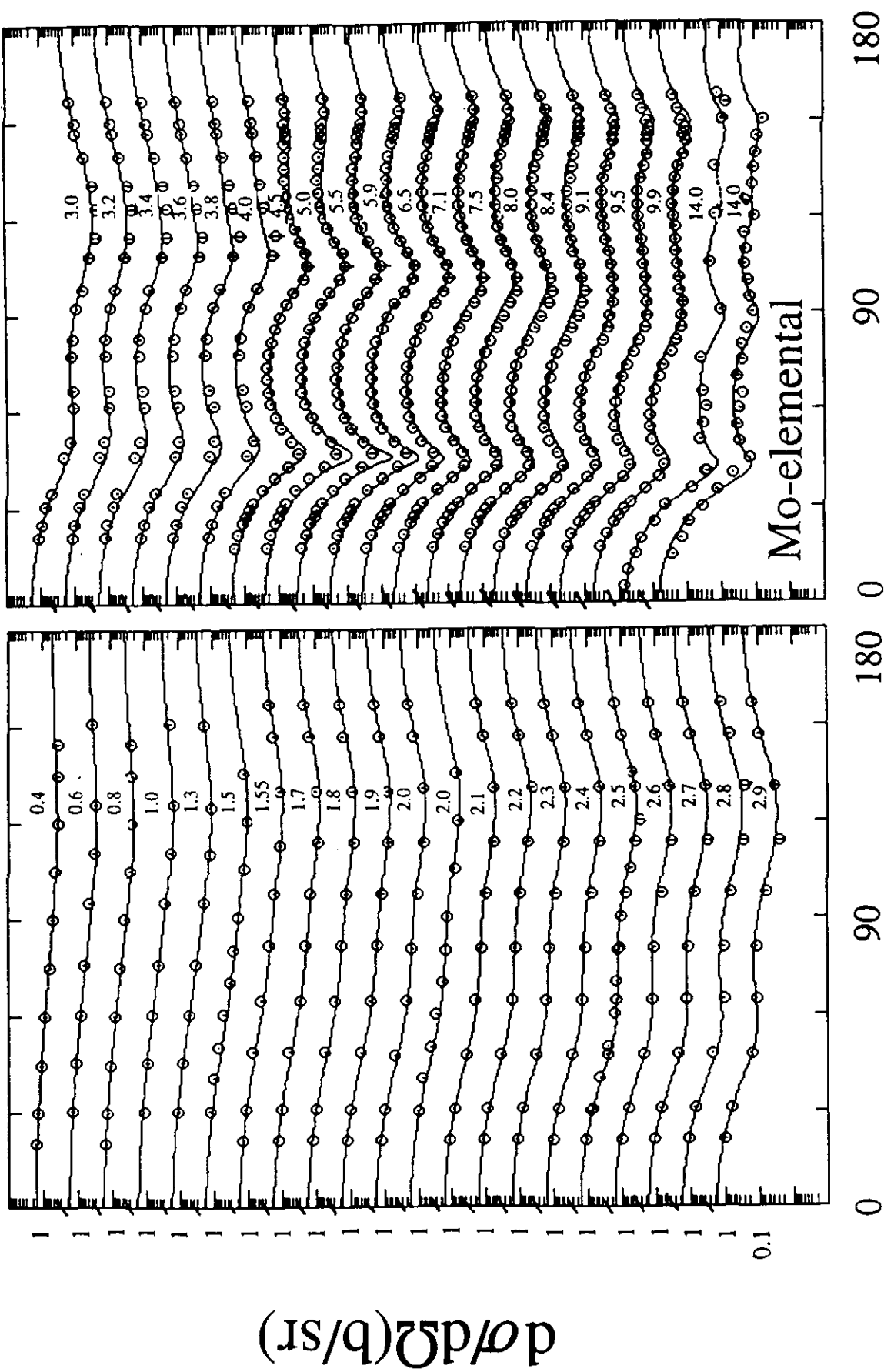


Fig. IV-1-E. Comparison of measured and calculated differential elastic-scattering cross sections of elemental Mo. The notation is identical to that of Fig. IV-1-A.

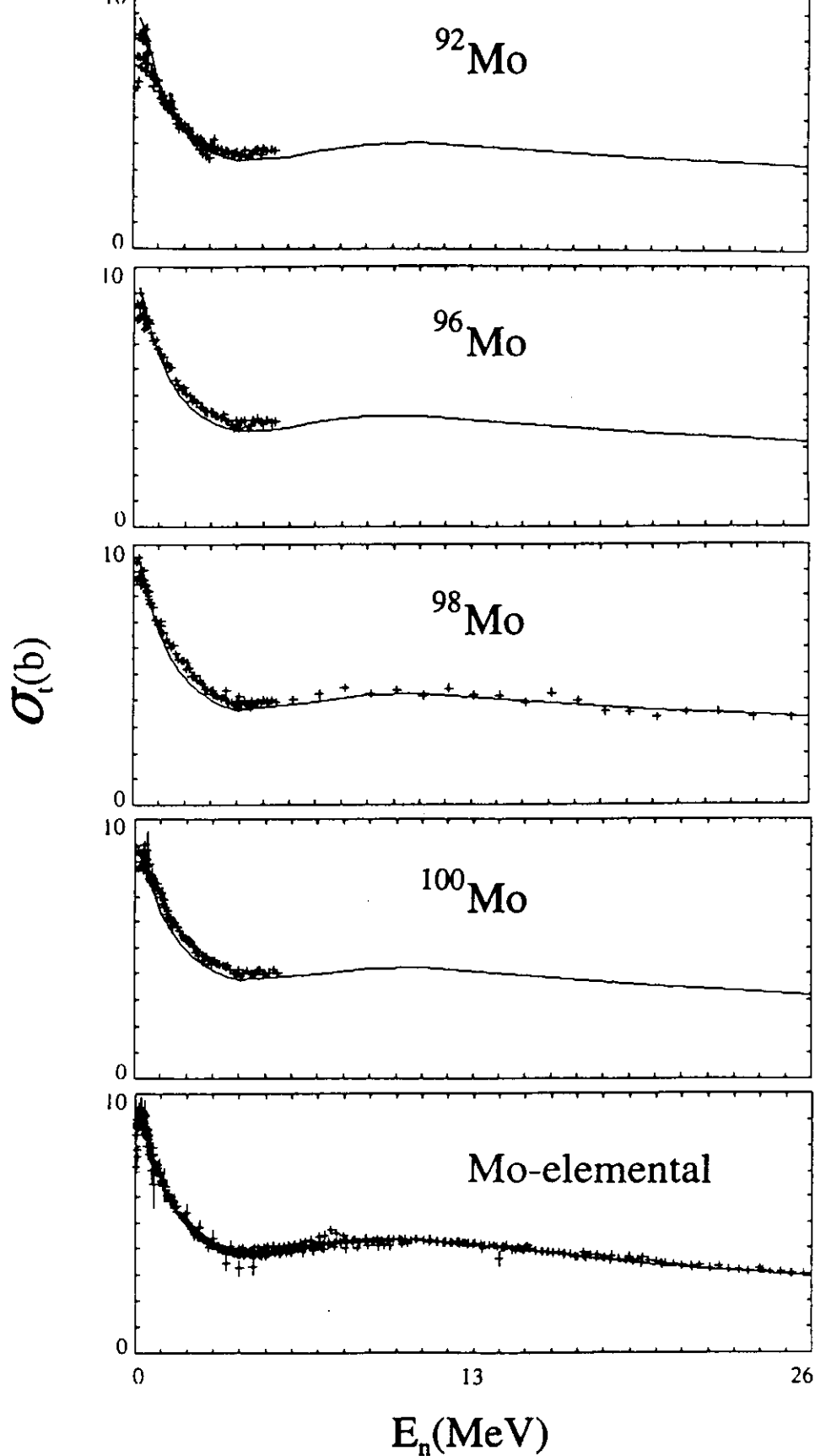


Fig. IV-1-F. Comparisons of measured and calculated neutron σ_t 's of ^{92}Mo , ^{96}Mo , ^{98}Mo , ^{100}Mo and elemental molybdenum. Symbols indicate energy averages of experimental values and curves the results of SOM calculations.

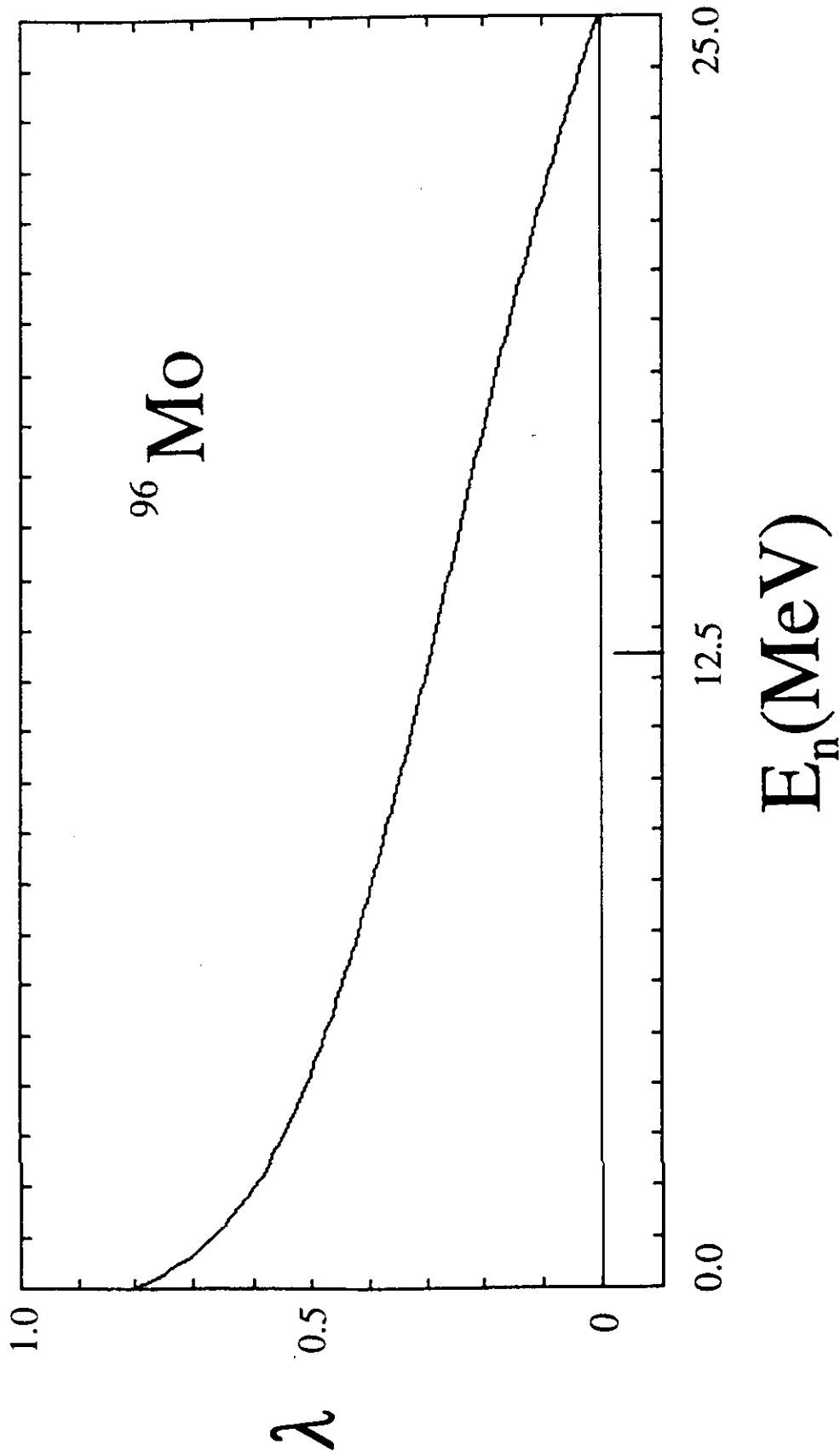


Fig. IV-4-A. The fraction, λ , of the surface-absorption potential of ^{96}Mo added to the real potential as a consequence of the dispersion effect.

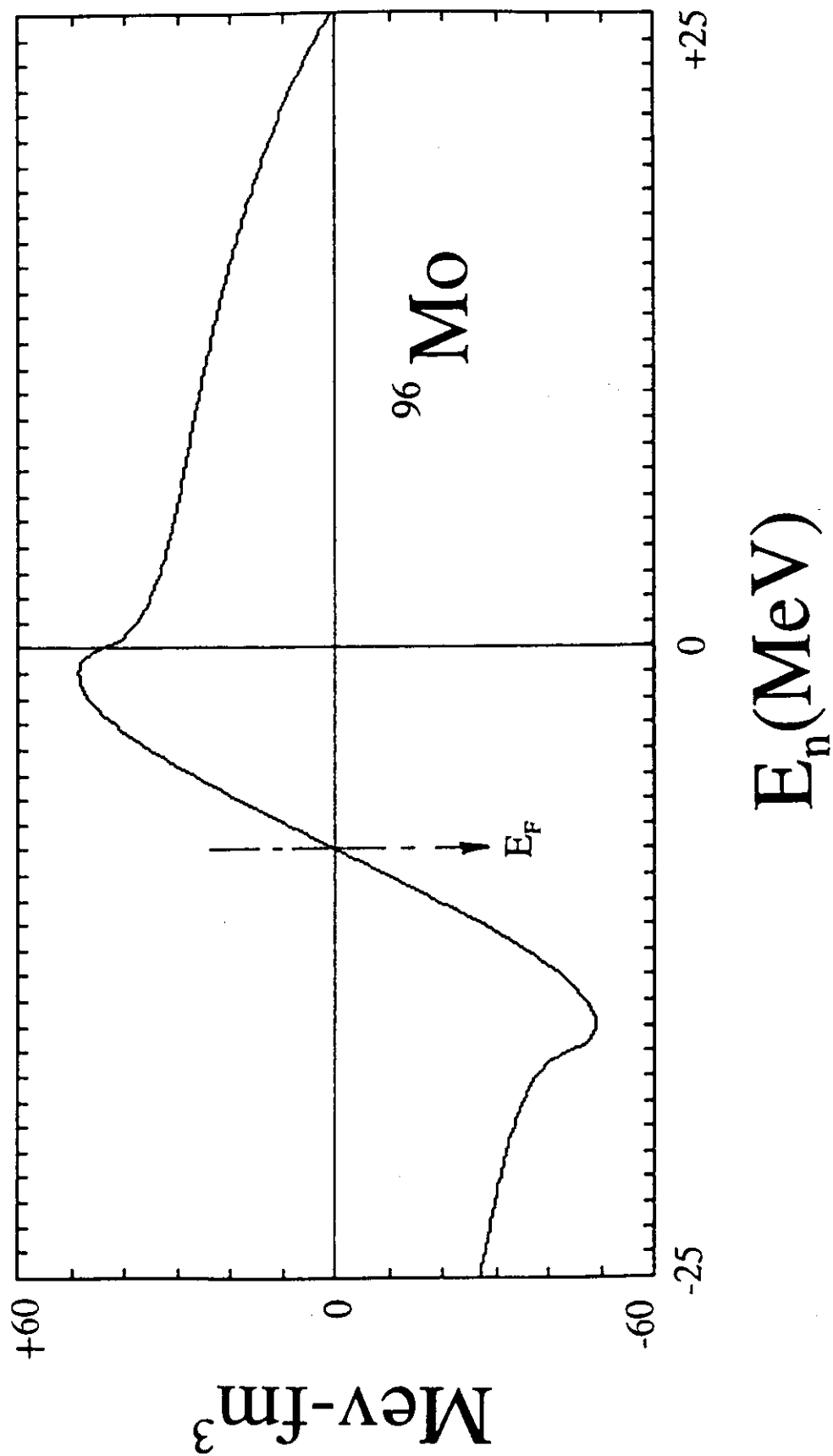


Fig. IV-4-B. The integral ΔJ_s of Eq. IV-4-2 as a function of energy for ${}^{96}\text{Mo}$.

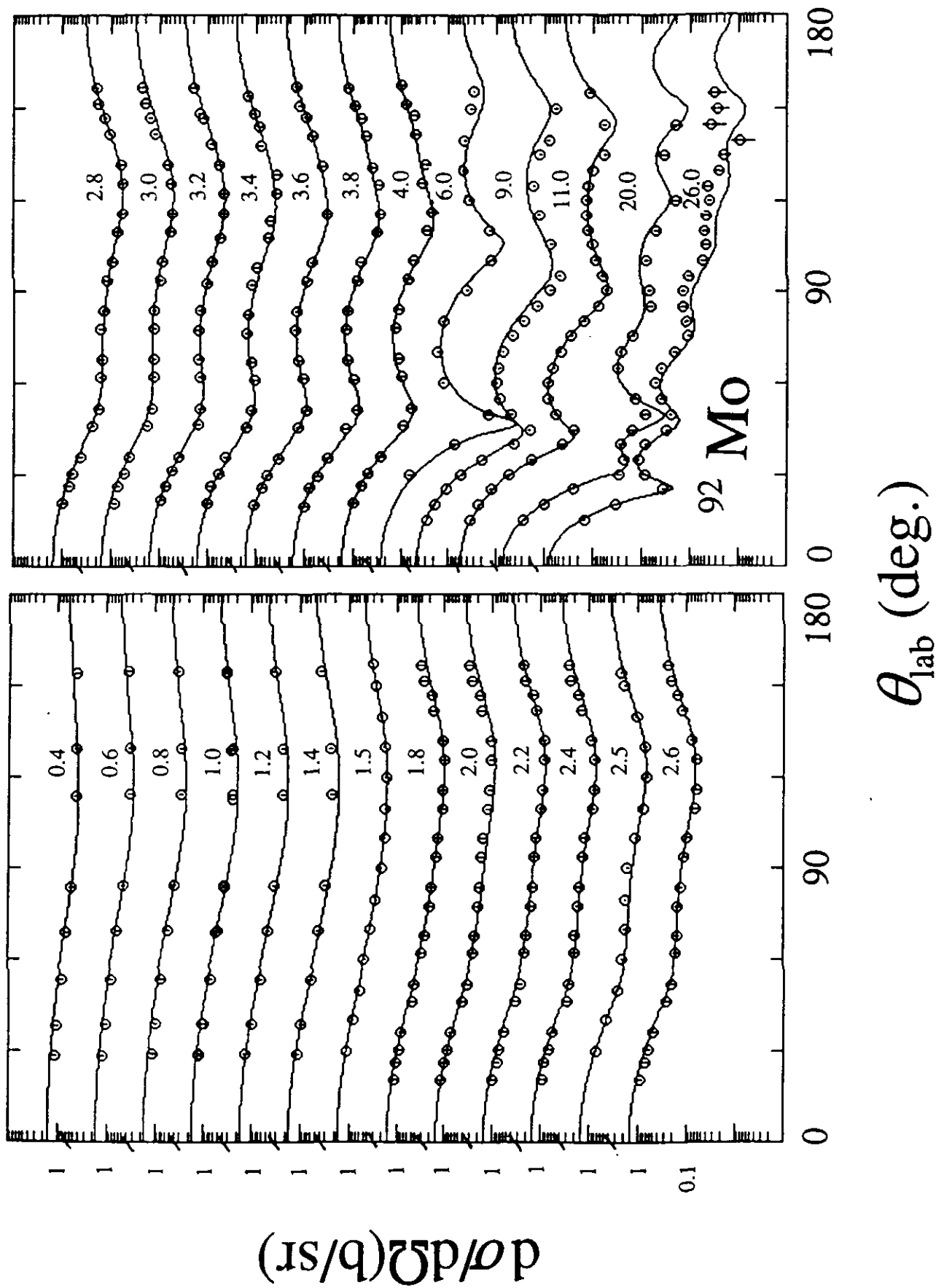
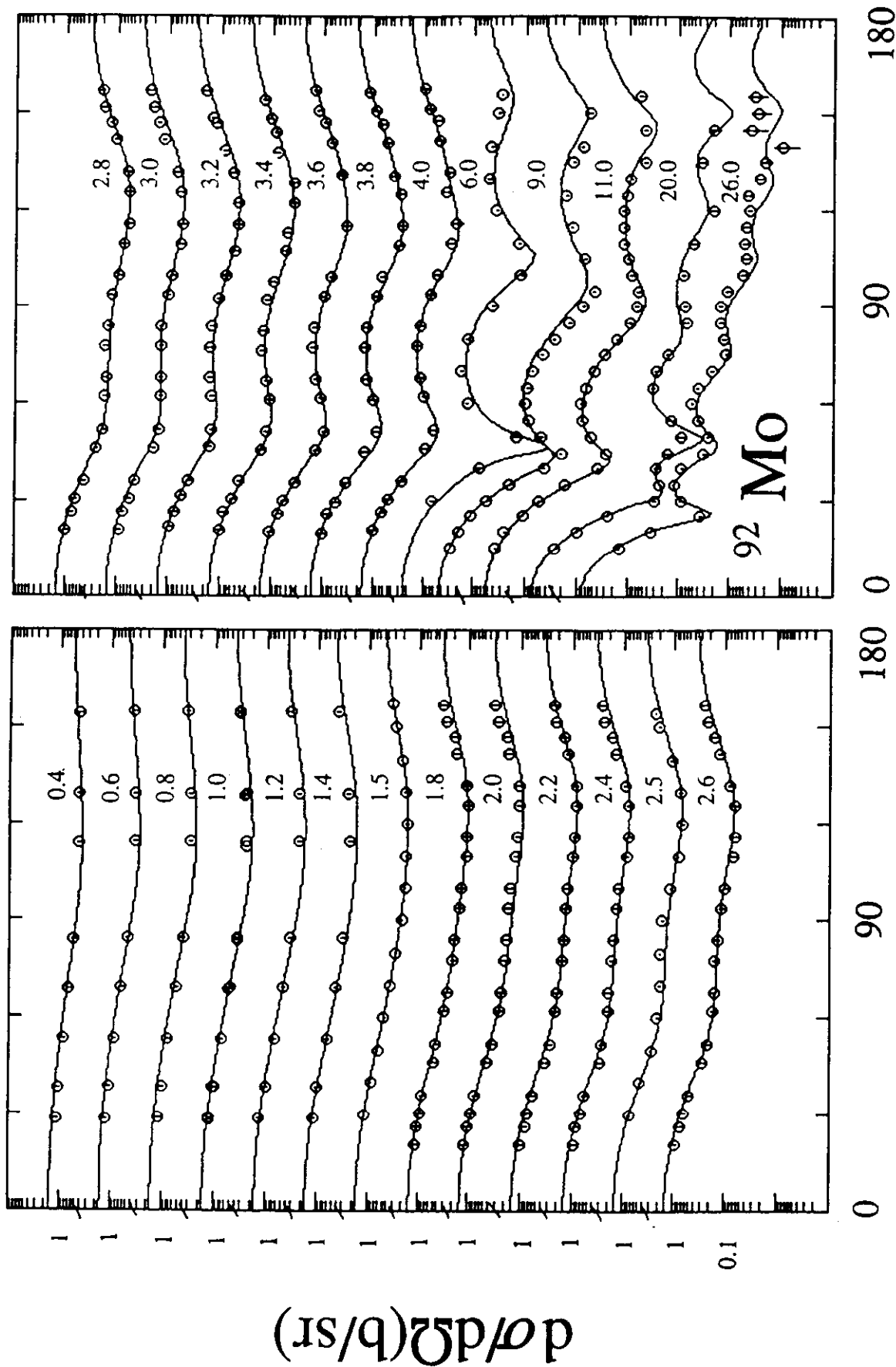


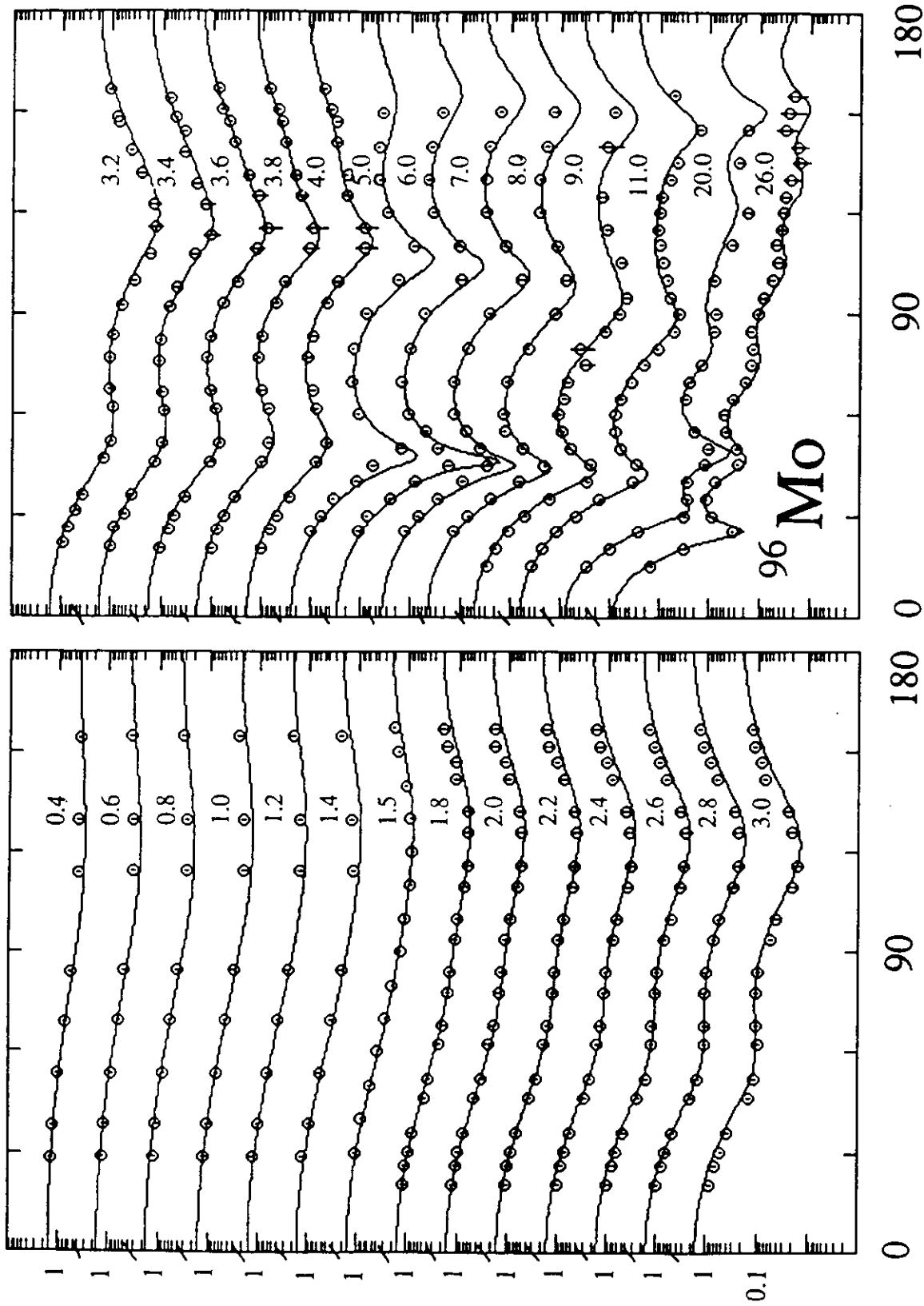
Fig. IV-4-C. Comparison of measured and DOM-calculated differential elastic-scattering cross sections of ^{92}Mo . The notation is identical to that of Fig. IV-1-A.



θ_{lab} (deg.)

Fig. IV-5-A. A comparison of measured (symbols) and CCM1 calculated (curves) neutron differential elastic-scattering cross sections of ^{92}Mo . Approximate incident energies are numerically noted in MeV.

$d\sigma/d\Omega$ (b/sr)



θ_{lab} (deg.)

Fig. IV-5-B. A comparison of measured (symbols) and CCM1 calculated (curves) neutron differential elastic-scattering cross sections of ^{96}Mo . The notation is identical to that of Fig. IV-5-A.

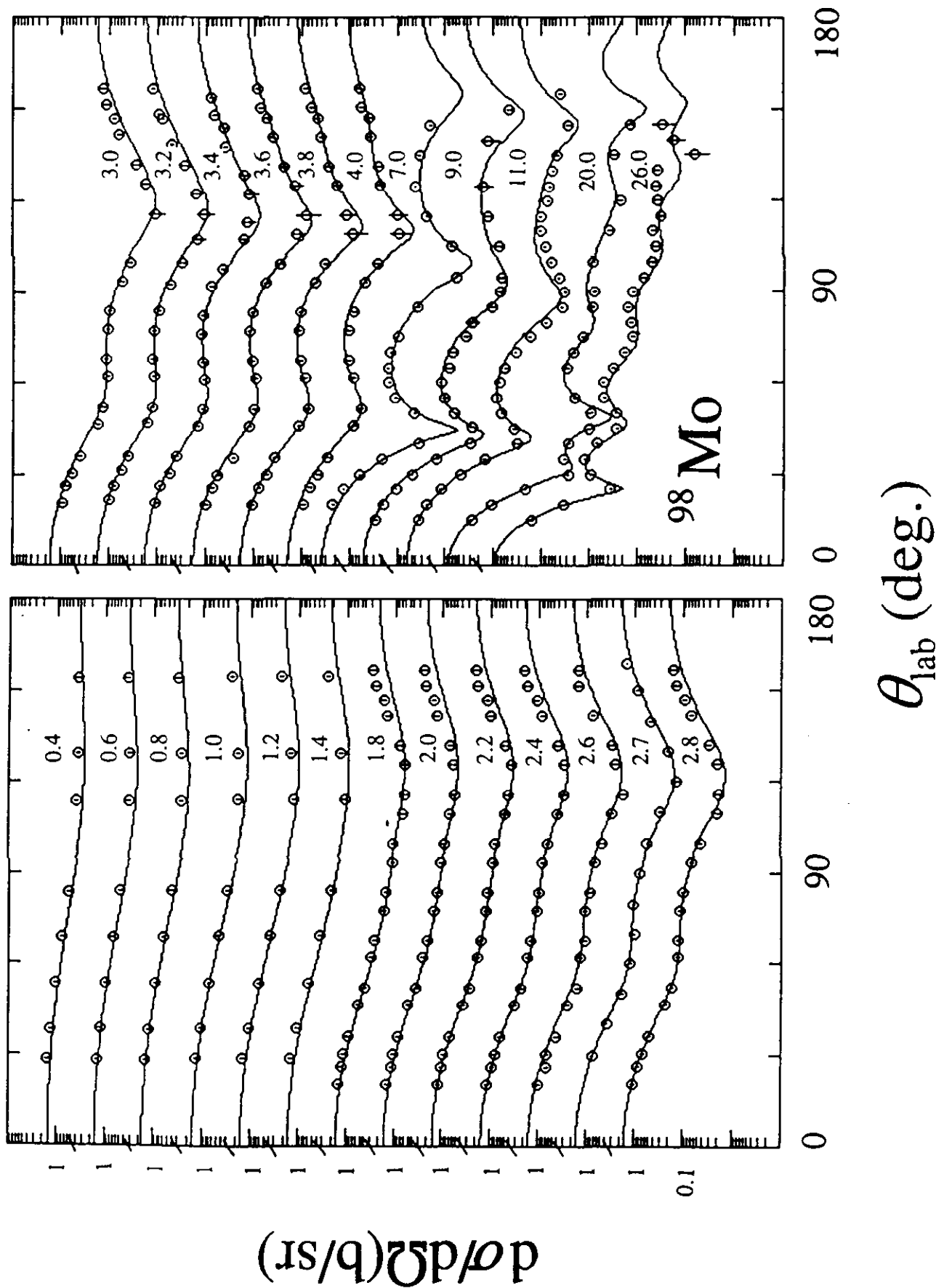
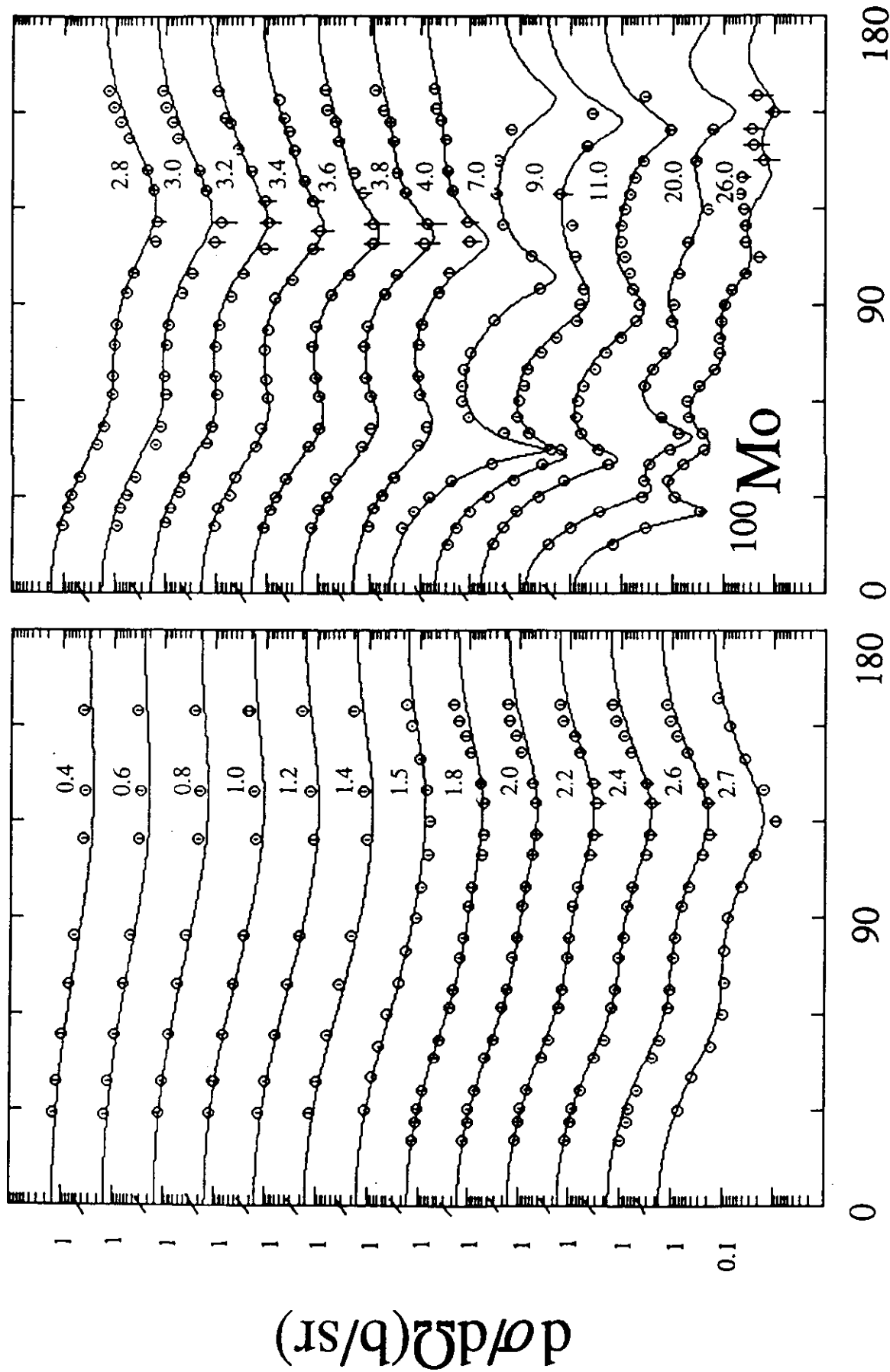


Fig. IV-5-C. A comparison of measured (symbols) and CCM1 calculated (curves) neutron differential elastic-scattering cross sections of ^{98}Mo . The notation is identical to that of Fig. IV-5-A.



θ_{lab} (deg.)

Fig. IV-5-D. A comparison of measured (symbols) and CCM1 calculated (curves) neutron differential elastic-scattering cross sections of ^{100}Mo . The notation is identical to that of Fig. IV-5-A.

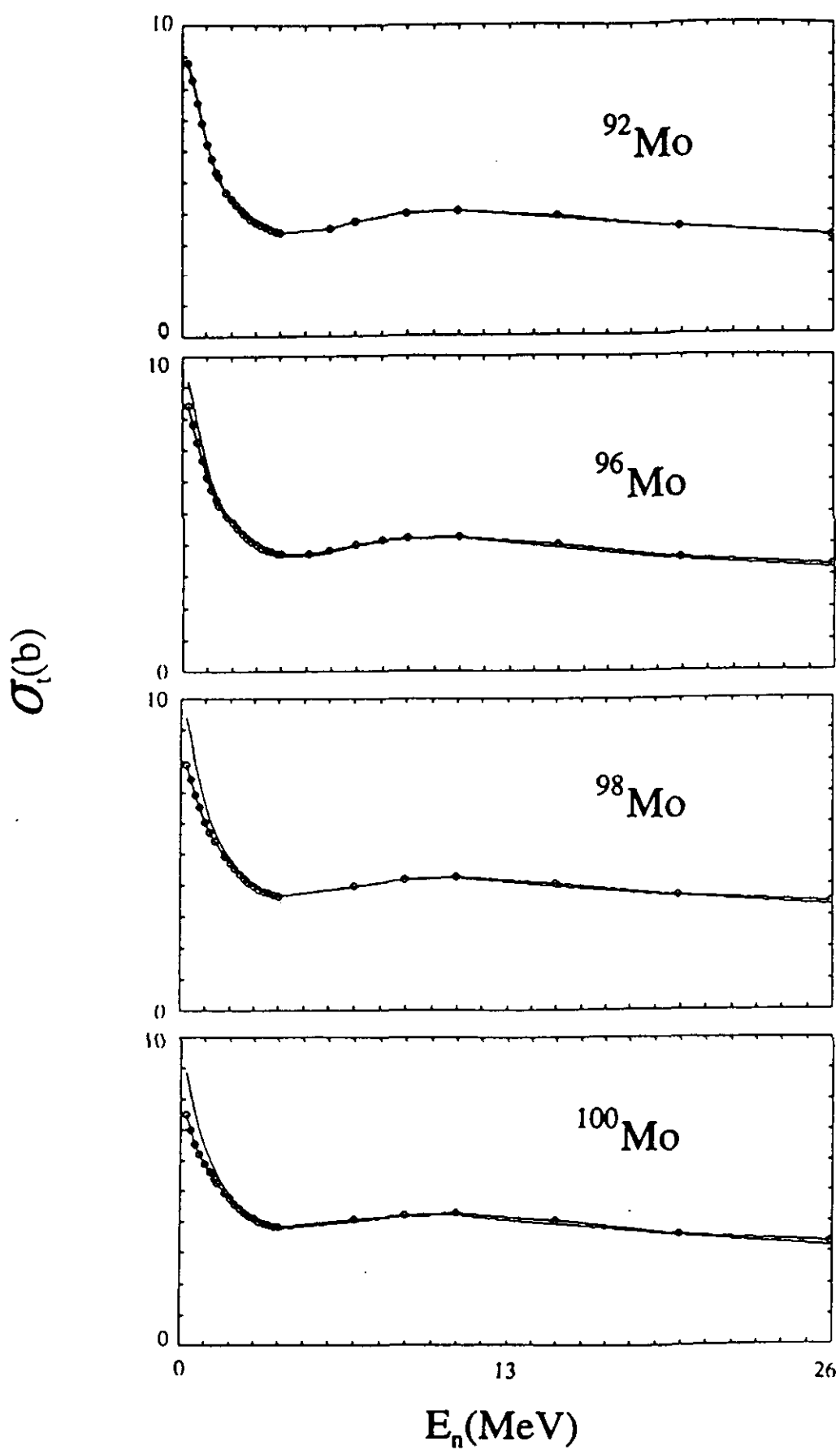


Fig. IV-5-E. Comparisons of calculated neutron σ_t 's. The simple curves were obtained with the SOM, and the curves with circular symbols with the CCM1 model.

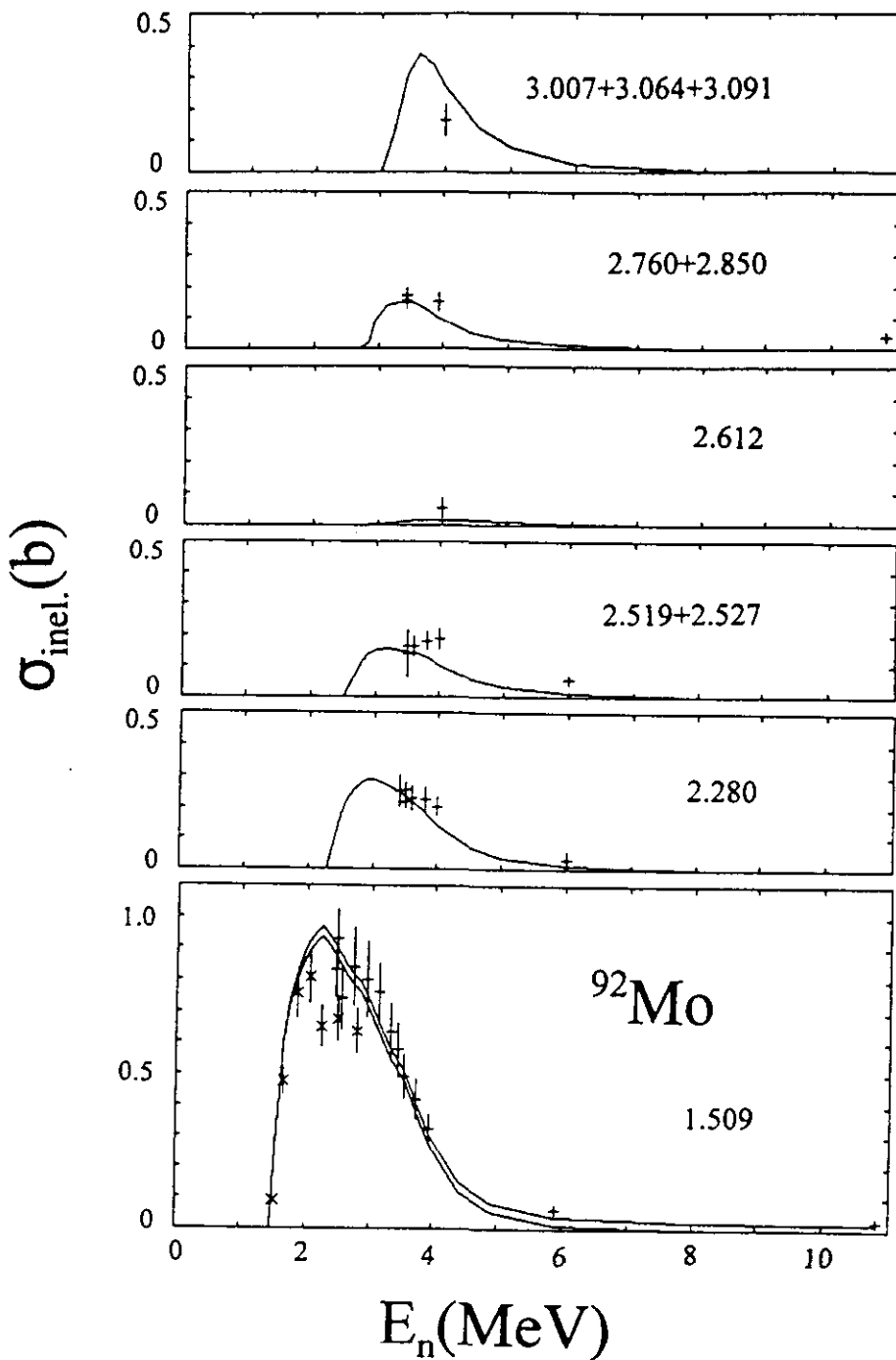


Fig. IV-5-F. Measured and calculated cross sections for the excitation of discrete levels in ^{92}Mo . "x" symbols indicate the results of $(n;n',\gamma)$ measurements [BWW97], primarily relevant to the yrast 2^+ levels. "+" symbols indicate the results of direct neutron measurements from a number of sources, largely from this laboratory. Curves indicate the results of calculations using the CCM1 model. All curves refer to compound-nucleus results, except for panels where there are two curves. In those instances the upper curve combines compound-nucleus and direct-reaction results, and the lower curve indicates compound-nucleus values alone. Excitation energies are numerically noted in MeV in each panel of the figure. Two or more values of excitation energies denote composite excitations comparable with the measured values.

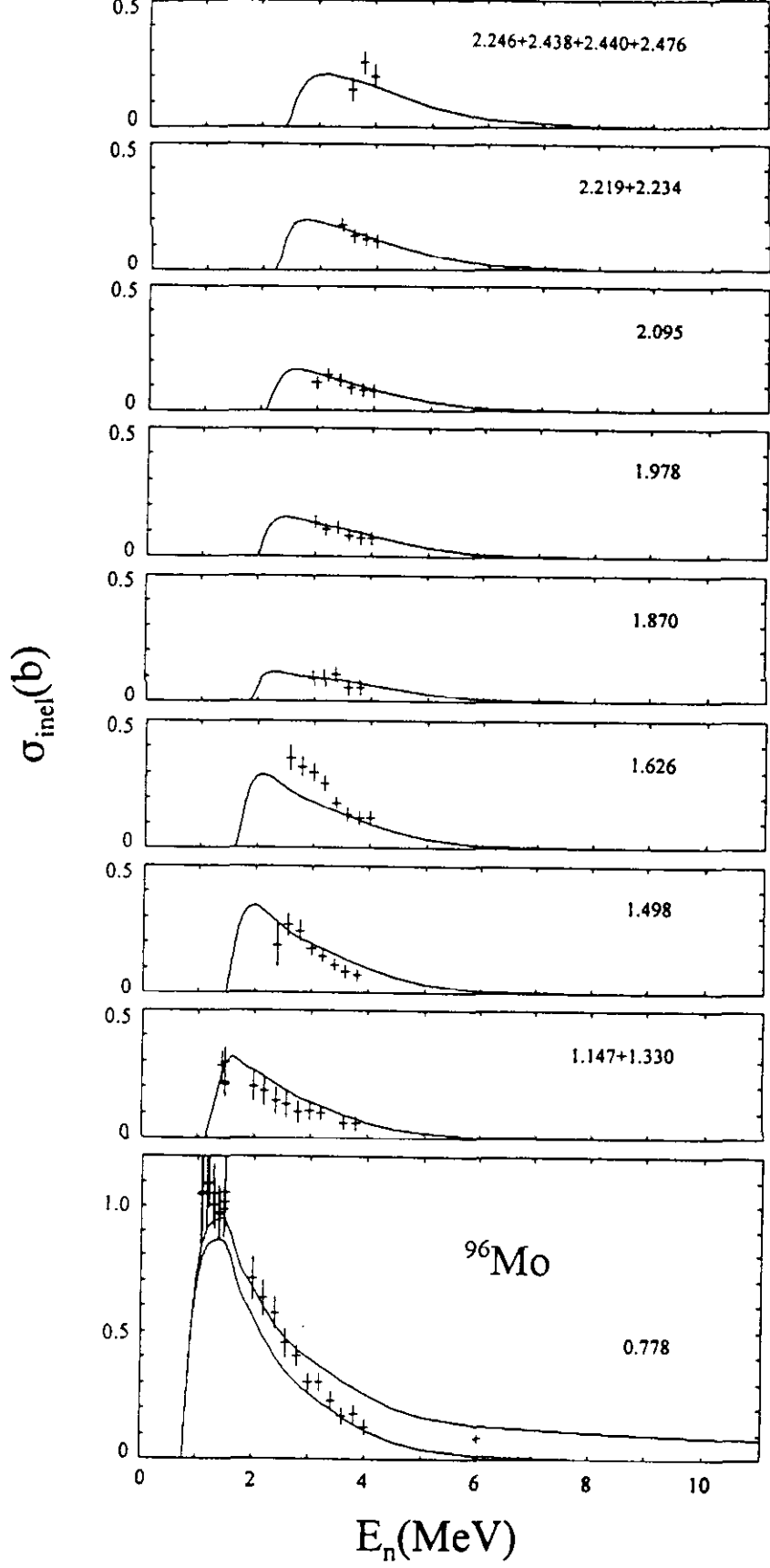


Fig. IV-5-G. Comparison of measured and calculated cross sections for the excitation of discrete levels in ^{96}Mo . The notation is identical to that of Fig. IV-5-F.

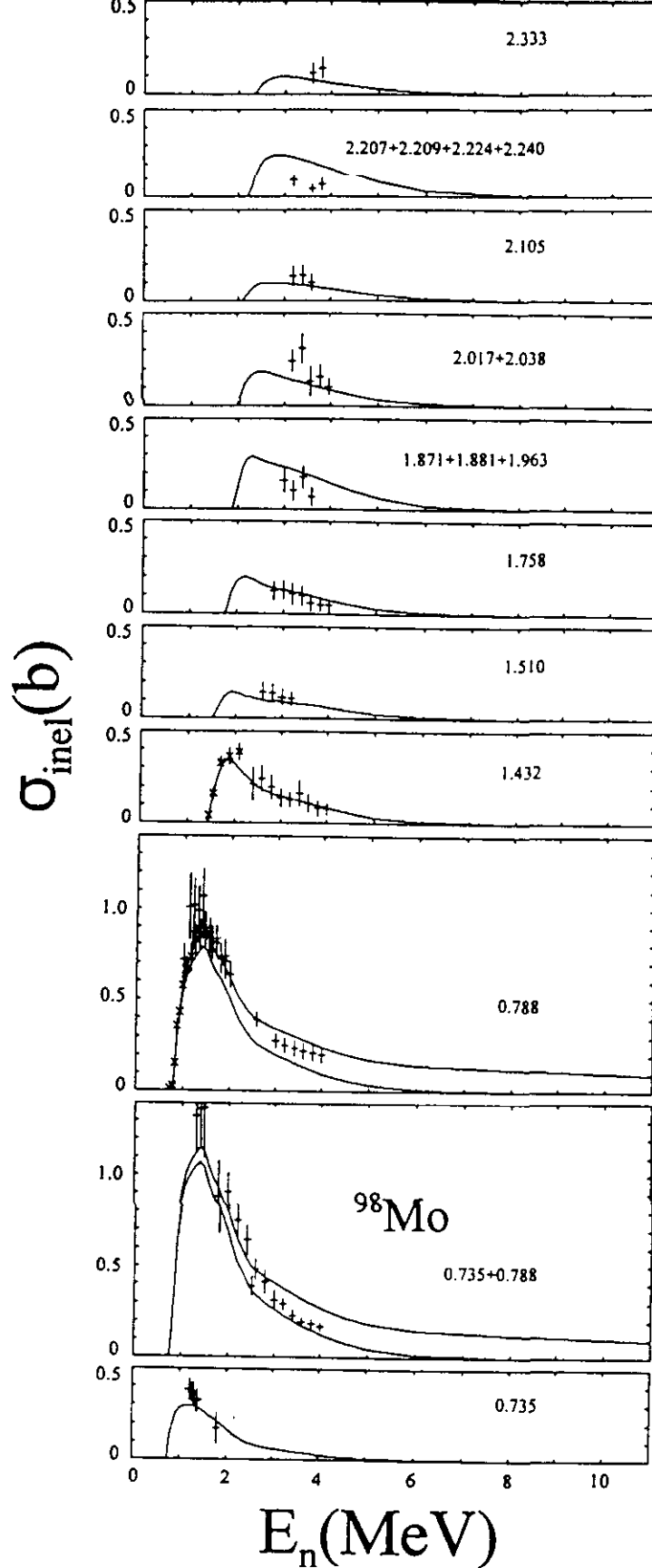


Fig. IV-5-H. Comparison of measured and calculated cross sections for the excitation of discrete levels in ^{98}Mo . The notation is identical to that of Fig. IV-5-F.

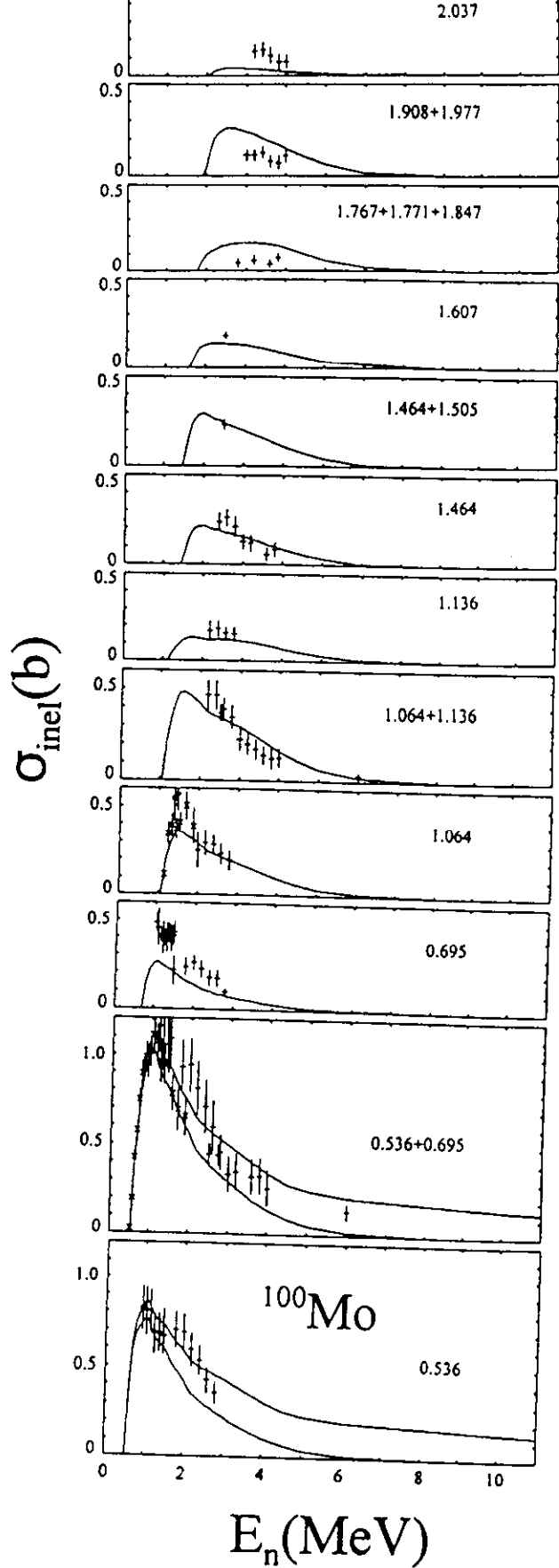


Fig. IV-5-I. Comparison of measured and calculated cross sections for the excitation of discrete levels in ^{100}Mo . The notation is identical to that of Fig. IV-5-F.

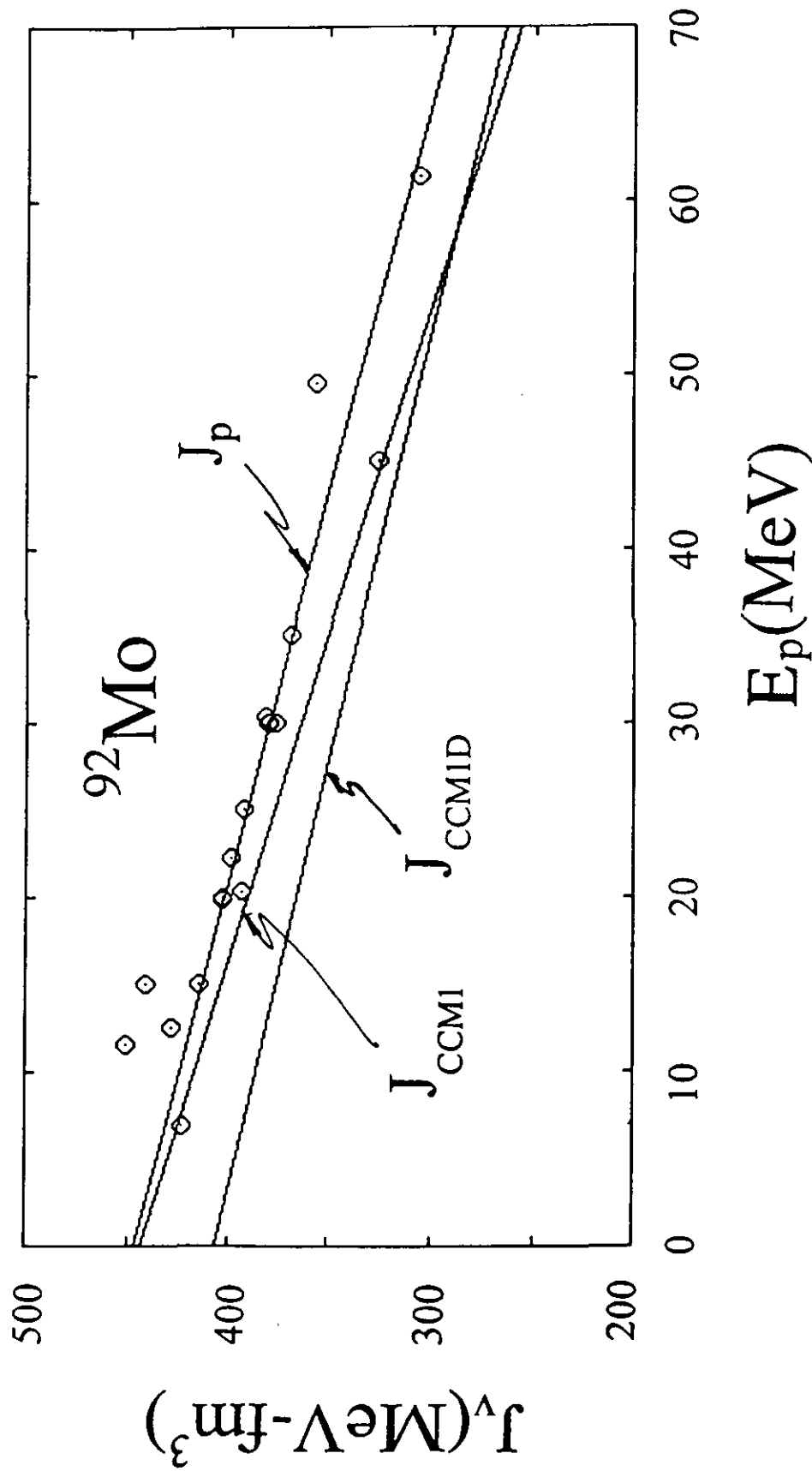


Fig. V-A. Proton and neutron J_v values for ^{92}Mo , Data symbols indicated proton J_v values deduced from measurements. The J_p curve is a least-square fit to the proton values as described in the text. The J_{CCM1} and J_{CCMID} curves represent the J_v results of the corresponding potentials of Section IV.

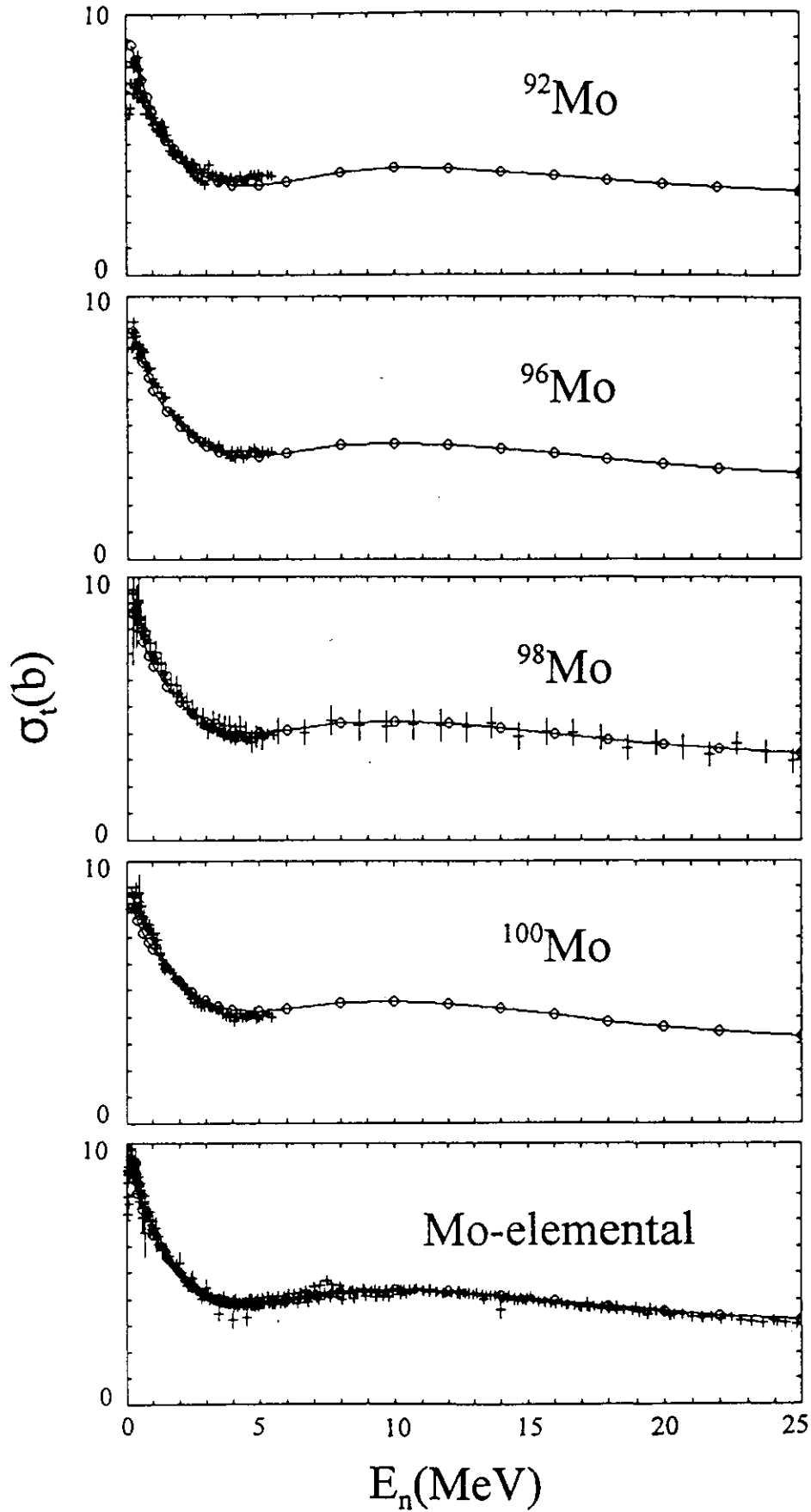


Fig. VI-A. Comparison of measured (+ symbol) σ_t 's with those calculated with the "regional" potential (curves with circular, "O" symbols). The upper sections present the four prominent even isotopes, and the lower section the elemental values.

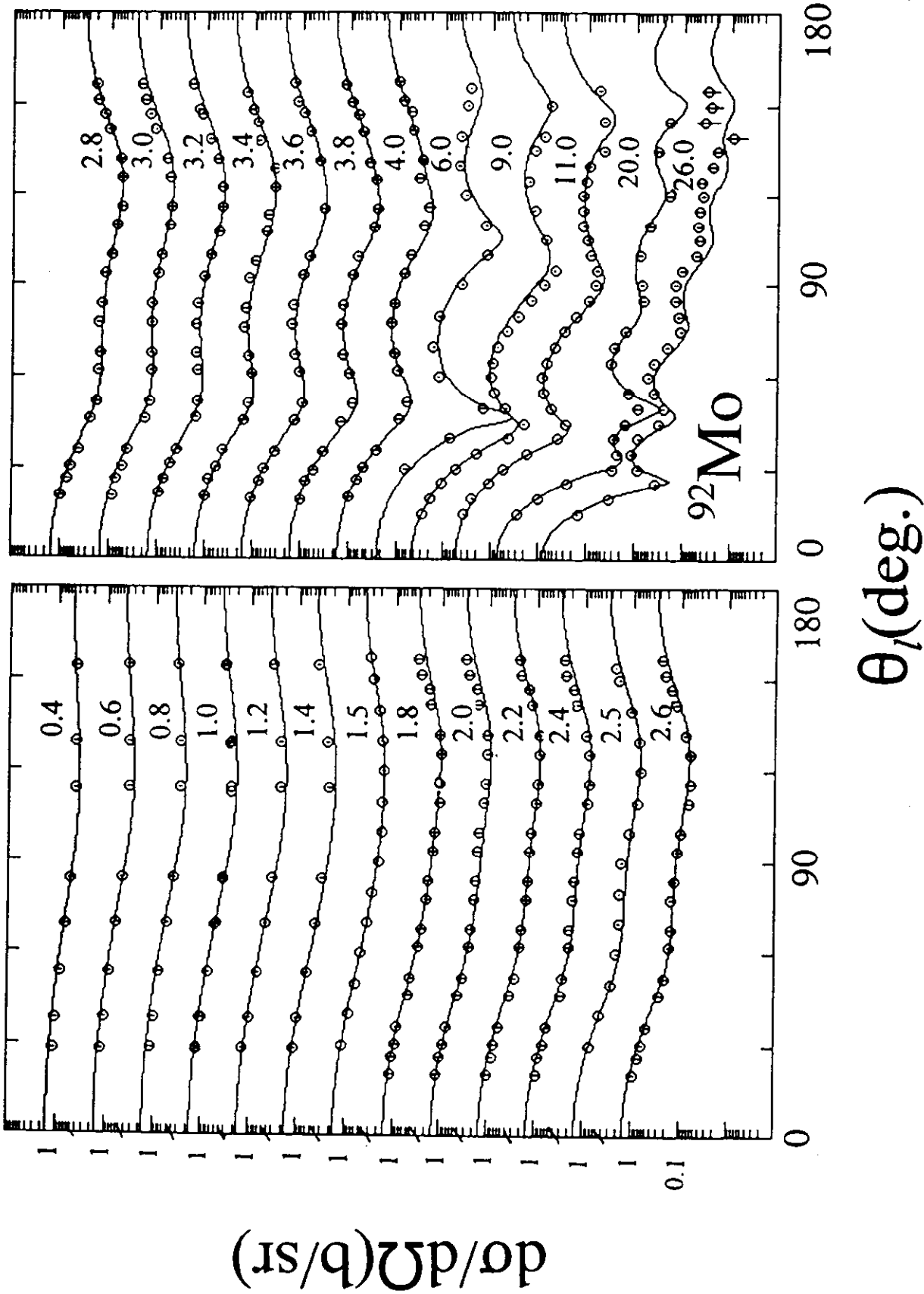


Fig. VI-B. Comparison of measured ^{92}Mo elastic-scattering distributions (data symbols) with results calculated with the "regional" potential (curves). Approximate incident energies are numerically cited in MeV.

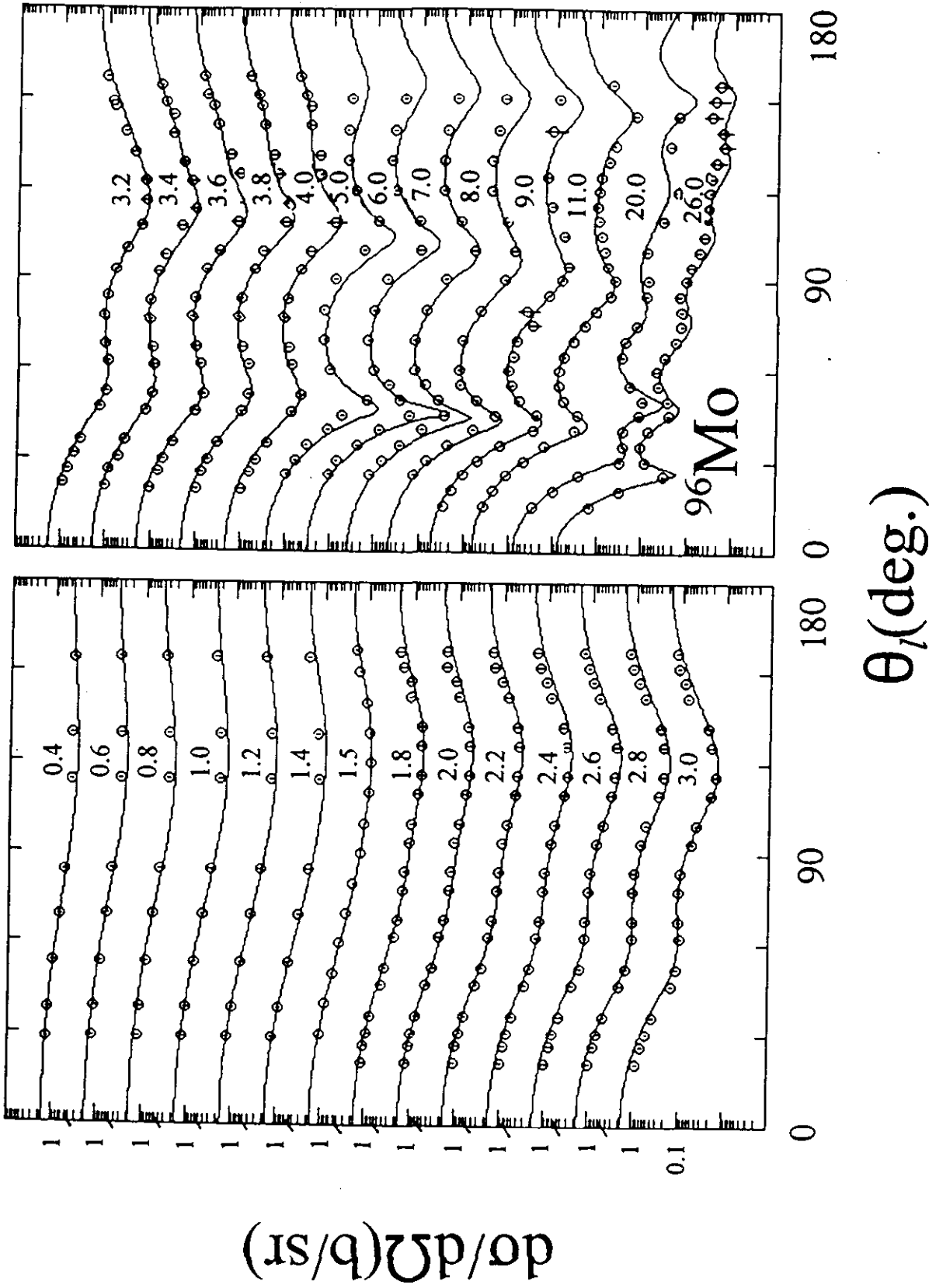


Fig. VI-C. Measured and calculated ^{96}Mo elastic-scattering distributions. The notation is identical to that of Fig. VI-B.

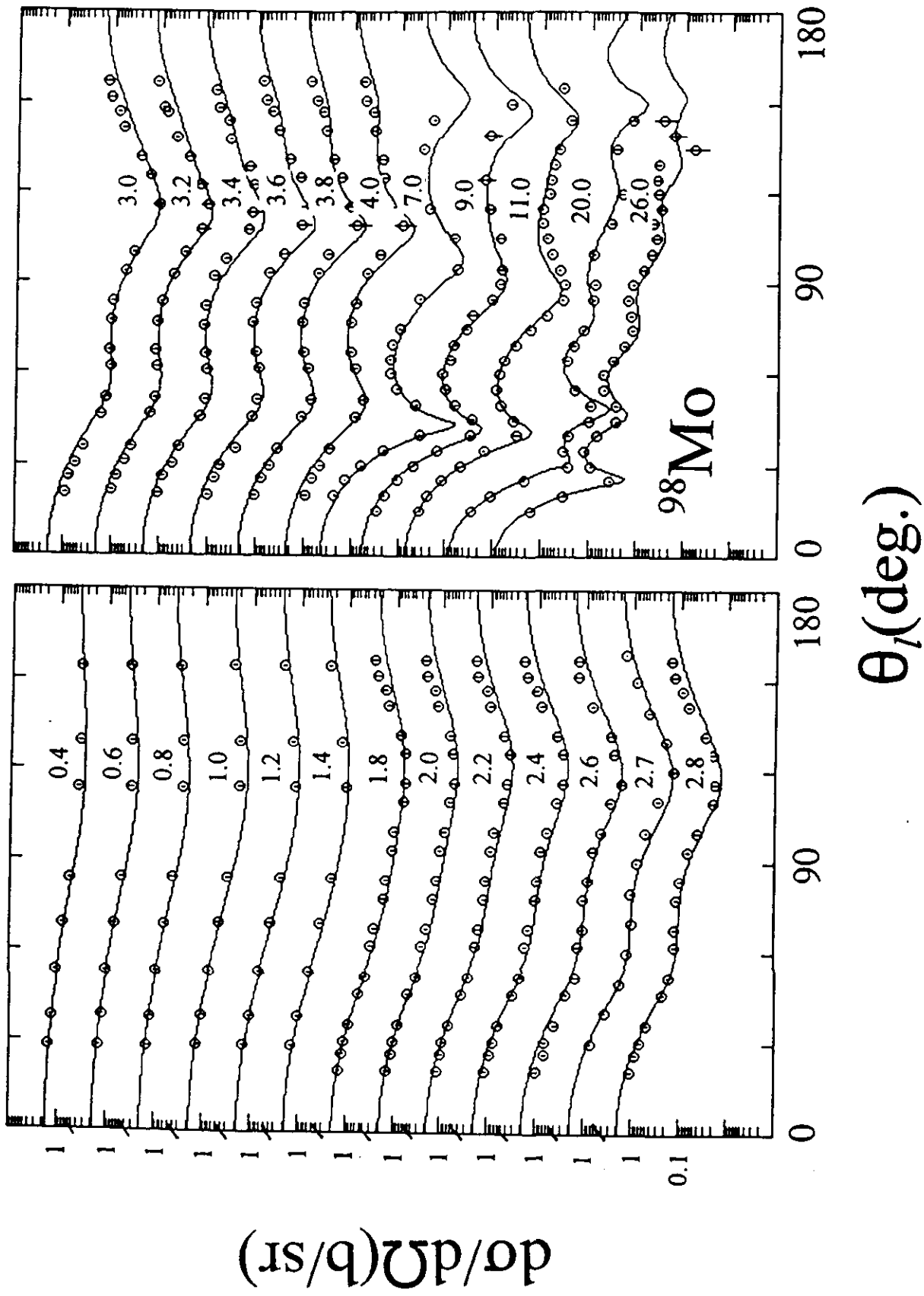


Fig. VI-D. Measured and calculated ^{98}Mo elastic-scattering distributions. The notation is identical to that of Fig. VI-B.

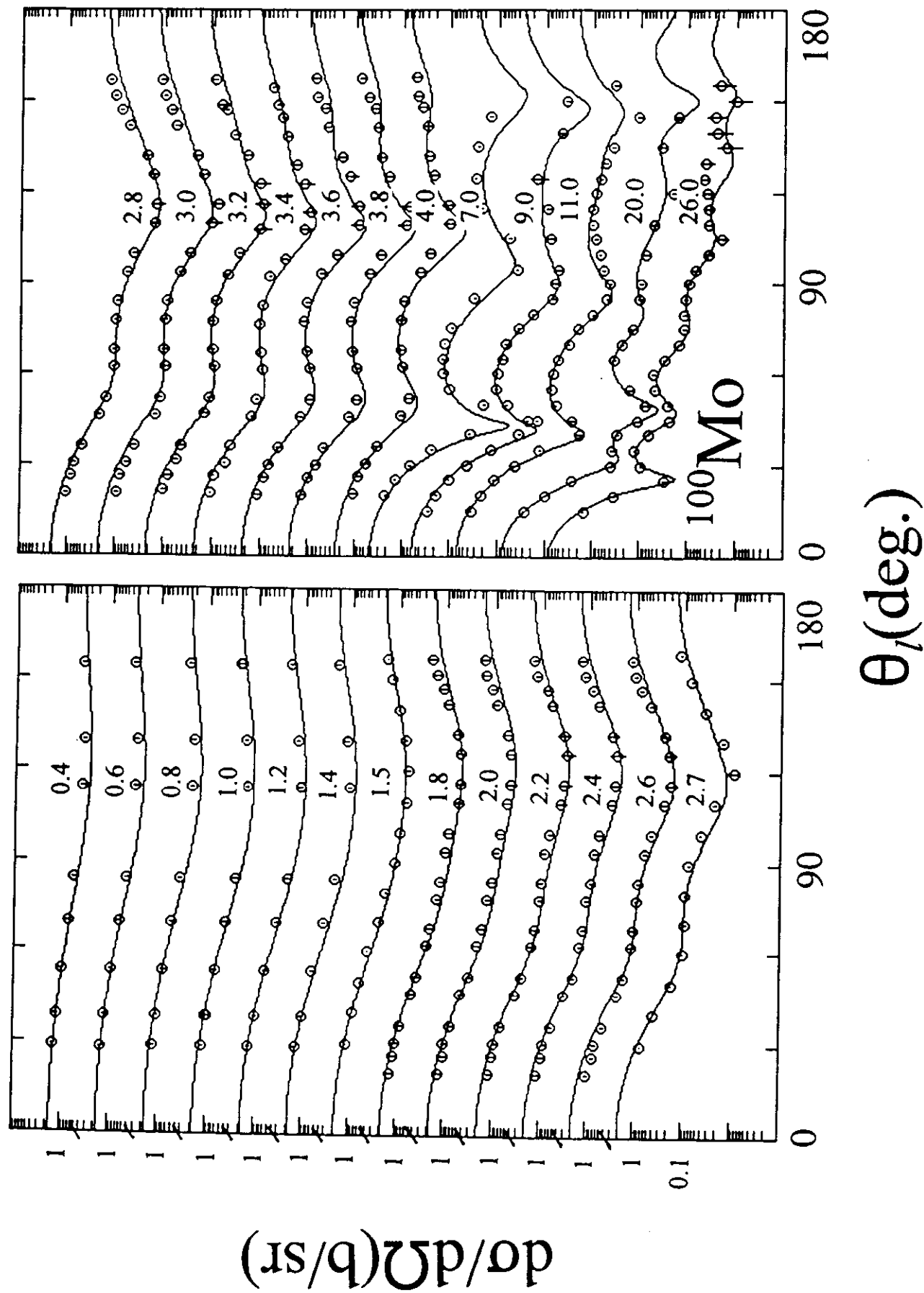


Fig. VI-E. Measured and calculated ^{100}Mo elastic-scattering distributions. The notation is identical to that of Fig. VI-B.

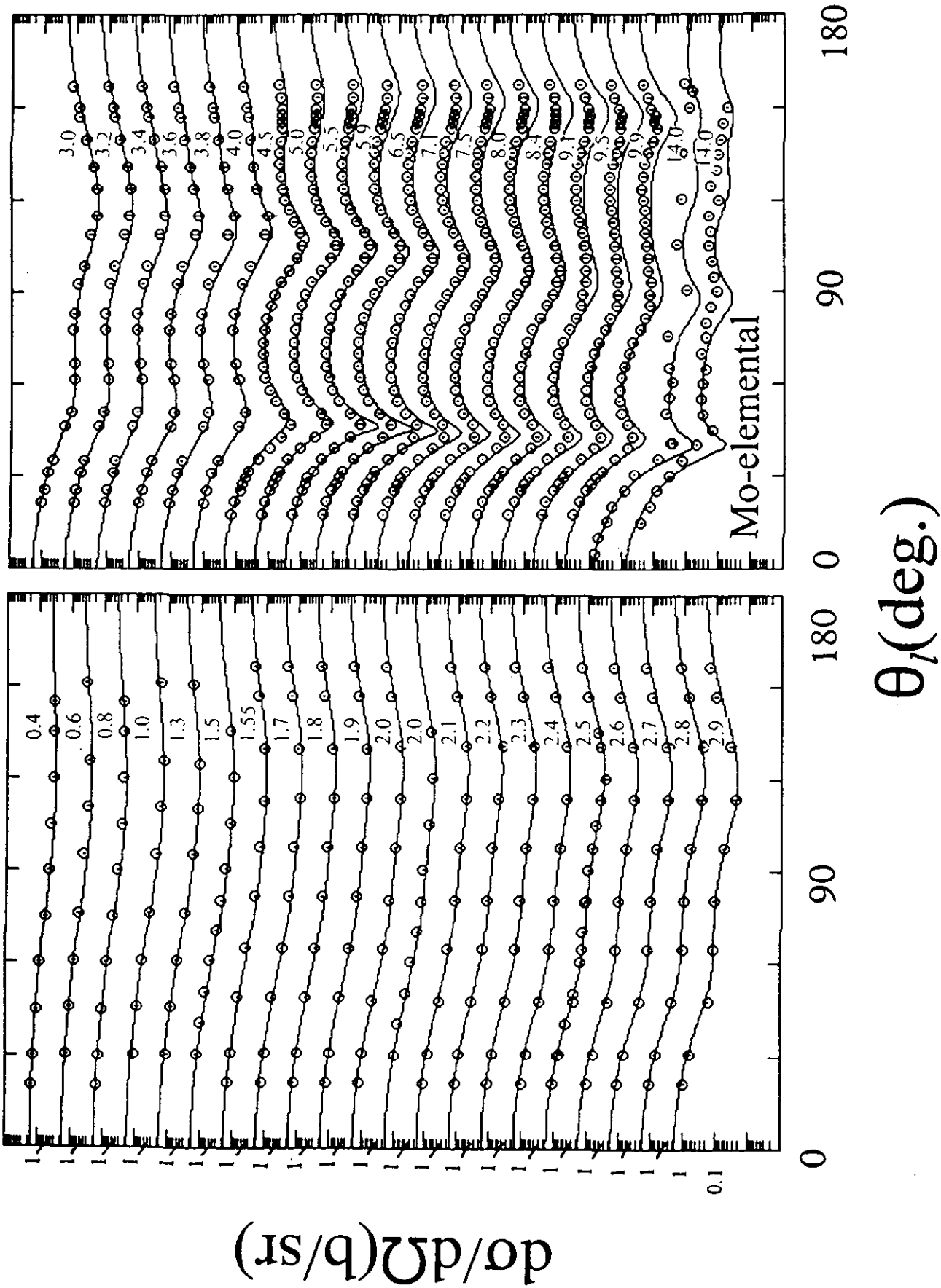


Fig. VI-F. Measured and calculated elemental molybdenum elastic-scattering distributions. The notation is identical to that of Fig. VI-B.

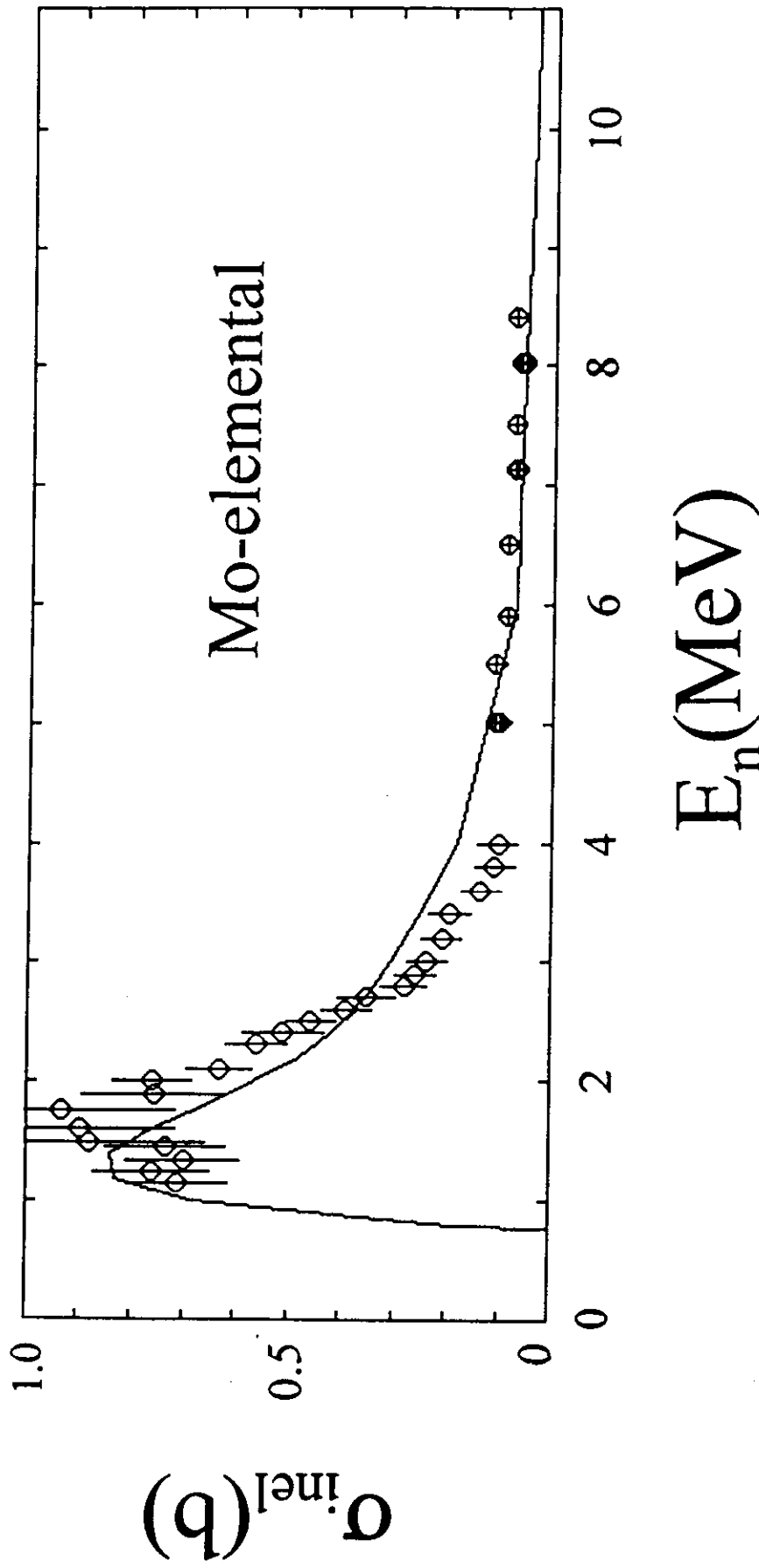


Fig. VI-G. Elemental molybdenum cross sections for the inelastic neutron excitation of levels between $\approx 0.7 \rightarrow 1.1$ MeV. The curve indicates the result of calculations as described in the text. Symbols indicate measured values, all from this laboratory. The circular symbols with crosses are the results of the present work.